Spring 2009

Photosynthetic and oxidative stress in the green alga Dunaliella tertiolecta: The effects of UV-B and UV-A radiation

Priya Sampath Wiley
University of New Hampshire, Durham

PHOTOSYNTHETIC AND OXIDATIVE STRESS IN THE GREEN ALGA *DUNALIELLA TERTIOLECTA*: THE EFFECTS OF UV-B AND UV-A RADIATON

BY

PRIYA SAMPATH WILEY

B.S. State University of New York College of Environmental Science and Forestry, 1999

M.S. University of New Hampshire, 2003

DISSERTATION

Submitted to the University of New Hampshire

In Partial Fulfillment of

the Requirements for the Degree of

Doctor of Philosophy

in

Plant Biology

May, 2009

DEDICATION

I dedicate this dissertation to the loves of my life. Abe, thank you for your support and encouragement throughout this long, long, LONG journey. Lila, you changed my life. Thank you for enlightening me on what is truly important in life. I love you both more than words can express.

ACKNOWLEDGEMENTS

I am so fortunate to have had the opportunity of working with Dr. Leland Jahnke. Lee was a patient, kind and wise advisor and I sincerely appreciate his guidance and direction throughout my graduate career. It was a privilege to have worked alongside Lee in the laboratory everyday. This type of experience is unique for a graduate student working in the biological sciences and I have gained so much more than just research knowledge from our time spent together in the lab. Ultimately, it was Lee's encouragement and belief in my abilities as a scientist that pushed me to achieve my goals and reach my utmost potential and I am so thankful for his support.

I am especially grateful to have had Dr. Christopher Neefus on my graduate committee. Chris was invaluable for help with statistical analyses, experimental design and soliciting research funding. Most importantly, he has always been a constant source of support and I greatly value his advice and friendship. I would like to extend my most sincere thanks to Dr. Subhash Minocha and Dr. Curt Givan for always taking the time out of their busy schedules to answer my questions, review manuscripts and provide helpful suggestions. I would also like to thank Dr. Michael P. Lesser for valuable research input and for graciously donating cellulose acetate and the chloroplastic APX antibodies. Thanks to Dr. Chris Lane for helping with the phylogenetic analyses, Dr. Kelly Thomas and everyone at the UNH Hubbard Center for Genome Studies for guidance on the molecular aspects of this project and Dr. Janet Sullivan for PAGE gel scanning assistance.

Many thanks are due to my fellow UNH graduate students (past and present) for their camaraderie, encouragement, advice and making me laugh out loud almost daily. In particular, Dr. Chery Whipple, Dr. Aaron Wallace, Dr. Troy Bray, Dr. Sridev Mohapatra, Lise Mahoney, Jeremy Nettleton, Laurie Hofmann, Agnes Mols Mortensen and Dr. (?) Scott Kavanaugh. Honorable mention to Melanie Shields for countless hours of stimulating conversation "over the wall" and for being the best listener I know. Finally, I would like to thank my parents for a lifetime of love and support. Thank you for believing in me. I love you.

This research was partially supported by a USDA Hatch grant awarded to Lee Jahnke as well as an UNH graduate school dissertation year fellowship, UNH marine program research awards, UNH graduate school teaching assistant summer fellowships, a College of Life Sciences and Agriculture graduate student summer fellowship and several travel grants funded by the UNH Graduate School and UNH Marine Program.

TABLE OF CONTENTS

LIST OF TABLES

LIST OF FIGURES

ABSTRACT

PHOTOSYNTHETIC AND OXIDATIVE STRESS IN THE GREEN ALGA *DUNALIELLA TERTIOLECTA*: THE EFFECTS OF UV-B AND UV-A RADIATON

by

Priya Sampath Wiley

University of New Hampshire, May 2009

The penetration of ultraviolet-B (UV-B; 290-320 nm) into the biosphere has increased in response to decreased stratospheric ozone. As a consequence, significant attempts have been made to elucidate the effects of UV-B radiation on primary producers such as phytoplankton and plants. Considerably less effort has been devoted to describing the role played by ultraviolet-A (UV-A; 320-400 nm) radiation, which is not attenuated by stratospheric ozone. The present work details the independent and combined effects of UV-B and UV-A radiation on photosynthetic and oxidative stress responses using the unicellular green alga *Dunaliella tertiolecta* as a model organism. A UV-B spectral profile comparable to natural solar irradiance was produced in the laboratory by filtering UV-B lamp emissions with a novel liquid urate solution (UA) and compared against the conventionally used cellulose acetate (CA) filter. Cells growing at 100, 200 or 600 μmol photons $m^{-2}s^{-1}$ photosynthetically active radiation (PAR) were exposed to 12-hour UV-B (6 μmol photons $m^{-2}s^{-1}$), UV-A (60 μmol photons $m^{-2}s^{-1}$) or UV-B + UV-A (6 + 60 μmol photons $m^{-2}s^{-1}$) radiation treatments after which, photosynthesis, fluorescence parameters, D1 protein contents and antioxidant enzyme activities were recorded. In almost all cases, the physiology of UA cultures remained comparable to controls, while CA cultures

suffered declines in photosynthesis and D1 protein content plus elevated antioxidant enzyme activities. UV-B: PAR ratios comparable to solar irradiance reduced UV-B induced photodamages, highlighting the significance of properly balanced irradiance environments within laboratory studies. Regardless of the PAR level applied, exposure to UV-A radiation resulted in acute photosynthetic and oxidative stress, which remained unchanged following the addition of UV-B flux. The findings of this study suggest that exposure to UV-A (and not UV-B) causes the direct impairment of photosynthesis and increased oxidative stress within plant cells. It is therefore recommended that laboratory based UV studies employ the use of UA filters and UV: PAR ratios that correspond to solar flux. Lastly, the discovery of at least two ascorbate peroxidase (APX) isoforms suggests that like higher plants, green algae also possess APX isoenzymes. This is the first report documenting the presence of multiple APX isoforms within green algae.

INTRODUCTION

Properties and absorption of light

Irradiance from the sun can be characterized both as electromagnetic waves and as particles called photons or quanta. Wavebands between 290-700 nm reach the Earth's surface as visible radiation (400 - 700 nm) and ultraviolet radiation (290 - 400 nm). Ultraviolet radiation is further differentiated into ultraviolet-C (UV-C; 190-280 nm), ultraviolet-B (UV-B; 280-320 nm) and ultraviolet-A (UV-A; 320-400 nm) radiation (Greenberg, *et al.*, 1997). Because the potential energy of a photon is inversely proportional to its wavelength, a photon from the blue region (400 nm) will have more potential energy than a photon from the red region (700 nm; Hall and Rao, 1999).

Plants harness the +2840 kJ/mol needed to fix six molecules of CO_2 into one hexose sugar through the absorption of light energy by pigment molecules (Buchanan *et al.*, 2000). A pigment in its ground state is a stable, low energy molecule. After absorbing a photon, an electron within the pigment is moved to a higher-energy molecular orbital and the pigment becomes "excited". Two states of excitation exist: (1) the short-lived singlet state, in which the outermost pair of electrons maintain their antiparallel spin in the excited state (2) the longer-lived triplet state, in which the excited electron undergoes spin reversal and the electron pair are aligned (parallel). To return to the ground state, singlet excited pigments can 1) transfer absorbed energy to a second, adjacent molecule 2) fluoresce the energy by re-emitting it as a photon of longer wavelength 3) release the energy as heat or 4) use the energy to reduce an acceptor molecule (Whitehead *et al.*,

2000). The latter mechanism is fundamental to the process of photosynthesis and is the means by which light energy is converted into a chemical product (i.e. photochemistry; Buchanan *et al.*, 2000). Of the four potential energy transfer options, energy transfer reactions are by far the fastest ($<10^{-14}$ s) and most efficient (> 95%). However, it is common for a plant to absorb energy in excess of what can be utilized photochemically. Incomplete utilization of absorbed light occurs commonly in plants experiencing full sunlight (or high light intensities) where the rate of energy absorption exceeds the capacity of the photosynthetic system to safely use it in photochemistry (Demmig-Adams and Adams, 2006). Under these conditions, excessive absorbed energy may be safely released as heat or as fluorescence to avoid physiological damage.

There are three main classes of pigments within photosynthetic organisms: the chlorophylls, phycobilins and carotenoids. Phycobilins are found within cyanobacteria and red algae, while carotenoids act as accessory photosynthetic pigments in most photosynthetic organisms; absorbing wavelengths of light not absorbed by other pigments. In addition, carotenoids also provide photoprotection to sensitive photosynthetic machinery by quenching excessive excitation energy and releasing it as heat (Siefermann-Harms, 1987; Niyogi, 1999). Chlorophyll pigment molecules are present in all photosynthetic organisms. They contain a central Mg atom surrounded by a tetrapyrrole (porphyrin) ring structure and a long hydrocarbon phytol tail (C_{20}). Although several forms of chlorophyll have been described, there are two forms present in higher plants and green algae: chlorophyll *a* (chl *a*) and chlorophyll *b* (chl *b*). Structural variations between these forms involve modifications on the porphyrin ring. Specifically, chl *a* contains a methyl (CH_3) group on ring II, while Chl *b* possesses a formyl group

(CHO; Buchanan *et al.*, 2000). Two additional types of chlorophylls have also been characterized from eukaryotic algae: chlorophyll *c* (chl *c*) and chlorophyll *d* (chl *d*). Chl *c* is classified as a porphyrin (not a chlorin) since ring D is not reduced and it also lacks an isopreniod tail (Figure 1; Blankenship, 2002). Chl *d* differs from chl *c* in that the substituent at the C-3 position is a formyl group instead of the vinyl group found in chl *a* (Figure 1; Blankenship, 2002). Chl *c* serves exclusively as an antenna pigment within marine algae such as diatoms and dinoflagellates, while chl *d* is found in trace amounts within algae and cyanobacteria (Blankenship, 2002). All chlorophylls contain two major absorption bands, one in the blue or near UV region and one in the red or near infrared region (Blankenship, 2002). The lack of significant absorption in the green region gives chlorophylls their characteristic green or blue-green color (Blankenship, 2002).

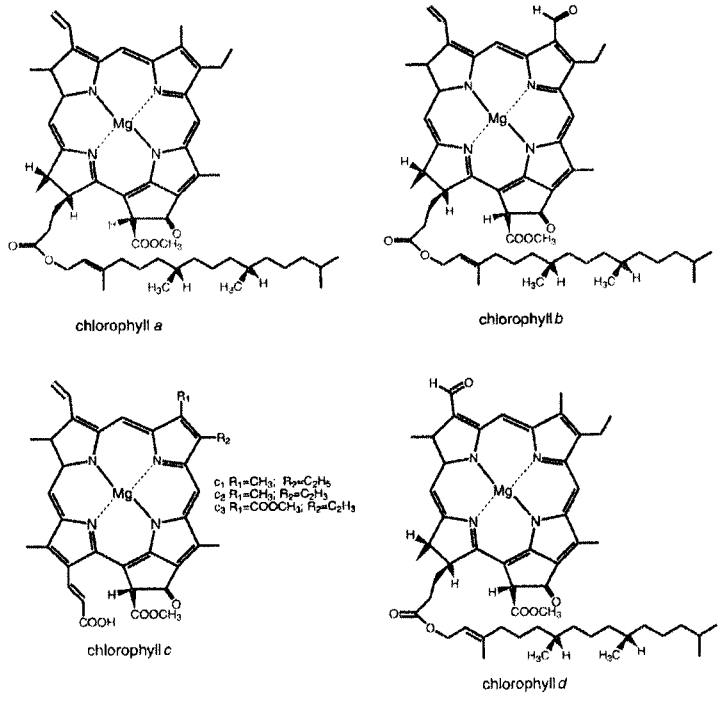

Figure 1. Chemical structures of chlorophylls *a*, *b*, *c* and *d*. R_1, R_2, etc. refer to ring substituents (taken from Blankenship, 2002).

The thylakoid membranes of higher plants and algae contain high concentrations of monogalactosyl and digalactosyl lipids (e.g. galactolipids). Embedded within these membranes are light absorbing pigment antenna systems organized into light harvesting complexes (LHC) that are responsible for funneling light energy into the reaction centers with which they are associated (Taiz and Zeiger, 2002). The size of LHCs varies with species. Some photosynthetic bacterial LHC possess 20-30 chlorophyll per reaction center while higher plant reaction centers may contain as many as 200-300 chlorophylls (Buchanan *et al.*, 2000; Taiz and Zeiger, 2002). Light captured by a LHC pigment is transferred to adjacent pigment molecules by a non-radiative process called resonance transfer (e.g. Förster energy transfer). This movement of energy is very efficient, with 95-99% of photon's energy absorbed by antenna pigments being transferred directly to reaction center chlorophyll molecules (Blankenship, 2002; Taiz and Zeiger, 2002).

The distances and orientation of particular pigments within the LHC antennae are optimized to ensure rapid and efficient transfer of light energy. *In vitro*, chl *a* and chl *b* molecules maintain absorbance maxima of 670 and 650 nm, respectively. However, the spectral properties of these pigments are significantly altered when they are incorporated into protein complexes. More specifically, the longest-wavelength maximum shifts to longer wavelength in pigment-protein complexes (Blankenship, 2002). Following energy transfer from pigment to pigment molecule, a small amount of energy is lost as heat and the excitation is moved closer to the reaction center (Blankenship, 2002). The energy lost as heat provides a degree of irreversibility to the process so that the excitation energy is funneled closer to the reaction center (Blankenship, 2002). Precise pigment arrangements within each LHC ensure that the majority of absorbed energy is directed toward the

reaction center and not lost to the system through reverse or "backward" transfers (Taiz and Zeiger, 2002). This means that the spatial and energetic ordering of the LHC is designed so that the shorter-wavelength absorbing pigments (carotenoids) are farthest away from the reaction center and the longest-wavelength absorbing pigments (chlorophylls) are closest (Blankenship, 2002).

Photosynthetic electron transport

The photochemical reactions of photosynthesis originate from reaction centers located within complex protein structures called photosystems. Each reaction center consists of a specially bound pair of chl *a* molecules that transfers an electron to an acceptor molecule following photon excitation. This reaction concurrently generates a positively charged chlorophyll radical that, in the case of oxygenic photosynthesis, is re-stabilized via electron donation from water. The oxidation of water not only establishes the electron transport chain reactions of the chloroplast, but also contributes to an electrochemical proton gradient across the thylakoid membranes used for the synthesis of ATP.

In most oxygenic phototrophs, two photosystems work in concert to drive photosynthetic electron transport. Photosystem II (PSII) is the site of the initial charge separation reactions and the oxidation of water. PSII is contained within a multi-subunit protein complex with a core reaction center consisting of two membrane proteins known as D1 and D2 (Buchanan *et al.*, 2000). The reaction center chlorophyll of PSII absorbs maximally at 680 nm and is therefore referred to as P_{680}. As the primary electron donor, P_{680} excited by a photon (P_{680}*), transfers an electron to a pheophytin acceptor molecule that subsequently donates an electron to a bound plastoquinone acceptor molecule (Q_A).

A second plastoquinone molecule (Q_B) sequentially accepts two electrons *via* Q_A forming a fully reduced plastohydroquinone (Q_BH_2), which dissociates from the reaction center complex and enters the thylakoid membrane (Taiz and Zeiger, 2002). Electrons liberated at PSII (as Q_BH_2) are transported through the thylakoid membranes to photosystem I (PSI). Electrons liberated from water reduce oxidized P_{680} (P_{680}^+) generated during the initial charge separation event.

The oxidation of water involves a complex series of reactions that occur on the luminal side of PSII (Buchanan *et al.*, 2000). Because single electron transfers would result in the formation of highly energetic oxidizing intermediates capable of destroying the photosynthetic membrane system, a "charge-storage apparatus" exists to couple the single positive charge generated in the PSII reaction center (i.e. P_{680}^+) with the multiple positive charges required for water oxidation (Buchanan *et al.*, 2000). The only known biological system capable of carrying out such a reaction is the oxygen-evolving complex (OEC) associated with PSII (Taiz and Zeiger, 2002). Four clustered Mn atoms ligated to amino acid residues of the D1 protein are central to each OEC (Buchanan *et al.*, 2000). Electrons liberated from water are individually transferred from Mn atoms to a redox active tyrosine residue (Tyr-Z) located within the D1 subunit. The Tyr-Z radical directly transfers an electron to P_{680}^+, returning it to its sable state or can shuttle an electron to a second tyrosine residue (Tyr-D) located on the D2 protein. Tyr-D radicals are also capable of reducing P_{680}^+, but they are not considered part of the water oxidation process (Taiz and Zeiger, 2002).

The efficiency of electrons moving through PSII can be quantified using various chl *a* fluorescence parameters. Dark-adapted chloroplasts will have fully oxidized (i.e.

open) electron acceptors Q_A and Q_B at their PSII reaction centers and will therefore exhibit a minimal level of fluorescence (F_o). Maximal fluorescence (F_m) is indicative of fully reduced (i.e. closed) PSII reaction centers because the quinone acceptors are fully reduced. Photochemical fluorescence quenching, termed variable fluorescence (F_v), is calculated by the difference between F_m and F_o. The efficiency of electron transport through PSII reaction centers is expressed by the ratio of F_v/F_m and represents the maximum quantum yield of PSII photochemistry (Baker, 2008).

In a continuation of the electron transport process, Q_BH_2 generated at PSII migrates to iron-containing cytochrome b_6/f complexes (Cyt b_6/f) located within the thylakoid membrane. Cyt b_6/f harvests electrons from Q_BH_2 and passes them on to the small soluble protein plastocyanin (PC), while simultaneously pumping protons into the thylakoid lumen to increase the electrochemical gradient needed for ATP synthesis. Reduced PC then donates an electron to oxidized PSI (P_{700}^+), which following excitation by a photon, had previously donated an electron to a PSI acceptor molecule (likely a chlorophyll; Buchanan *et al.*, 2000). Successive electron transfers through a series of acceptor molecules within the PSI protein complex terminates at the stroma-associated flavoprotein ferredoxin-NADP reductase, which reduces $NADP^+$ to NADPH (Buchanan *et al.*, 2000).

Inhibition of photosynthesis

Maximum quantum efficiency (Φ_{max}) is achieved when photosynthesis rates increase linearly with increasing irradiance and is often referred to as the light-limiting region of photosynthesis (Figure 1A). Following exposure to high light intensities, the relationship

between absorbed light and photosynthesis becomes non-linear and quantum efficiency (Φ) decreases (Baker, 1996). In a protective measure to avoid physiological damage and photobleaching, high light-induced photosynthetic decline is associated with the dissipation of excess excitation energy as heat. In situations where excessive energy cannot be dissipated safely, over-excited PSII reaction centers are damaged which results in the decline of both Φ_{max} and light-saturated photosynthetic rates (Baker, 1996; Figure 1C). The inhibition of maximum photosynthesis as a result of light-induced damage to PSII is termed photoinhibition (Tyystjärvi, 2008).

The effects of decreased Φ are often temporary, and photosynthetic rates usually recover upon exposure to decreased irradiances. A temporary decline in Φ that results in decreased light-saturated photosynthesis is called dynamic photoinhibition (Osmond, 1994). Dynamic photoinhibition can occur naturally during mid-day hours when irradiance levels are at their peak. The main target of photodamage is the D1 protein of PSII, which is especially sensitive to high light and must be repaired or replaced once damaged. During dynamic photoinhibition, the repair of D1 protein occurs as fast as the damage is happening thereby preventing long term or permanent impairments to PSII. Under these circumstances, plants can function at decreased photosynthetic rates for a period of time until the irradiance levels decrease, the D1 repair mechanisms "catch up" and PSII reaction center efficiencies fully recover.

There are situations in which plants are unable to efficiently repair D1 protein damage. When repair rates cannot keep pace with the rate of PSII damage, the plant undergoes chronic photoinhibition and the net rate of photosynthesis decreases (Osmond, 1994; Tyystjärvi, 2008). Chronic photoinhibition is the consequence of failing or

overloaded protective systems that severely impact Φ and the rate of light-saturated photosynthesis.

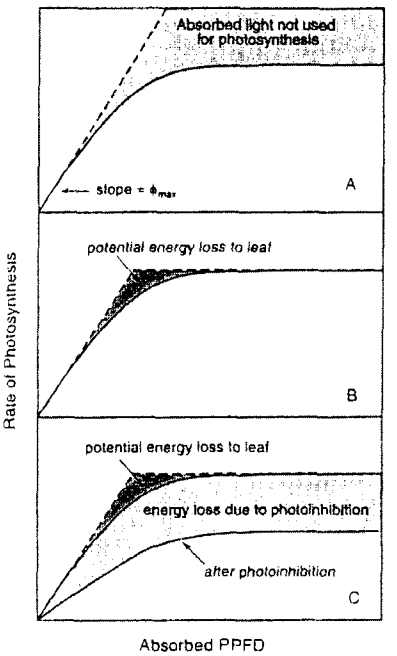

Figure 2. The rate of photosynthesis to light intensity (photosynthetic photon flux density, PPFD). A) The Φ_{max} of photosynthesis is determined from the initial slope of the response curve. The shaded area above the response curve indicates the amount of absorbed light that is not used for photosynthesis. B) The dashed line represents a theoretical response where photosynthesis operates at Φ_{max} until light saturation occurs and photosynthesis is limited by carbon fixation reactions. Shaded area represents the absorbed light energy that could potentially be used for photosynthesis, but is lost due to intrinsic characteristics and regulatory processes of the photosynthetic apparatus. C) Effect of severe photoinhibition on the light response curve. Shaded area between normal and photoinhibited curves represents the absorbed light energy lost due to photoinhibition of the system (from Baker, 1996).

Two main theories exist on how photoinhibitory damages facilitate the inhibition of PSII electron transfer and the degradation of D1 protein (1) the acceptor-side hypothesis and (2) the donor-side hypothesis (Baker, 1996). Under high light, acceptor-

side damages originate at the highly reduced plastoquinone pools connecting PSII and PSI. Depletion of available oxidized plastoquinone decreases the efficiency of Q_B molecule binding to the D1 protein and initiates the formation of a doubly reduced quinone acceptor ($Q_A \rightarrow Q_A^{-2}$) that is then protonated to form Q_AH_2, which leaves its binding site on the D1 protein (Baker, 1996). With the Q_A site unoccupied, excitation of P_{680} results in the formation of triplet state chlorophyll that reacts with oxygen to form singlet oxygen (Tyystjärvi, 2008). Singlet oxygen ($^1O_2$) is a strong oxidizing agent and therefore short-lived; rapidly reacting with molecules in its immediate vicinity including proteins, pigments and membrane lipids (Krieger-Liszkay, 2004). $^1O_2$ will also react directly with the D1 protein, triggering PSII destruction and exacerbating photoinhibition (Baker 1996; Krieger-Liszkay, 2004).

Obstruction of OEC reactions results in the inhibition of PSII electron transfer and is the basis for the donor-side hypothesis (Tyystjärvi, 2008). An obstruction in the water oxidation process leaves the highly reactive P_{680}^+ free long enough to oxidize neighboring molecules like chlorophyll, β-carotene and the D1 protein (Baker 1996). Donor-side inhibition has been demonstrated in plants in experiments that chemically remove or deactivate the OEC *in vitro* (Tyystjärvi, 2008). These data suggest that direct absorption of light by the Mn cluster plays a crucial role; specifically that UV-induced inhibition of the S-state cycle causes slowing of P_{680}^+ reduction (Tyystjärvi, 2008).

Biological effects of ultraviolet radiation

Stratospheric ozone removes all ultraviolet-C (UV-C; < 290 nm) and strongly attenuates the UV-B irradiance reaching the Earth's surface. However, in recent times,

the concentrations of anthropogenic contaminants such as chlorofluorocarbons (CFCs) within the stratosphere have shown a steady increase with a corresponding decrease in ozone (Kerr and McElroy, 1993; Greenberg *et al.*, 1997; Whitehead *et al.*, 2000). CFCs are very stable in the troposphere but following exposure to UV-C radiation, release chlorine molecules that attack and destroy ozone (Whitehead *et al.*, 2000). Because ozone is responsible for the mitigation of UV-B irradiance, a direct consequence of its degradation is the increased transmission of UV-B wavelengths into the troposphere.

As a result, the biological effects of increased UV-B radiation on primary producers like phytoplankton and higher plants have been heavily researched. UV-B radiation has been shown to cause direct damage to DNA, proteins, membranes, photosynthetic pigments and phytohormones (Greenberg *et al.*, 1997). In addition, negative responses in growth, motility and photosynthesis of phytoplankton to UV-B irradiance have also been reported (Jahnke *et al.*, 2009). Conversely, there is also the perception that increased UV-B exposure (as a result of depleted ozone) will not adversley affect the physiology of phototrophs (Nogues, 2006; Caldwell and Flint, 2006). These reports suggest that when laboratory studies carefully consider principal environmental factors (such as the UV-B: PAR ratio and/or the inclusion of UV-A radiation), the adverse signs of UV-B induced damages do not occur and/or are greatly reduced. A large part of this hypothesis arises from observations that plants acclimatize to naturally increasing UV-B irradiances by altering their morphology and/or biochemistry to protect against potential UV-B induced damage (Greenberg *et al.*, 1997). However, because these acclimation processes are triggered by UV-B specific photoreceptors, phytochrome and the UV-A/blue light receptors, the combination of UV-B, UV-A and

PAR irradiances in addition to the level of UV-B incident on the plant becomes relevant (Greenberg *et al.*, 1997).

In order to draw ecologically relevant conclusions regarding the effects of elevated UV-B radiation on biological processes, it is important that laboratory-based UV-B studies replicate naturally occurring UV-B: PAR ratios. For example, in experiments designed to highlight the sensitivity of soybean (*Glycine max* (L.) Merr.) to UV-B radiation, Caldwell *et al.* (1994) observed significant reductions in plant growth only when both PAR and UV-A radiations were reduced to levels half of that present in natural solar flux. Similarly, Deckmyn *et al.* (1994) showed that bean plants (*Phaseolus vulgaris* cv. Label) failed to exhibit significant declines in growth, photosynthesis and pigment concentrations following UV-B treatments when PAR levels similar to that of solar flux were applied concomitantly.

Another common problem in UV-B research is the application of UV-B radiation with a spectral profile dissimilar to solar flux. Since the differences between solar UV-B flux and the radiation emitted by UV-B lamps are also quantitative as well as qualitative, the use of Biological Weighting Functions (BWFs) is absolutely necessary to compare experiments. BWFs permit quantitative comparisons between exposure conditions in different experiments using non-natural spectral irradiances (Cullen *et al.*, 1992; Neale, 2000; Day and Neale, 2002). Specifically, BWFs are used to compensate for the differences between the experimental radiation conditions and solar radiation, particularly in the UV-B region. Determining which BWF to apply to a particular experimental study can be problematical. BWFs are quite variable since they are a function of specific conditions including species, environment and the physiological response measured

(Caldwell, 1986; Cullen and Neale 1997; Flint and Caldwell, 2003). In microalgal UVR research, the most frequently applied BWFs are those of Behrenfeld *et al.* (1993), Cullen *et al.* (1992), Caldwell (1971) and Jones and Kok (1966). The BWFs of Beherenfeld *et al.* (1993) and Cullen *et al.* (1992) were designed to measure the inhibition of carbon fixation in natural populations of marine phytoplankton. The method of Cullen *et al.*, (1992), is used frequently in UVR studies because it is capable of predicting the biological effects of short-term exposures to both UV-A and UV-B radiation. More recently, new weighting factors have been described for assessing the effects of UV-B radiation on photosynthetic oxygen evolution in *Dunaliella salina* (Ghetti *et al.*, 1999) and carbon fixation in *D. tertiolecta* (Andreasson and Wängberg, 2006).

In contrast to UV-B radiation, UV-A wavelengths are not altered by stratospheric ozone and consequently, research focused on elucidating its physiological effects are less common. Nonetheless, UV-A-induced photoinhibition comprises more than 50% of the photodamage occurring naturally in macroalgae and phytoplankton (Bühlmann *et al.*, 1987; Helbling *et al.*, 1992; Holm-Hansen *et al.*, 1993; Kim and Watanabe, 1993; Herrmann *et al.*, 1995; Dring *et al.*, 1996; West *et al.*, 1999) including *Dunaliella* (Herrmann *et al.*, 1997). In a laboratory study, Jahnke (1995) demonstrated that UV-A exposure reduced initial growth rates in *Dunaliella parva* by 80% and decreased photosynthetic efficiencies by 50%. In a similar study, White and Jahnke (2002) treated *Dunaliella* cultures with either UV-A or UV-B radiation and concluded that UV-A (and not UV-B) was the primary inhibitor of photosynthesis and photosynthetic efficiency.

Production and scavenging of ROS

A free radical is defined as any chemical species capable of independent existence with one or more unpaired electrons (Halliwell and Gutteridge, 1999). Although molecular oxygen ($^3O_2$) in the ground state is technically a radical (with two unpaired electrons of parallel spin occupying different molecular orbitals), it is not particularly reactive and will not oxidize cellular components without the aid of enzymes. This is largely because most organic molecules have pairs of electrons with opposite spins and $^3O_2$ cannot accept a complete pair of electrons, but must receive electrons individually (Asada and Takahashi, 1987; Apel and Hirt, 2004). As a result, $^3O_2$ will openly react with other free radicals and is easily reduced into several highly reactive oxygen species (ROS) including superoxide ($O\cdot^-_2$).

A majority of the $O\cdot^-_2$ generated within plant cells comes from the electron transport chains of photosynthesis and respiration, which leak approximately 1- 4% of their electrons to molecular oxygen to form $O\cdot^-_2$ (Apel and Hirt, 2004; Wolfe-Simon *et al.*, 2005). While $O\cdot^-_2$ itself has been shown to damage membranes, degrade DNA and inactivate enzymes, the most dangerous consequence of $O\cdot^-_2$ production is its dismutation into hydrogen peroxide (H_2O_2) and ultimately hydroxyl radicals ($HO\cdot$) *via* Haber-Weiss reaction: $H_2O_2 + O\cdot^-_2 \rightarrow O_2 + OH^- + OH\cdot$ (Halliwell and Gutteridge, 1999).

With the exception of $^1O_2$ all ROS species are derived from superoxide and peroxides. Because all superoxide is defensively converted into peroxides, peroxides themselves are at the center of ROS cellular damages (Figure 2). In both algae and higher plants, three major defense systems have evolved to protect against superoxide radicals

and the subsequent formation of H_2O_2: the superoxide dismutases (SODs), peroxidases and catalases (Asada, 1999).

SOD (EC 1.15.1.1) family of enzymes is responsible for catalyzing the disproportionation of $O^{\cdot -}_2$ to molecular oxygen and H_2O_2. Different metalloproteins of SOD have iron (Fe), manganese (Mn) or copper/zinc (Cu/Zn) cofactors and function in different compartments of the cell. The most primitive form of SOD is the Fe isoform, as it evolved during an era in which soluble iron [Fe (II)] was in abundance. In algae, FeSODs are located within the chloroplast and cytosol and are homodimers or tetramers with 14-30 kDa subunits (Alscher *et al.*, 2002; Wolfe-Simon *et al.*, 2005). Following the oxygenation of the Earth's atmosphere, mineral components were oxidized and the amount of soluble Fe (II) decreased causing a shift in the SOD metal cofactor to a more available metal, Mn (II) (Alscher *et al.*, 2002). The Mn and Fe isoforms share ~50% similarities in amino acid sequence homology and are speculated to have evolved from a gene duplication event in a common ancestor (Wolfe-Simon *et al.*, 2005). Unicellular green algae like *Dunaliella* possess the Fe and Mn isoforms in the chloroplast/cytoplasm and mitochondria/ peroxisomes, respectively (Wolfe-Simon *et al.*, 2005).

The Cu/Zn isoform of SOD is structurally different from the Fe and Mn forms and is thought to have evolved separately (Alscher *et al.*, 2002; Wolfe-Simon, *et al.*, 2005). The Cu/Zn SODs are homodimeric or homotetrameric with 150-160 amino acids subunits and are present within the chloroplasts and cytosol of higher plants, but are lacking in some unicellular green algae like *Dunaliella*. In the chloroplast, Cu/ZnSOD exists as both a free stromal and thylakoid bound form eliminating $O^{\cdot -}_2$ produced by the univalent

photoreduction of dioxygen in PSI (i.e. Mehler reaction; Figure 2; Miyake and Asada, 1992; Alscher *et al.*, 2002).

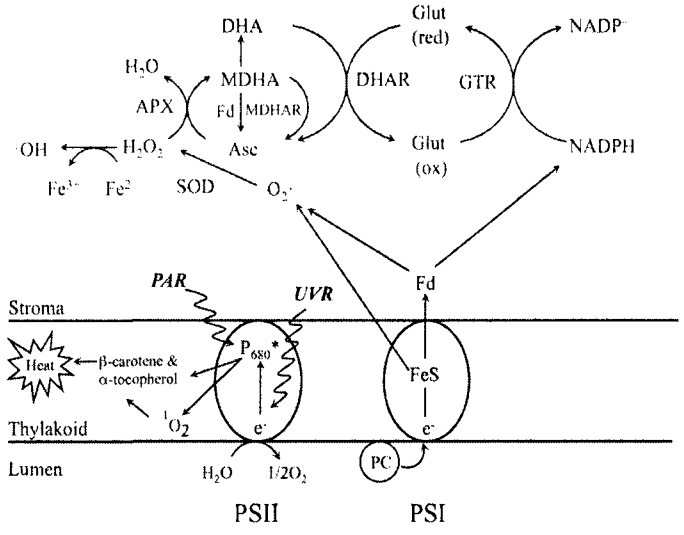

Figure 3. Generation and scavenging of ROS within the chloroplast. Ascorbate (Asc); ascorbate peroxidase (APX); dehydroascorbate (DHA); dehydroascorbate reductase (DHAR); iron-sulfur center (FeS); ferredoxin (Fd); glutathione (Glut); glutathione reductase (GTR); hydrogen peroxide (H_2O_2); monodehydroascorbate (MDHA); monodehydroascorbate reductase (MDHAR); singlet excited oxygen ($^1O_2$); superoxide ($O_2^{\cdot-}$); hydroxyl radical ($\cdot OH$); reaction center chlorophyll in PSII (P_{680}); photosynthetically active radiation (PAR); plastocyanin (PC); superoxide dismutase (SOD); UV radiation 280-400nm (UVR). Adapted from Jahnke *et al.* (2009).

Ascorbate peroxidase (APX; EC 1.11.1.11) is a homodimeric, heme-containing enzyme that utilizes ascorbate as its specific electron donor to reduce H_2O_2 to H_2O with the concurrent generation of monodehydroascorbate (MDA), a univalent oxidant of ascorbate (Shigeoka *et al.*, 2002). MDA is reduced back to ascorbate either by the NAD(P)H-dependent enzyme monodehydroascorbate reductase (MDHAR; Figure 2) or by reduced ferredoxin (Asada, 2006). The functionality of APX is highly dependent on

the availability of reduced ascorbate acid and therefore the recycling of ascorbate between its oxidized and reduced states is essential for APX operation. During this catalytic cycle, APX initially reacts with H_2O_2 and is converted into the two electron oxidized intermediate, Compound I; in which the heme moiety is oxidized to the oxyferryl ($Fe^{VI} = O$) species and an organic group (R) is oxidized to a free radical (R•; Figure 3). Compound I is subsequently reduced back to the resting ferric (Fe^{III}) state by two successive one-electron reactions with ascorbate, generating two molecules of the one-electron oxidized product of ascorbate MDA in the process (Miyake and Asada, 1996; Dabrowska *et al.*, 2007).

(1) APX (Fe^{III})R + H_2O_2 → APX ($Fe^{IV} = O$)R• + H_2O
Compound I

(2) APX ($Fe^{IV} = O$)R• + AsA → APX ($Fe^{IV} = O$)R + MDA
Compound II

(3) APX ($Fe^{IV} = O$)R + AsA → APX (Fe^{III})R + H_2O+ MDA

Figure 4. Catalytic cycle of ascorbate peroxidase. Ascorbate peroxidase (APX) converts hydrogen peroxide (H_2O_2) into two molecules of water using ascorbate (AsA) as an electron donor. Two molecules of monodehydroascorbate (MDA) are concomitantly generated. Compound I and II denote APX forms with different oxidation levels.

Unlike many peroxidase enzymes, which are also present within animal cells, APX is unique to plants and algae and functions in conjunction with the glutathione reductase (GTR; EC 1.8.1.7) enzyme pathway that is responsible for replenishing the reduced ascorbate pool (Figure 2; Shigeoka *et al.*, 2002). The rapid removal of H_2O_2 from the

chloroplast is of particular importance to a plant cell, as the failure to do so will lead to the formation of $OH^{\cdot}$ by the Haber-Weiss or Fenton reactions (Figure 2).

A great deal of attention has been focused on elucidating the properties of APX isoenzymes, which have been identified within many higher plants including *Spinacia*, *Oryza* and *Arabidopsis* (Yoshimura *et al.*, 1998; Shigeoka *et al.*, 2002; Mittler and Poulos, 2005; Teixeira *et al.*, 2006). APX isoenzymes have been detected in almost all cellular compartments, most notably the cytosol, the chloroplast (stromal and thylakoid bound forms), the microbody (glyoxysome and peroxisome), and the mitochondria (Leonardis *et al.*, 2000; Yoshimura *et al.*, 2000). All APX isoenzymes have demonstrated specificity for ascorbate as the electron donor, however some isoforms harbor heightened sensitivities to ascorbate depletion (i.e. chloroplast APXs) compared to others (cytosolic APXs; Yoshimura *et al.*, 1998). Interestingly, only one APX isoenzyme (chloroplast isoform) has been isolated and molecularly characterized from unicellular organisms like *Chlorella* (Takeda, *et al.*, 1998), *Chlamydomonas* (Takeda *et al.*, 2000) and *Euglena* (Ishikawa *et al.*, 1996). It has been proposed that the absence of additional APX isoforms within unicellular phototrophs is attributable to the heightened presence of alternative H_2O_2 scavenging enzymes such as glutathione peroxidase (GPX; EC 1.11.1.9) and catalase which provide similar/analogous protection against reactive oxygen, particularly H_2O_2 (Shigeoka *et al.*, 2002).

Catalase (EC 1.11.1.6) differs from peroxidases in that it dismutates H_2O_2 to H_2O [$2H_2O_2 \rightarrow O_2 + 2H_2O$], whereas peroxidases convert H_2O_2 into H_2O with the help of a reducing substrate (e.g. ascorbate). Catalases are tetrameric, heme-containing enzymes with a molecular mass between 220-270 kDa. They are present within all aerobic

organisms, but within higher plants, catalases localized within the microbody (peroxisome or glyoxysome), are responsible for degrading the H_2O_2 generated during photorespiration and the β-oxidation of fatty acids.

Three distinct catalase isoenzymes have been identified in maize (CAT-1, CAT-2 and CAT-3; Redinbaugh, *et al.*, 1990), tobacco (Willekens *et al.*, 1994) and *Arabadopsis* (Frugoli *et al.*, 1996). The CAT-3 isoform is structurally and biochemically unique compared to its counterparts. It is cyanide insensitive, possesses enhanced peroxidase activity and is localized within the mitochondrion (Scandalios, 1994). In their 1997 study, Kato *et al.* showed that catalase in the green alga *Chlamydomonas reinhardtii* was localized within the mitochondria. This association is note worthy because unlike higher plants, the photorespiratory process of *Dunaliella* does not involve the peroxisome-localized generation of H_2O_2 by glycolate oxidase. Instead, unicellular green algae utilize mitochondrial glycolate dehydrogenase (GD) during photorespiration, which does not result in the production of H_2O_2 (Frederick *et al.*, 1973). The GD photorespiratory pathway was originally thought to be exclusive of unicellular green algae like *Dunaliella*, *Chlorella* and *Chlamydomonas*, however recent identification of mitochondrial GD enzymes within *Arabadopsis* have prompted suggestions that the GD pathway may also be conserved within higher plants (Bari *et al.*, 2004). Such findings imply that the role of catalase within all plant cells may be more diverse than previously suspected. For example, changes in catalase regulation have been found to coincide with metabolic processes such as embryogenesis, germination, circadian regulation, pathogen attack and oxidative stress response (Scandalios, 1994; McClung, 1997; Scandalios *et al.*, 1997).

Therefore, it is likely that catalase in *Dunaliella* is involved with other metabolic processes in addition its role as an antioxidative H_2O_2 scavenger.

Photoinactivation of catalase has been thoroughly researched because of the enzymes extreme sensitivity to blue light. Catalase is photoinactivated directly following light absorption by the heme moiety (Feierabend and Engel, 1986) and indirectly through chloroplast-mediated ROS production (Shang and Feierabend, 1999). Catalase's sensitivity to moderate levels of light (~ 70- 400 μmol photons m^{-2} s^{-1}; Feierabend and Engel, 1986; Shang and Feierabend, 1999) is compensated for in "healthy" plants by continual *de novo* synthesis of new protein to maintain constant functional steady state levels. Therefore, any declines in catalase activity and/or contents are considered an early indication that a plant is experiencing some form of oxidative stress.

Dunaliella as a model organism

Compared to higher plants, microalgae have considerably greater phenotypic plasticity, which allows them to acclimate to wide variations in environmental conditions including irradiance, nutrient supply and temperature. Among the various algal groups, the Chlorophytes are the most similar to higher plants, possessing a double membrane enclosed chloroplast, thylakoids grouped into grana, chlorophyll *a*/*b*, accessory pigments (carotenoids), chloroplastic pyrenoids and starch as their primary reserve polysaccharide (van den Hoek *et al.*, 1978).

The genus *Dunaliella* (Volvocales, Chlorophyta) consists of some larger species (~12-16 μm x 6-9 μm) like *D. salina* and *D. bardawil* plus smaller species (~12 x 8 μm) such as *D. tertiolecta*, *D. parva* and *D. viridis* (Chen and Jiang, 2009). In addition to

their higher plant-like biochemistry, *Dunaliella* also possess several unique characteristics that distinguish them from other commonly studied green algae genera. Growing predominantly within hypersaline waters, *Dunaliella* regulates its halotolerance using glycerol as an osmoticum (Goyal, 2007). When exposed to hypersaline conditions, *Dunaliella* respond by accumulating intracellular levels of glycerol that can reach concentrations as high as 8M; or 55% of the cell weight under saturating NaCl (5.5M NaCl; Chen and Jiang, 2009). Glycerol is a particularly desirable compatible solute for a variety of reasons as it: 1) is chemically inert and non-toxic 2) is an end-product metabolite and will not offset major metabolic pathways 3) requires a low amount of energy to synthesize and 4) does not depend on the availability of nitrogen (Chen and Jiang, 2009). The resources utilized to sustain such massive quantities of intracellular glycerol come from products generated during light-dependent photosynthesis and from the breakdown of stored starch molecules (Goyal, 2007). While some *Dunaliella* species like *D. tertiolecta* will thrive under NaCl concentrations typical of most marine environments (0.5M NaCl), other species (i.e. *D. salina*) are able to withstand NaCl concentrations as high as 5.5M without accumulating high amounts of intracellular sodium (Chen and Jiang, 2009).

A second distinguishing feature of some *Dunaliella* species (e.g. *D. salina* and *D. bardawil*) is the ability to accumulate large amounts of inter-thylakoidal β-carotene (Jahnke, 1999; Raja *et al.*, 2007; Jahnke *et al.*, 2009). It is hypothesized that large quantities of this particular pigment allow *Dunaliella* to shield themselves from ROS damages arising from excessive irradiance, quench triplet-state chlorophyll and block more harmful wavebands from reaching sensitive photosynthetic machinery (Raja *et al.*,

2007; Jahnke *et al.*, 2009). This theory seems particularly probable since β-carotene molecules absorb the strongest in the blue to UV-range of the spectrum. Indeed, research has shown that globules of β-carotene within *D. bardawil* effectively screen blue light, offer significant protection against PAR induced photoinhibition (Ben-Amotz *et al.*, 1989) and are correlated with reduced UV damage to photosynthesis (White and Jahnke, 2002; Jahnke *et al.*, 2009). Although much research has linked β-carotene accumulation with high PAR and UV exposure, a variety of other environmental stresses also trigger β-carotene buildup, including salinity and temperature extremes as well as deficiencies in either sulfate or nitrate (Jahnke *et al.*, 2009).

Finally, although *Dunaliella* species are highly attractive for the commercial production of both glycerol and the protective pigment β-carotene, the absence of a rigid polysaccharide cell wall makes this genus particularly suitable for commercial and physiological research purposes. In particular, research focused on elucidating the biochemistry of plant metabolic processes benefit from the fast growth rates and easily accessible cellular contents characteristic of this genus.

CHAPTER I

SIGNIFICANCE OF EXCESSIVE SHORT-WAVELENGTH UV-B RADIATION AND IMBALANCED UV-B: PAR RATIOS ON PHOTOSYNTHESIS AND OXIDATIVE STRESS IN THE GREEN ALGA *DUNALIELLA TERTIOLECTA*.

ABSTRACT

Recognition of the Antarctic ozone hole has prompted considerable research aimed at elucidating the effects of increased ultraviolet-B (UV-B) radiation on primary producers such as phytoplankton and higher plants. A fundamental design limitation in laboratory UV-B experiments results from the spectral composition of radiation emitted by UV-B lamps, which does not accurately mimic solar radiation. The most commonly used lamps generate shorter wavelengths not present in ground level solar flux (i.e. ultraviolet-C [UV-C]), contain excessive short wavelength UV-B and also emit a substantial amount of ultraviolet-A (UV-A) radiation. A second concern is that UV-B is commonly applied concomitantly with photosynthetically active radiation (PAR) in ratios not comparable to solar flux (i.e. 1:100). In past research (Jahnke and Sampath-Wiley, 2009), liquid urate (UA) filters containing an aqueous solution of uric acid have provided a more realistic mimic or solar UV-B radiation than conventionally used cellulose acetate (CA) in removing UV-C and short wave UV-B radiation from UV-B lamp emissions. In the current study, comparisons between CA and UA suggest that seemingly small differences in the shortwave length UV-B spectrum result in significantly different physiological

responses. *Dunaliella tertiolecta* cells growing under 100, 200 and 600 μmol photons m^{-2} s^{-1} PAR were exposed for 12 hours to 6 μmol photons m^{-2} s^{-1} *unweighted* UV-B radiation filtered by either CA or UA. In almost all cases, the physiology of UA cultures remained comparable to that of controls receiving no UV-B, while CA cultures growing at 100 μmol photons m^{-2} s^{-1} PAR suffered significant declines in light-saturated photosynthesis ($P_{LS;}$ 58%↓), variable to maximal fluorescence (F_v/F_m; 50%↓) and D1 protein contents (57%↓). Conversely, the activities of the antioxidant enzymes ascorbate peroxidase (APX) and superoxide dismutase (SOD) increased 167% and 77%, respectively. Furthermore, UV-B induced photoinhibition was alleviated in cultures exposed to high PAR, highlighting the relevance of photoreactivation processes. Lastly, removal of UV-A radiation from UV-B lamp emissions did not result in UV-B induced stress, implying that the protective nature of UA filtration stems from the removal of excessive short-wavelength UV-B, not from increased transmission of UV-A radiation and/or heightened photoreactivation repairs.

INTRODUCTION

Energy from the sun covers the whole electromagnetic spectrum, from short gamma rays to long radio waves. Stratospheric ozone removes all ultraviolet-C (UV-C) and strongly attenuates the solar irradiance of ultraviolet-B (UV-B) by several orders of magnitude within a very narrow range of wavelengths. Solar radiation between 290-700nm reaches the earth's surface yielding an approximate 1:10:100 ratio of UV-B (280-320nm) to ultraviolet-A (UV-A; 320-400nm) to visible light (Photosynthetically Active

Radiation (PAR); 400-700nm; Greenberg, *et al.*, 1997). Absorption of UV-B by O_3 is the phenomenon that protects the earth against much greater UV-B radiation exposures. Therefore, depletion of the ozone layer will principally lead to an increase in only UV-B radiation (Kerr and McElroy, 1993; Greenberg *et al.*, 1997).

The escalating trend of UV-B radiation transmittance into our biosphere has raised many questions regarding the effects of short wave radiation on photosynthesis. Research has shown that photosynthetic organisms are experiencing considerable UV-B stress at current solar flux levels (Cullen and Lesser, 1991; Smith *et al.*, 1992; Häder *et al.*, 2003; Day and Neale, 2002). Investigations into the effects of increased UV-B typically involve ultraviolet radiation (UVR) and PAR blended from various combinations of lamps and filters with or without sunlight. In experiments designed to yield ecologically useful results, two major difficulties arise with respect to the UV-B radiation environment: (1) the wavelength distribution (i.e. spectral profile) of UV-B radiation emitted by lamps is different, especially at shorter wavelengths and (2) a ratio imbalance of UV-B: PAR flux densities exists; usually with low PAR. The effects of these variables should be evaluated separately. Yet, even in outdoor studies when natural sunlight is supplemented with artificial UV-B radiation, the initial problem of wavelength distribution remains.

The fundamental limitation in UV-B experimental design is caused by the spectral composition of radiation emitted by the UV-B lamps. Supplemental UV-B lamps emit shorter wavelengths that are not present in natural solar flux reaching ground level (i.e. UV-C) and emit excessive short wavelength UV-B compared to solar flux (Caldwell *et al.*, 1983). The Q-Panel 313, the National Biological Corporation FS40/UV and the

Phillips TL12 are widely used UV-B lamps. They have nearly identical emission spectra (with a peak at 313nm) and significant emission into the UV-C. This emission is typically altered with either cellulose acetate (CA) plastic or glass filters to remove UV-C and a portion of the excess short wavelength UV-B. In either case, the resultant emission in the UV-B region remains quite different from the solar spectrum (Caldwell *et al.*, 1983; Adams and Britz, 1992; Döhring *et al.*, 1996; Johanson and Zeuthen, 1998; Holmes, 2002). This is of particular concern since even small deviations from solar UV-B can produce major effects.

Although a spectral composition that more closely resembles natural flux can be achieved by using Q- panel 340 lamps, their output in the UV-B represents only 12% of the total emission (< 6 μmol photons $m^{-2}s^{-1}$; < 2.4 Wm^{-2}). This makes it difficult to simulate conditions of increasing UV-B radiation or recreate UV-B conditions utilized in previous studies. Following Bowen (1932, 1946), a liquid urate anion solution (UA) filter was developed that has proven effective at removing UV-C and the excessive short-wave UV-B radiation emitted by fluorescent UV-B lamps (Jahnke and Sampath-Wiley, 2009). The urate anion produces a sharp transmission cutoff in the middle of the UV-B range and is varied by adjusting the concentration of urate (Figure 1.1).

Fluorescent UV-B lamps with peak emission at 313 nm emit UV-C and a spectral profile in the UV-B range that deviates critically from the ground level solar spectrum (Figure 1.2). The widespread use of plastic (i.e. CA) removes UV-C, but yields UV-B radiation that remains dissimilar to solar (Figure 1.2). A 0.26 mM UA filter was shown to remove much of the excess radiation < 320 nm rendering the UV-B spectrum nearly identical to that of sunlight (Figure 1.2; Jahnke and Sampath-Wiley, 2009).

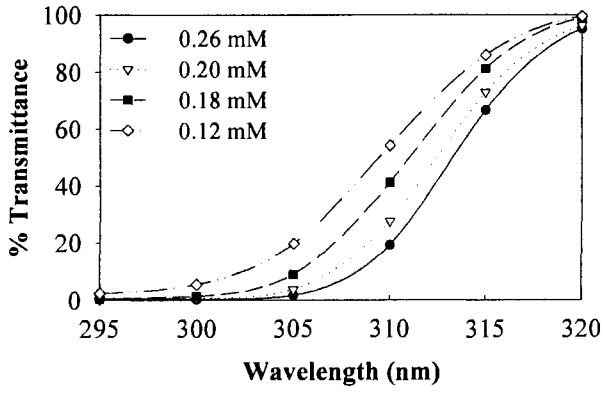

Figure 1.1 Transmittance spectra of liquid urate solutions. Concentrations of urate were 0.26mM (closed circles), 0.20mM (open circles), 0.18 mM (open triangles) and 0.12mM (closed triangles). Each filter solution contained 15mM Na azide as a quencher to prevent photo-oxidation. Measured spectrophotometrically using a Shimadzu UV-160 spectrophotometer with a 1 cm path length. Adapted from Jahnke and Sampath-Wiley (2009).

The complex interactions between UV-B and longer wavelength radiation (PAR: 400-700nm) are of additional interest. These interactions are inadequately understood and involve quantitative parameters such as inhibition of photosynthesis, DNA repair and alterations in enzyme activities (Krizek, 2004). Consequently, many studies may report exaggerated effects because unrealistic levels of UV-B radiation are applied and/or synergistic effects between UV-B and PAR are ignored (Krizek, 2004). Generally, when photosynthetic organisms are exposed to supplemental UV-B with low levels of UV-A and PAR there is an observable inhibition of photosynthesis, alteration in pigment ratios and a reduction in biomass. However, manipulating the Photosynthetic Photon Flux Density (PPFD; 400-700 nm) and UV-A irradiance levels has proven to be effective at preventing some UV-B induced damage (Caldwell *et al.*, 1994; Shelly *et al.*, 2003; Krizek, 2004). UV-B induced declines in photosynthetic pigment content, F_v/F_m and

oxygen evolution are minimized if UV-A radiation is applied *in tandem* (Joshi *et al.*, 2007) and/or if the PPFD level is sufficient to drive the synthesis of ATP needed for UV-B recovery processes (Shelly *et al.*, 2003). Caldwell *et al.* (1994) reported that amelioration of UV-B induced damage by UV-A wavebands was most prevalent when PPFD was low. Interestingly, at higher PPFDs, PAR wavebands contributed the greatest to recovery processes, while UV-A radiation failed to provide further substantial benefit (Caldwell *et al.*, 1994).

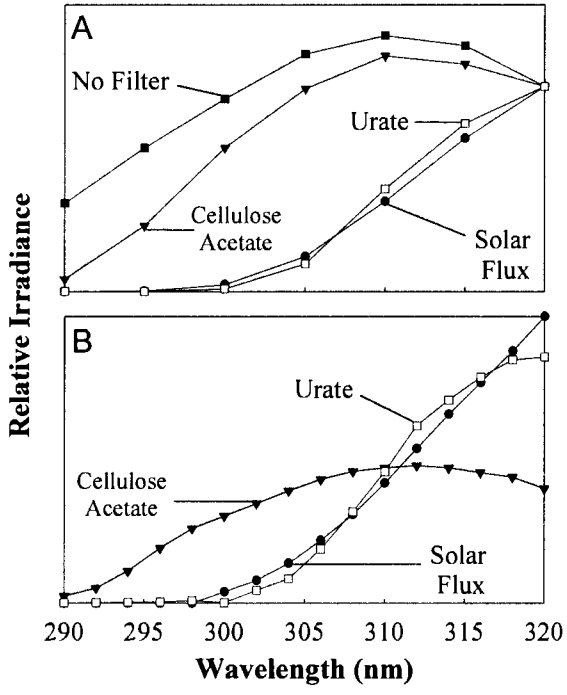

Figure 1.2. Irradiance spectra of UV-B solar flux compared with UV-B radiation emitted by National Biological Corporation FS40/UV lamps. A) Lamp emissions were unfiltered (diamonds) or filtered by solarized cellulose acetate (closed triangles) or 0.26mM liquid urate solution (open triangles) and normalized to 320 nm B) Comparisons between solar radiation (closed circles) and lamp emissions filtered by cellulose acetate or 0.26 mM urate solution at *identical total UV-B flux densities*. Solar flux data taken from Gerstl *et al.* (1986). Relative irradiance measurements were recorded using a spectroradiometer fiber optics probe placed within culture tubes *in situ*. Adapted from Jahnke and Sampath-Wiley (2009).

Of further concern are that approximately one-half of emissions from UV-B lamps are in the UV-A region (Jahnke and Sampath-Wiley, 2009; Figure 1.3). Neither CA nor UA filters are able to remove the UV-A "contamination". Even though this amount of UV-A radiation is far less than that present in solar flux, its presence makes it more difficult to clearly separate UV-B *vs.* UV-A induced effects. Therefore, to focus on the specific effects of UV-B, it was necessary to limit the UV-A portion of lamp emissions without changing the UV-B radiation exposure. UV-B lamps used in combination with a potassium chromate (K_2CrO_4) solution have previously been effective at removing UV-A from UV lamp emissions (White and Jahnke, 2004). The chromate anion strongly absorbs both UV-A and UV-C, but not UV-B (White and Jahnke, 2004).

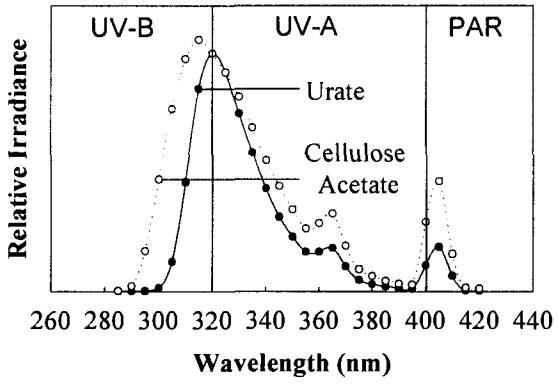

Figure 1.3. Relative Irradiance of National Biological Corporation FS40/UV lamps. Lamp emissions were filtered by either cellulose acetate (open circles) or 0.26mM liquid urate anion solution (closed circles) and normalized at 320 nm. Relative irradiance measurements were taken using a spectroradiometer fiber optics probe placed within culture tubes *in situ* as described in Materials and Methods.

Although much research has focused on the effects of increased UV-B radiation on growth and photosynthesis, UV-B is also known to induce oxidative stress in plants. UV-B radiation is responsible for directly facilitating the production of reactive oxygen species (ROS) including superoxide radicals ($O^{\cdot -}_2$), hydroxyl radicals ($\cdot OH$) and hydrogen peroxide (H_2O_2; Malanga and Putarulo, 1995; Halliwell and Gutteridge, 1999; Mackerness *et al.*, 1999; Langebartels *et al.*, 2002). Antioxidant enzyme and substrate responses, that scavenge and purge ROS before they react with surrounding molecules, are triggered by elevated levels of ROS at both the gene and protein levels to coordinate the most effective response(s) and avoid excessive oxidative damage (Asada and Takahashi, 1987; Estevez *et al.*, 2001).

To achieve an accurate and realistic understanding of the effects of decreased stratospheric ozone, experimental conditions that mimic solar UV-B are needed. Thus, the goals of this project were to (1) Compare/contrast conventional UV-B radiation filtration methods (i.e. CA) against the novel UA filter whilst examining the effect of the UV-B: PAR ratio and (2) determine whether the UV-A radiation emitted from UV-B lamps contributes to ascribed UV-B physiological effects. Specifically, this research sought to evaluate the divergences of UV-B radiation from solar flux and observe its effects on photosynthesis and oxidative stress responses in *Dunaliella tertiolecta* (Chlorophyta), a marine phytoplankton species.

MATERIALS AND METHODS

Culture and radiation procedures

Dunaliella tertiolecta (Chlorophyta) was chosen for this study as a model organism because it is easily grown/maintained and possesses comparable photosynthetic chemistry and ROS defenses to that of higher plants (Jahnke *et al.*, 2009). Cultures were grown in medium TK containing 0.5M NaCl as per Jahnke and White (2003). Air was bubbled through the cultures at a rate of approximately 150-200 ml min^{-1} for a 150 ml culture. Cultures were grown in 38 x 300 mm Pyrex tubes maintained at 24°C in a water bath constructed of UV-transmitting plastic (Acrylite OP-4; Cadillac Plastics, Manchester, NH) as per the methods of White and Jahnke (2004). All experiments were conducted using cell suspensions within 28 x 200 mm quartz tubes. PPFD was provided by two cool-white fluorescent lamps on one side of the water bath producing irradiances in the range of 50-100 μmol photons m^{-2} s^{-1}. Following the addition of two high-output fluorescent lamps, 200□μmol photons m^{-2} s^{-1} PAR was achieved. PPFD intensities above 200□μmol photons m^{-2} s^{-1} were generated using a bank of eight 42W compact fluorescent white light bulbs (Commercial Electric). All experiments began using cultures acclimated to experimental PAR treatment levels (100, 200 or 600 μmol photons m^{-2} s^{-1}; 100, 200 or 600 PAR) without UVR exposure and a chlorophyll density between 1.5-2.0 mg chl ml^{-1}. Because fluorescent lamps are known to emit a small flux of UVR, a layer of UV blocking plastic film that absorbs all radiation below 395nm (Edmund Scientific, Barrington, NJ type T39-426) was placed between the water bath and the fluorescent light bank to remove any extraneous UVR.

UV-B radiation was supplied by National Biological Corporation FS40/UV lamps placed on the side of the water bath opposite the cool-white lamps so that manipulation could occur independently of PAR. UV-B flux densities were altered by changing the distance of the lamp to the culture and/or by inserting stainless steel neutral density screens between the UV lamp and the culture tube. To promote comparisons of artificial UV-B radiation with ground level solar radiation, pre-solarized ($\geq$ 24 hours) cellulose acetate (CA) film was compared against urate solution liquid filters. Liquid urate (UA) filters with 0.95 cm depth containing a 0.26 mM aqueous solution of uric acid (pH 7.5) were used to remove UV-C and short-wave UV-B radiation from UV-B lamps. The urate can be photo-oxidized by UVR exposure over a period of hours, thus 15 mM sodium azide was added to the UA solution to avoid urate photooxidation. With azide, the UV-B absorption spectrum of the urate anion was unchanged and the urate remained photochemically stable for up to 92 hours of UVR exposure (Jahnke, unpublished). To further minimize photooxidation of the urate solution, a sheet of pyrex glass (3 mm) was placed between the UV-B lamps and the water bath.

The K_2CrO_4 filters were made with UVR transmitting plastic (Acrylite OP-4), which had an internal thickness (depth) of 0.55 cm and were filled with an aqueous 1.0 mM K_2CrO_4 solution (pH 8.0) as per White and Jahnke (2004). A majority of UV-A was removed from lamp emissions facilitating an inquiry into the effect of the UV-B: PAR ratio and more specifically, the direct effect of UV-B on physiological parameters. During experiments requiring the use of both UA and K_2CrO_4 filters (K_2CrO_4 + UA), one filter was placed in line so that the UV-B radiation passed through both filters prior to reaching the cell cultures (Figure 1.4). The order of filter placement with respect to the

UVR lamps did not make a difference in the spectral profile achieved (Sampath-Wiley, unpublished). Experiments comparing UA *vs.* UA + K_2CrO_4 were performed at 600 μmol photons m^{-2} s^{-1} PAR using 12 hour exposures to 6 μmol photons m^{-2} s^{-1} (2.4 Wm^{-2}) UV-B radiation (see Appendix A for flux density and cumulative dose values).

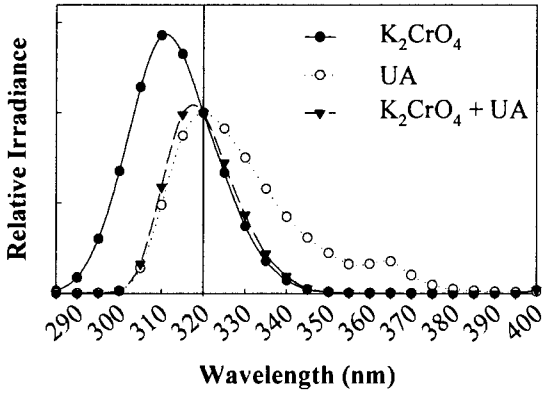

Figure 1.4. Relative irradiance transmission of chromate and 0.26mM urate solutions. UV-B radiation was supplied by two National Biological Corporation lamps filtered through a liquid K_2CrO_4 solution (closed circles), a 0.26 mM urate solution (open circles) or both K_2CrO_4 and urate liquid solutions (closed triangles) as described in Materials and Methods. Radiation was measured with a spectroradiometer fiber optics probe placed within culture tubes *in situ*. Wavelengths were normalized at 320 nm for comparison.

The total UVR irradiance flux incident on experimental cells was determined *in situ* using the potassium ferrioxalate chemical actinometer of Hatchard and Parker (1956), which counts photons in the UV and far-blue radiation regions. The actinometer fluid was placed within the culture tubes *in situ* to reproduce the UVR exposure geometry of the cultures. The actinometer measurements of total radiation intercepted were partitioned into UV-B, UV-A and blue wavebands for each lamp based on previously described

fractional distributions (Jahnke and Sampath-Wiley, 2009; White and Jahnke, 2004). The spectral distribution of the UVR was determined using a spectroradiometer (International Light model 1700/760D/783, Newburyport, MA) with a 2 nm band pass and a fiber-optics probe calibrated by International Light. Cultures not receiving UV-B radiation (i.e. controls) were established using UV-blocking film (Edmund Scientific). The PPFD was determined using a Li-Cor LI-185 D quantum radiometer.

UV-B irradiance range and time course experiments

Preliminary inquiries into the influence of UV-B on *D. tertiolecta* physiology were performed prior to starting the primary UV-B radiation experiments. The purpose was to establish an UV-B irradiance and exposure duration that generated significant physiological stress, without causing lethal photobleaching. This UV-B treatment would then be used for all subsequent physiological studies. F_v/F_m values and ascorbate peroxidase (APX) enzyme activities were selected as parameters that responded to the preliminary UV-B treatments. Two sets of preliminary experiments were performed: 1) UV-B irradiance experiments and 2) UV-B time course experiments. For the UV-B irradiance experiments, *D. tertiolecta* cultures endured 24-hour exposures to a variety of UV-B irradiance levels (0-14 μmol photons m^{-2} s^{-1} [0- 4 Wm^{-2}]). All UV-B radiation in these initial studies was filtered by pre-solarized CA and applied in combination with a constant PPFD of 200 μmol photons m^{-2} s^{-1} PAR. Time course experiments were performed using a constant UV-B radiation level of 6 μmol photons m^{-2} s^{-1} (2.4 Wm^{-2}; Appendix A) filtered by CA or 0.26 mM UA for a maximum of 24 hours. Three replicate experiments were conducted under 100, 200 and 600 μmol photons m^{-2} s^{-1} PAR; which

yielded UV-B: PAR ratios of 1:17, 1: 33 and 1:100, respectively. An UV-B radiation level of 6 μmol photons m^{-2} s^{-1} (2.4 Wm^{-2}) was selected for time course experiments based on results obtained from the UV-B range study. It was not evident whether an exposure time of 24 hours produced the peak physiological response, thus *D. tertiolecta* samples were collected for analysis at three-hour intervals for the first 12 hours of UV-B exposure and then again following 24 hours exposure. All experiments started with cultures that had received no UV radiation and were acclimated to experimental PPFD.

Photosynthesis rates, pigments and active fluorescence

Polarographic measurement of light-saturated (500 μmol m^{-2} s^{-1} PAR; P_{LS}) and light-limited (100 μmol m^{-2} s^{-1} PAR; P_{LL}) photosynthetic rates were measured at 25°C using Rank Brothers Clark-type oxygen electrodes as described by Delieu and Walker (1972). Rates were calculated on a per mg chlorophyll basis and on a per mg protein basis. Photosynthetic efficiency as determined by the ratio of variable to maximal fluorescence (F_v/F_m) was measured at room temperature with an Opti-Science OS500 modulated fluorometer (Tyngsboro, MA). Samples were equilibrated in darkness for 10 minutes (to allow for complete oxidation of photosystem II (PSII) quinone acceptors) before F_v/F_m measurements were performed. Chlorophyll and carotenoid contents were assessed from sample extracts using the equations of Lichtenthaler (1987).

Antioxidant enzyme activities

Extracts for enzyme and total protein analysis were prepared by centrifuging 10 mL of cells and re-suspending the pellet in 0.5M hypoosmotic glycerol, 50mM phosphate buffer

(pH 7.0). A second centrifugation of the cell suspension was immediately followed by ultrasonication of the pellet in buffer A (0.5 μmol ascorbate, 0.5M sorbitol and 50mM phosphate buffer, pH 7.0) and microfugation. The supernatant was stored on ice and used for ascorbate peroxidase (APX), monodehydroascorbate reductase (MDHAR), glutathione reductase (GTR) and catalase analyses. Extracts for superoxide dismutase (SOD) analysis were prepared as described above except ascorbate was omitted from the extraction buffer. Total protein was quantified using the methods of Sedmak and Grossberg (1977).

APX activity was determined using a modification of the procedure by Nakano and Asada (1981) as per Jahnke and White (2003). The activity of GTR was measured as a decrease in absorbance at 340nm as described by Schaedle and Bassham (1977). MDHAR activity was measured using the method of Hossain *et al.* (1984). Catalase was quantified as oxygen evolution rates via Clark-type oxygen electrodes calibrated at 25°C using the techniques of Del Rio *et al.* (1977) and Delieu and Walker (1972). Each chamber was filled with 5 ml of 50 mM phosphate buffer (pH 7.0) and oxygen was removed by bubbling nitrogen gas. Once oxygen was depleted, 10 mM H_2O_2 was added to the chamber and the chamber sealed. Background oxygen evolution activity was recorded until a stable rate was obtained, after which sample extract was injected into the chamber using a Hamilton syringe. The subsequent oxygen evolution rate was recorded and catalase activity was calculated by subtracting the background rate from the sample rate.

SOD activity was measured using the Bioxytech SOD-525 spectrophotometric assay for superoxide disumutase (Oxis Research™, Portland, OR). This method is based on the SOD-mediated increase in the rate of autoxidation of 5,6,6a, 11b-tetrahydro-3,9,10-

trihydroxybenzo[c]fluorine in aqueous alkaline solution to yield a chromophore with maximum absorbance at 525nm. Prior to the initiation of the SOD reaction, 0.2 Units ascorbate oxidase were added to the sample + buffer mixture and incubated for 1 minute at 37°C. The purpose for this modification was to remove any remaining ascorbate in the sample that would interfere with the assay.

SDS PAGE and Western Blotting

Total protein extracts were prepared by initially centrifuging ~50 mL cell suspensions at 1000 x g for 5 minutes, washing the cell pellet with 0.5M glycerol, 50 mM phosphate buffer (pH 7.0) and re-centrifuging the samples. Cell pellets were suspended in 1 mL 0.5M sorbitol, 50 mM phosphate (pH 7.0), sonicated and centrifuged at 12,000 x g (top speed) for 3 minutes. Centrifugation was repeated twice more to thoroughly remove course cellular debris still remaining in the extract. For each sample, 15 μg total protein was loaded into a 4-12% gradient polyacrylamide gel (BioRad) and separated by SDS-PAGE. Gels were processed at 200V for ~ 45 minutes until loading dye ran through. Gels were subsequently equilibrated in 25 mM Tris, 192 mM glycine and the proteins transferred onto polyvinylidene difluoride (PVDF) membranes (BioRad). Electroblotting was performed at 100V for one hour. The D1 protein was detected using rabbit anti-PsbA antibodies (Agrisera, AS05084) at a dilution of 1: 3,000 followed by an incubation with goat anti-rabbit IgG(Fc) HRP-conjugated secondary antibodies (Pierce, 31463) at a dilution of 1: 62,500. Detection of HRP was performed using SuperSignal® West Pico chemiluminescent substrate (Pierce). Quantification of D1 protein was conducted with Image J gel analysis software (NIH).

Statistical Analysis

Individual and interactive effects of filter type and PAR treatments on all measured parameters were tested as 3 x 3 factorial ANOVAs with filter type (UV- blocking, CA or UA) and PAR level (100, 200 or 600 μmol photons m^{-2} s^{-1}) as experimental factors. For the preliminary UV-B time course experiments, a third factor (Time [hours]) was added into the analysis. Pairwise comparisons (Tukey's) were made where applicable. Western blot quantifications were performed by initially $\log_{10}$ transforming optical density data (obtained from ImageJ) prior to ANOVA analysis. Graphical data are representative of back-transformed mean values and standard errors. All calculations were done using SYSTAT v. 12 (Systat, Inc.).

RESULTS

Preliminary UV-B Intensity and Time Course Studies.

The purpose for performing preliminary experiments was to establish an appropriate UV-B radiation dose to use throughout the duration of the study. Initial inquiry revealed that *D. tertiolecta* cultures could withstand approximately 5-8 μmol photons m^{-2} s^{-1} (2.0-3.2 Wm^{-2}) CA filtered UV-B over a 24 hour period. F_v/F_m values decreased linearly as UV-B radiation levels increased from 0 – 10 μmol photons m^{-2} s^{-1} ($R^2 = 0.67$; Figure 1.5A). Photobleaching occurred above 8.5 μmol photons m^{-2} s^{1} (3.6 Wm^{-2}), while cultures receiving less than 5 μmol photons m^{-2} s^{1} (2.0 Wm^{-2}) did not demonstrate significant physiological stress (Figure 1.5A).

APX enzyme activities also responded dramatically to increased levels of UV-B radiation. As UV-B radiation levels increased from zero to 5 μmol photons m^{-2} s^{-1} (2.0 Wm^{-2}), APX activities tripled (Figure 1.5B). Between 5-8 μmol photons m^{-2} s^{-1} (2.0- 3.2 Wm^{-2}), APX activities leveled (Figure 1.5B). At UV-B radiation fluxes above 8 μmol photons m^{-2} s^{-1} (3.2 Wm^{-2}), observable photobleaching occurred and APX activities declined sharply (Figure 1.5B). It was therefore determined that 6 μmol photons m^{-2} s^{-1} (2.4 Wm^{-2}) UV-B was suitable for generating substantial photosynthetic stress without initiating lethal photobleaching.

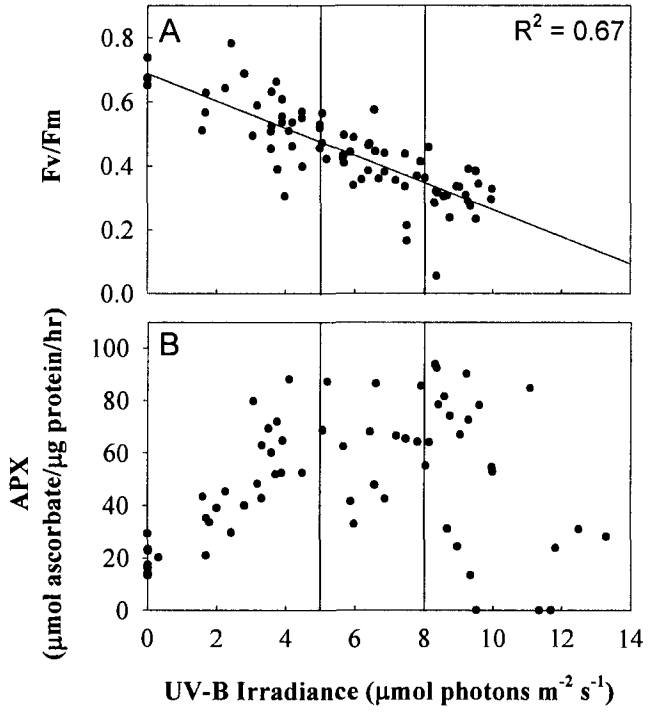

Figure 1.5. Response of *D. tertiolecta* to 24 hours UV-B radiation filtered by pre-solarized cellulose acetate. Cultures were maintained at 200 μmol photons m^{-2} s^{-1} PPFD and exposed to a range of UV-B radiation intensities (0-14 μmol photons m^{-2} s^{-1}; 0 - 5.8 Wm^{-2}). A) Variable to maximal fluorescence (F_v/F_m) values and B) APX activity rates were recorded as described in Materials and Methods.

Exposure to UV-B radiation for 24 hours did not represent a scenario experienced by phytoplankton in the natural environment. Therefore, a dosage of 6 μmol photons m^{-2} s^{-1} (2.4 Wm^{-2}) UV-B was applied for 24 hours under three varying PAR intensities; during which samples of *D. tertiolecta* were collected and analyzed every three hours. This served to establish an UV-B exposure time for subsequent experiments that was comparable to natural irradiances and which would highlight any differences between CA and UA filtration. Results from the time course experiments suggested that PPFD had no influence on F_v/F_m ($p = 0.315$), regardless of which UV-B filter was used (PAR x Filter type; $p = 0.970$). Conversely, the effect of UV-B filter type on F_v/F_m was dependent on the duration of UV-B exposure ($p = 0.015$). Following 3 hours of UV-B exposure, CA cultures maintained 20% lower F_v/F_m values than UA cultures (Figure 1.6). Interestingly, F_v/F_m remained consistent for both filter types from 3-12 hours (Figure 1.6). After 24 hours, CA cultures possessed 38% lower F_v/F_m values compared to UA cultures (Figure 1.6). In all cases, F_v/F_m values were higher in UA cultures, but this difference was only determined to be significantly different after 3, 12 and 24 hours (Figure 1.6).

The effect of PPFD on APX was dependent on whether CA or UA filtration was used ($p = 0.003$). After six hours of exposure, APX activities of cultures receiving UV-B filtered by CA at 100, 200 and 600 PAR increased 126%, 107% and 177%, respectively. Following 12-hours, APX had increased 159%, 165% and 177%, respectively (Figure 1.7A). APX in UA cultures did not change, regardless of the PPFD or UV-B exposure time ($\alpha > 0.05$; Figure 1.7B). Therefore, a 12-hour exposure to 6 μmol photons m^{-2} s^{-1} (2.4 Wm^{-2}) UV-B was utilized for all subsequent experiments.

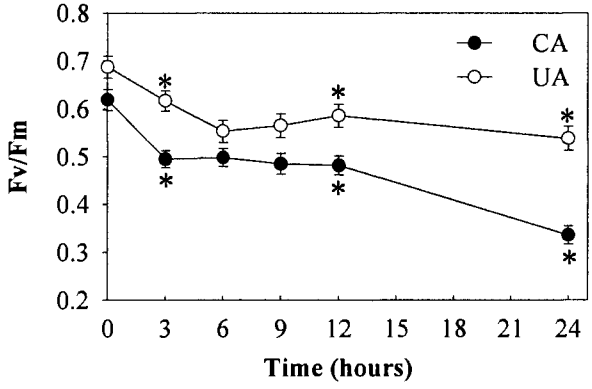

Figure 1.6. Effect of UV-B radiation exposure duration on F_v/F_m. Cultures received 6 μmol m^{-2} s^{-1} (2.4 Wm^{-2}) UV-B radiation filtered by cellulose acetate (closed circles) or 0.26 mM urate solution (open circles) for varying exposure durations (0-24 hours). Experiments were conducted at 100, 200 and 600 μmol photons m^{-2} s^{-1} PAR. Asterisks (*) indicate significant differences between filter types for a particular time (a = 0.05). Data are n = 20 samples per treatment. Error bars are ± one standard error.

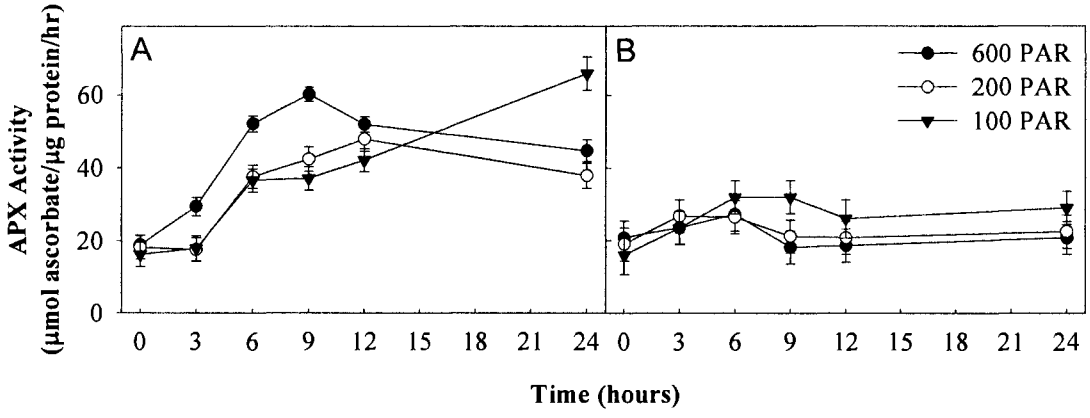

Figure 1.7. Effect of UV-B radiation exposure duration on APX activity. Cultures received 6 μmol m^{-2} s^{-1} (2.4 Wm^{-2}) UV-B radiation filtered by A) cellulose acetate or B) 0.26 mM urate solution for varying durations of time (0-24 hours). Experiments were conducted at 100 (triangles), 200 (open circles) and 600 (closed circles) μmol photons m^{-2} s^{-1} PAR. Data are n = 4 samples per treatment. Error bars are ± one standard error.

UV-B Radiation Effects on Photosynthesis and Pigments.

The effect of PPFD on P_{LS} and P_{LL} depended on the UV-B filter type used (Table 1.1). For all PPFDs, P_{LS} rates of CA cultures were significantly lower than both control (UV-blocking film) and UA cultures (Figure 1.8A). Specifically, P_{LS} dropped 58%, 67% and 36% from control rates at 100, 200 and 600 PAR, respectively (Figure 1.8A). In contrast, P_{LS} in UA cultures did not vary from controls, regardless of the PPFD applied (Figure 1.8A). In other words, cultures receiving 6 μmol photons $m^{-2}s^{-1}$ (2.4 Wm^{-2}) UV-B filtered through 0.26 mM urate solutions maintained P_{LS} rates comparable to cultures receiving no UV radiation, while cultures receiving the same unweighted UV-B dose (i.e. no BWF applied) filtered by CA experienced acute inhibition of P_{LS}.

P_{LL} rates of CA cultures fell 73% and 72% under 100 and 200 PAR, respectively yet, when 600 PAR was used, P_{LL} rates were unchanged (Figure 1.8B). Alternatively, only cultures growing at 100PAR were affected by UA filtered UV-B radiation, with P_{LL} dropping 40% compared to control rates. At 200 and 600 PAR, P_{LL} rates were unaffected ($p = 0.397$ and $p = 0.980$, respectively; Figure 1.8B).

Light limited: light saturated photosynthetic ratios (P_{LL}: P_{LS}) declined from control values only when 100 PAR was used (Figure 1.9). This difference occurred with both CA (43% decrease) and UA (29% decrease; Figure 1.9). Interestingly, when PAR was elevated to 200 or 600 μmol photons $m^{-2}s^{-1}$, P_{LL}: P_{LS} ratios for all three filter types were identical ($\alpha > 0.5$; Figure 1.9).

Table 1.1. ANOVA results (p-values) for photosynthesis and pigment parameters following exposure to UV-B radiation. *D. tertiolecta* cultures were treated for 12 hours with 6 μmol photons m^{-2} s^{-1} (2.4 Wm^2) UV-B radiation. Experimental factors were PAR (100, 200 or 600 μmol photons m^{-2} s^{-1}) and Filter type (UV-blocking, 0.26 mM UA or CA). P_{LS} (light-saturated) and P_{LL} (light-limited) photosynthesis rates (μmol O_2 mg chl^{-1} h^{-1}), F_v/F_m (variable to maximal fluorescence ratio), F_o (dark adapted minimal fluorescence), *Chl* (total chlorophyll), Chl *a* (chlorophyll *a*), Chl *b* (chlorophyll *b*), *Car* (total carotenoids). P-values are results from 2 x 2 factorial ANOVAs. Bolded values represent statistical significance. Values < 0.05 that are not bolded indicate that a significant interaction with another experimental factor is present.

Response	Main Effects		Interactive Effect
	PAR	Filter Type	PAR x Filter Type
P_{LS}	< 0.001	< 0.001	**0.052**
P_{LL}	0.667	< 0.001	**0.003**
P_{LL}: P_{LS}	0.002	0.002	**0.006**
F_v/F_m	< 0.001	< 0.001	**0.002**
Relative quantity D1 protein	0.648	**0.017**	0.986
F_o	**0.007**	**< 0.001**	0.741
Chl	**0.001**	0.112	0.546
Car	**0.001**	**0.019**	0.944
Chl *a*	**< 0.001**	0.386	0.605
Chl*b*	0.11	**0.014**	0.457
Chl *a*/*b*	0.166	**0.017**	0.713

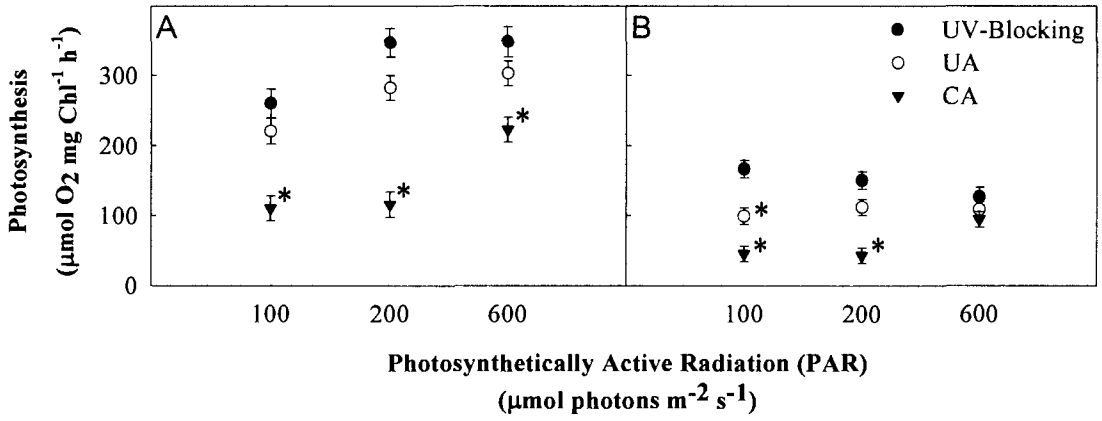

Figure 1.8. Oxygenic photosynthetic rates of *D. tertiolecta* following a 12-hour exposure to 6 μmol photons $m^{-2}s^{-1}$ (2.4 Wm^{-2}) UV-B radiation. Measurements were recorded under A) Light-saturating (500 μmol photons $m^{-2}s^{-1}$) and B) Light-limiting (100 μmol photons $m^{-2}s^{-1}$) PPFDs. Experiments were conducted at 100, 200 and 600 μmol photons $m^{-2}s^{-1}$ PAR. UV-B radiation was filtered by UV-blocking film (closed circles; control), 0.26 mM urate solution (open circles) or cellulose acetate (closed triangles). Data are mean of n = 12 samples per treatment. Error bars are ± one standard error. For a particular PAR, asterisk's (*) indicate significant differences from control.

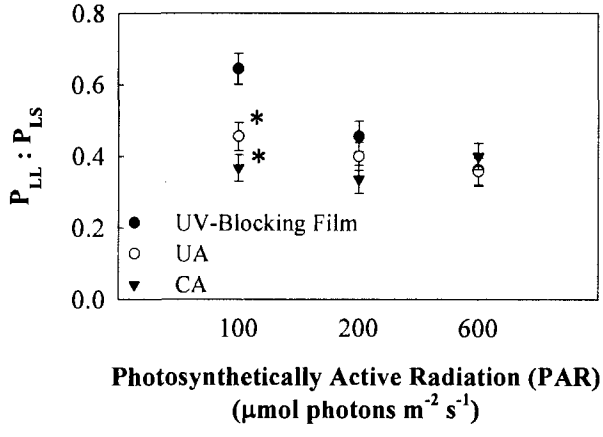

Figure 1.9. Effect of UV-B radiation on P_{LL}: P_{LS}. Cultures were exposed to 12 hours of 6 μmol photons m^{-2} s^{-1} (2.4 Wm^{-2}) UV-B radiation filtered by UV-blocking film (closed circles), 0.26 mM urate solution (open circles) or cellulose acetate (closed triangles). Experiments were performed at 100, 200 or 600 μmol photons $m^{-2}s^{-1}$ PAR. Data are mean of n = 12 samples per treatment. Error bars are ± one standard error. For a particular PAR, asterisks (*) indicate significant difference from control (UV-blocking film).

The effect of UV-B radiation on F_v/F_m was a function of both PPFD intensity and whether CA or UA filtration was used (Table 1.1). Across all PPFDs, Fv/Fm values of CA cultures were significantly lower compared to any other treatment (Figure 1.10). At 100, 200 and 600 PAR, F_v/F_m values of CA cultures dropped 50%, 34% and 22%, respectively (Figure 1.10). F_v/F_m values in UA cultures fell 18% and 17% under 100 and 200 PAR, respectively ($p = 0.007$, $p = 0.019$). UA cultures receiving 600 PAR experienced no change in F_v/F_m values following UV-B treatment ($p = 0.519$; Figure 1.10).

The severity of UV-B induced D1 protein degradation was dependent on the filtration type (Table 1.1). Compared to control cultures that received no UV-B radiation, the relative amount of D1 protein decreased 56.9% in CA cultures and 23.44% in UA cultures (Figure 1.11A). Variations in PPFD intensity did not affect D1 protein content ($p = 0.686$; Figure 1.11B). That is, regardless of PPFD, CA cultures always contained 33.5% less D1 protein compared to UA cultures (Figure 1.11A).

There were no interactive effects on F_o between PPFD and UV-B filter type, however individual effects of both experimental factors were observed (Table 1.1). Compared to the F_o values of 100 PAR cultures, F_o within 200 and 600 PAR cultures dropped 23% and 28%, respectively (Figure 1. 12A). F_o values increased 63.6% and 48.3% in CA and UA cultures, respectively following exposure to UV-B (Figure 1.12B).

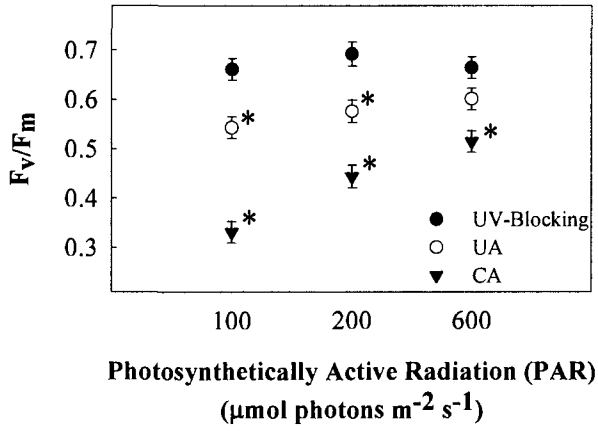

Figure 1.10. Effect UV-B radiation on the photosynthetic efficiency of PSII (F_v/F_m). Cultures were exposed to 12 hours of 6 μmol photons m^{-2} s^{-1} (2.4 Wm^{-2}) UV-B radiation filtered by UV-blocking film (closed circles), 0.26 mM urate solution (open circles) or cellulose acetate (closed triangles). Experiments were performed at 100, 200 or 600 μmol photons $m^{-2}s^{-1}$ PAR. Data are mean of n = 12 samples per treatment. Error bars are ± one standard error. For a particular PAR, asterisks (*) indicate significant difference from control (UV-blocking film).

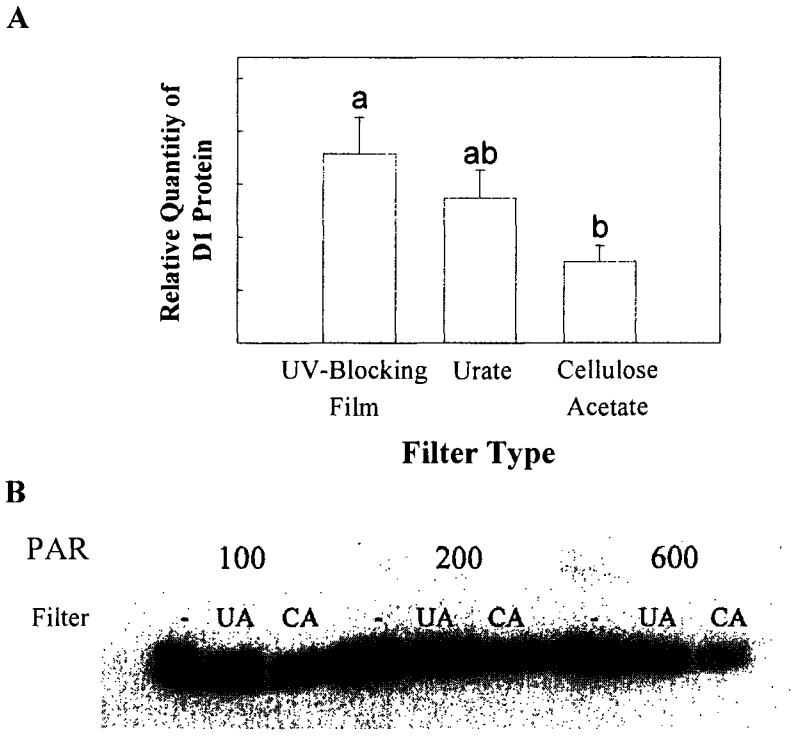

Figure 1.11. Effect of short wavelength UV-B radiation on D1 protein turnover. A) Relative quantity of D1 protein in *D. tertiolecta* following a 12 hours exposure to 6 μmol photons $m^{-2}s^{-1}$ (2.4 Wm^{-2}) UV-B radiation filtered by cellulose acetate (CA), 0.26 mM urate (UA) or UV-blocking film (-). Experiments were performed at 100, 200 or 600 μmol photons $m^{-2}s^{-1}$ PAR. Data are mean of n = 3 samples per treatment. Error bars are ± one standard error. B) Representative western blot of D1 protein.

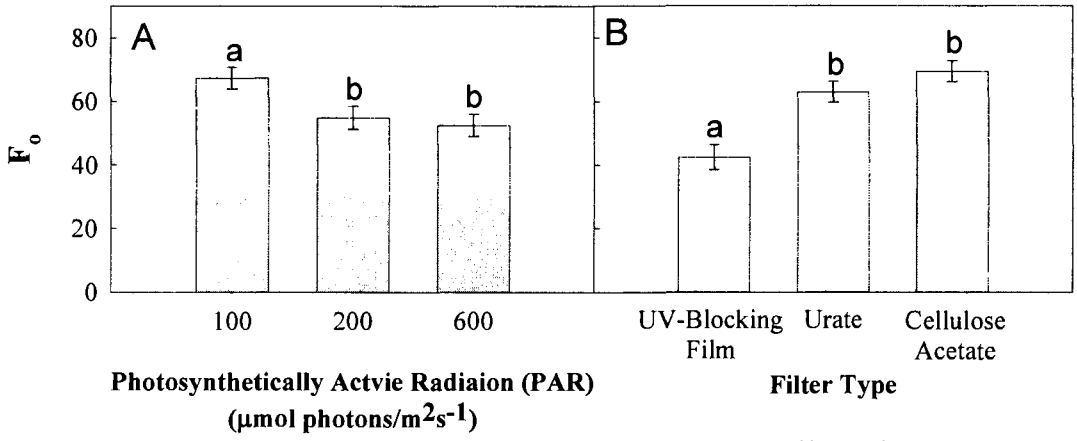

Figure 1.12. Damage to LHC as measured by F_0 values. A) Effect of PPFD on F_0 values. Cultures grown at 100, 200 and 600 µmol photons $m^{-2}s^{-1}$ PAR B) Effect of UV-B radiation on F_0 values. Cultures received 12 hours of 6 µmol photons $m^{-2}s^{-1}$ (2.4 Wm^{-2}) UV-B radiation filtered by UV-blocking film, 0.26 mM urate or cellulose acetate. Data are mean of n = 30 samples per treatment. Error bars are ± one standard error.

Total chlorophyll (total *chl*), total carotenoids (*car*) and chlorophyll *a* (chl *a*) contents varied depending on the PAR level applied (Table 1.1). As PPFD increased, pigment levels decreased (Figure 1.13). More specifically, total *chl, car* and chl *a* contents fell 32%, 24% and 35%, respectively between 100 and 600 PAR treatments (Figure 1.13A, B & C). Chlorophyll *b* (chl *b*) was not affected by changes in PPFD (Table 1.1; Figure 1.13D).

Chl *b* and *car* contents, as well as the chl *a*: chl *b* ratio, changed depending on the UV-B filtration type used (Table 1.1). In all cases, UA values did not differ from controls (Figure 1.14). Following exposure to UV-B, CA cultures contained 51% and 27% more chl *b* and *car*, respectively than control cultures (Figure 1.14A & B) Alternatively, CA cultures possessed 26% lower chl *a*: chl *b* ratios than controls. (Figure 1.15C). Chl *a* contents did not change with varying UV-B filter type (p = 0.386; Table 1.1).

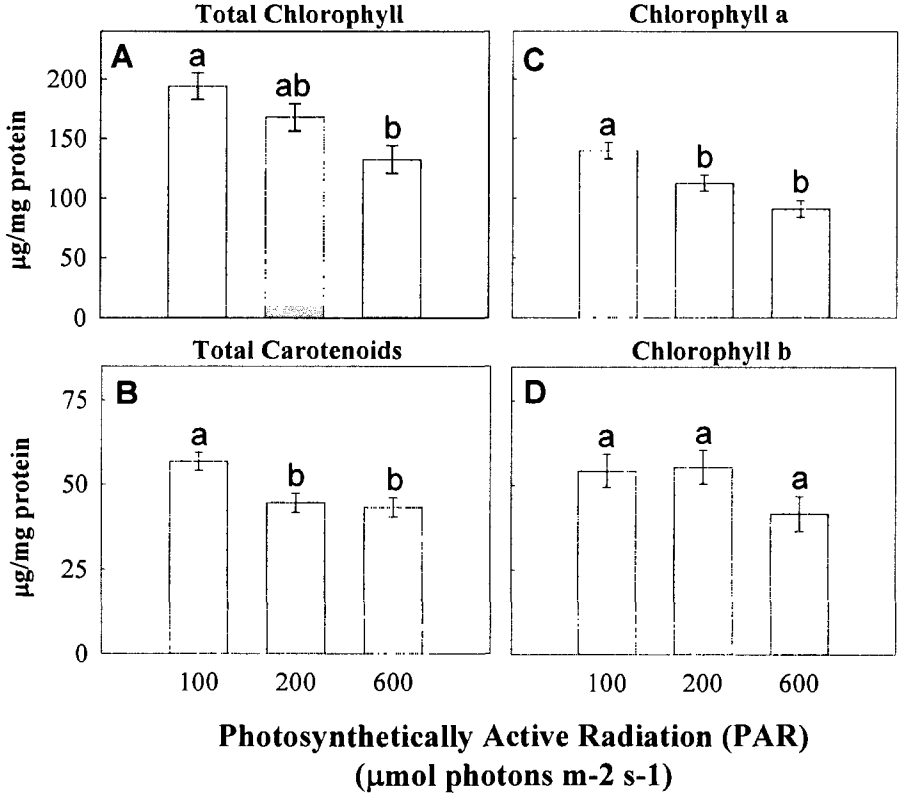

Figure 1.13. Pigment contents of *D. tertiolecta* grown at 100, 200 and 600 µmol photons $m^{-2}s^{-1}$ PAR. The quantities of A) total *chl* B) *car* C) chl *a* and D) chl *b* were measured following 12 hour exposure to 6 µmol photons m^{-2} s^{-1} (2.4 Wm^{-2}) UV-B radiation filtered with UV-blocking film, CA and UA. Data represent mean of n= 30 samples per treatment. Error bars are ± one SE. For a particular pigment, means with the same letter are not significantly different ($\alpha = 0.05$).

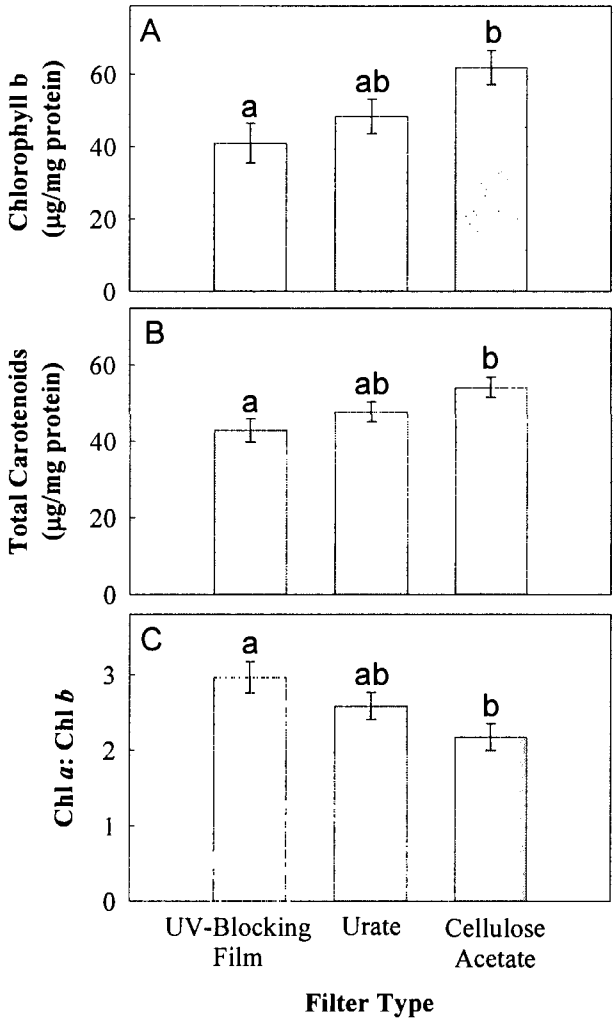

Figure 1.14. Effect of UV-B filter type on *D. tertiolecta* pigments. Quantities of A) chlorophyll *b* and B) total carotenoids in addition to C) the chl *a*/*b* ratio of *D. tertiolecta* were measured following 12 hour exposure to 6 µmol photons $m^{-2}s^{-1}$ (2.4 Wm^{-2}) UV-B filtered by UV-blocking film, UA or CA. Experiments were conducted at 100, 200 and 600 µmol photons $m^{-2}s^{-1}$ PAR. Data represent mean of n= 30 samples per treatment. Error bars are ± one SE. For a particular parameter, means with the same letter are not significantly different ($\alpha = 0.05$).

Oxidative Stress Responses.

Alterations in APX, SOD and catalase enzyme activities depended on the UV-B filtration type used (Table 1.2). Compared with controls, APX and SOD rates within CA cultures increased 167% and 77%, respectively, while no changes were observed in UA cultures (Figure 1.15A & B). Exposure to UV-B radiation resulted in decreased catalase activity, regardless of whether CA (56%) or UA (32%) filtration was employed (Figure 1.15C).

Table 1.2. ANOVA results (p-values) for antioxidant enzyme responses to UV-B radiation. *Dunaliella tertiolecta* cultures were treated for 12 hours with 6 μmol photons m^{-2} s^{-1} (2.4 Wm^{-2}) UV-B radiation. Experimental factors were PAR (100, 200 or 600 μmol photons m^{-2} s^{-1}) and Filter type (UV-blocking, 0.26 mM UA or CA). APX (ascorbate peroxidase), SOD (superoxide dismutase), MDHAR (monodehydroascorbate reductase), GTR (glutathione reductase). P-values are results from 2 x 2 factorial ANOVAs. Bolded values represent statistical significance.

Response	Main Effects		Interactive Effect
	PAR	Filter Type	PAR x Filter Type
APX	0.073	**<0.001**	0.607
SOD	0.87	**<0.001**	0.322
Catalase	**<0.001**	**<0.001**	0.945
MDHAR	**0.002**	0.236	0.652
GTR	0.367	0.332	0.641

Although SOD and APX did not change with varying PPFD, MDHAR and catalase enzyme rates changed significantly (Table 1.2). As PPFD increased from 100 to 600 PAR, MDHAR rates also increased 63% (Figure 1.16A). Alternatively, catalase rates

at 100 PAR were 25% higher than under 200 or 600 PAR (Figure 1.16B). GTR activity remained constant under all experimental conditions (Table 1.2).

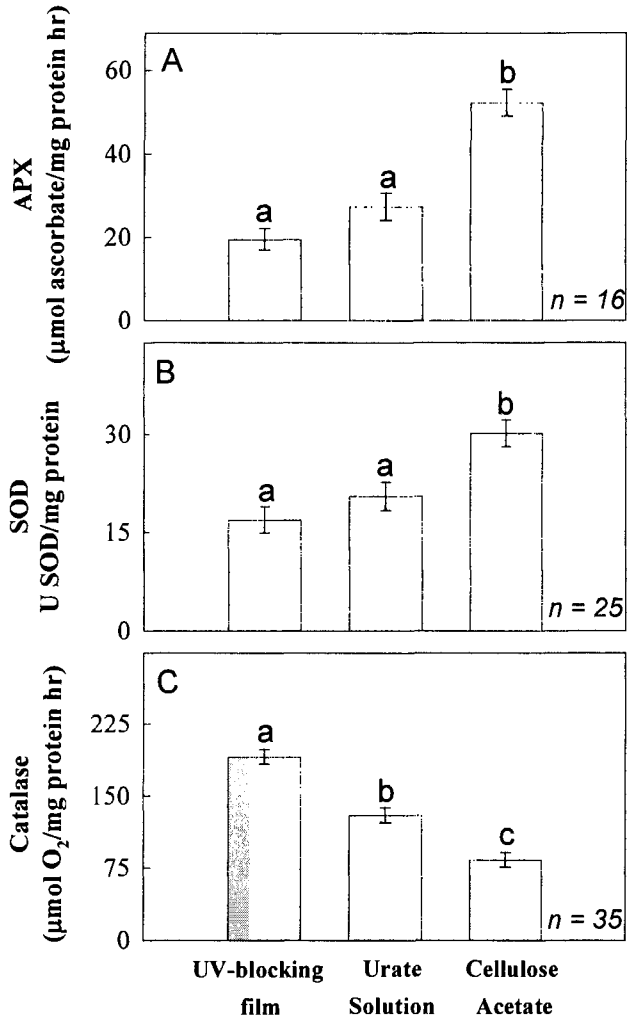

Figure 1.15. Effect of UV-B filter type on antioxidant activities. *D. tertiolecta* were grown at 100, 200 and 600 µmol photons m^{-2} s^{-1} PAR and exposed to 6 µmol photons m^{-2} s^{-1} (2.4 Wm^{-2}) UV-B radiation filtered by UV-Blocking film, UA or CA. Enzyme rates of A) APX B) SOD and C) catalase were recorded as described in Materials and Methods. Error bars are ± one SE. For a particular enzyme, means with the same letter are not significantly different ($\alpha = 0.05$).

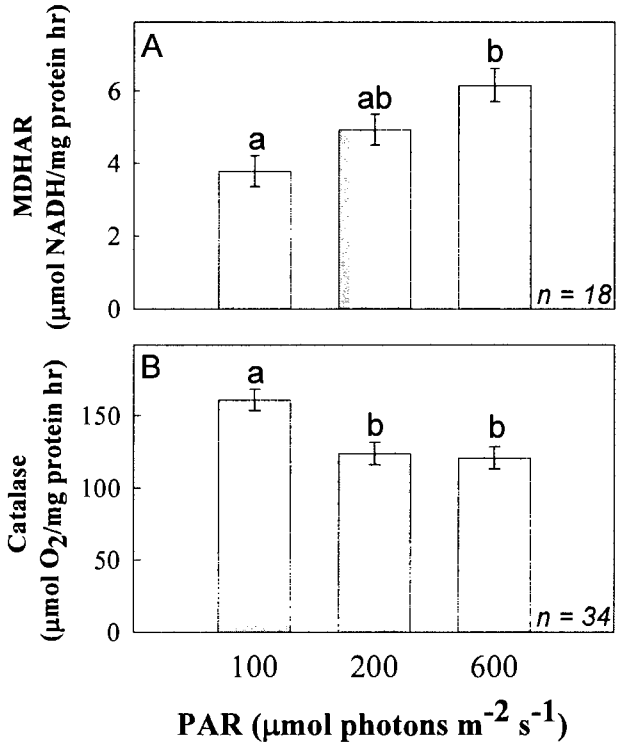

Figure 1.16. Effect of PPFD on antioxidant activities. *D. tertiolecta* were exposed to 6 μmol photons m^{-2} s^{-1} (2.4 Wm^{-2}) UV-B radiation filtered by UV-Blocking film, UA or CA at 100, 200 and 600 μmol photons m^{-2} s^{-1} PAR. Enzyme rates of A) MDHAR and B) catalase were recorded as described in Materials and Methods. Error bars are ± one SE. For a particular enzyme, means with the same letter are not significantly different (α = 0.05).

Removing UV-A from UV-B Lamp Emissions.

Comparisons between UV-B radiations filtered by UA and UA used in conjunction with K_2CrO_4 solutions were made to establish whether the UV-A wavebands emitted by the UV-B lamps had any significant physiological effects on *D. tertiolecta*. For all measured photosynthetic and antioxidative parameters there were no differences observed (Table 1.3). That is, identical physiological responses were obtained from using UA or UA + K_2CrO_4 filtered UV-B lamp emissions at a constant UV-B flux.

Table 1.3. Effect of removing UV-A radiation from UV-B lamp emissions on photosynthesis, pigment contents and antioxidant enzymes. *Dunaliella tertiolecta* growing at 600 μmol photons m^{-2} s^{-1} PAR were treated for 12 hours with 6 μmol photons m^{-2} s^{-1} (2.4 Wm^{-2}) UV-B radiation filtered by 0.26 mM urate solution (pH 7.0; UA) or 0.26 mM urate solution plus 1.0 mM K_2CrO_4 solution (pH 8.0; UA + CrO_4). P_{LS} (light-saturated) and P_{LL} (light-limited) photosynthetic rates (μmol O_2 mg chl^{-1} h^{-1}), F_v/F_m (variable to maximal fluorescence ratio), F_o (dark adapted minimal fluorescence), *Chl* (total chlorophyll), Chl *a* (chlorophyll *a*), Chl *b* (chlorophyll *b*), *Car* (total carotenoids), APX (ascorbate peroxidase), MDHAR (monodehydroascorbate reductase), GTR (glutathione reductase). F-ratios and probability values (P-values) are results from one-way ANOVAs.

Response	Filter Type	Mean ± SE	F - ratio	P - value
P_{LS} (μmol O_2 mg chl a^{-1} hr^{-1})	UA	252.3 ± 23	2.257	0.148
	UA + CrO_4	302.2 ± 23		
P_{LL} (μmol O_2 mg chl a^{-1} hr^{-1}))	UA	62.5 ± 8.8	0.633	0.435
	UA + CrO_4	72.7 ± 9.1		
F_v/F_m	UA	0.535 ± 0.18	0.037	0.849
	UA + CrO_4	0.504 ± 0.18		
F_o	UA	136.2 ± 8.7	0.956	0.339
	UA + CrO_4	123.8 ± 9.1		
Total *Chl* (μg/mg protein)	UA	132.6 ± 11.5	0.03	0.863
	UA + CrO_4	129.7 ± 12.0		
Chl *a* (μg/mg protein)	UA	91.2 ± 7.0	0.001	0.977
	UA + CrO_4	91.5 ± 7.3		
Chl *b* (μg/mg protein)	UA	41.4 ± 4.7	0.215	0.647
	UA + CrO_4	38.2 ± 5.0		
Car (μg/mg protein)	UA	42.3 ± 2.3	0.382	0.543
	UA + CrO_4	44.4 ± 2.4		
APX (μmol ascorbate/mg protein/hr)	UA	26.6 ± 2.3	0.274	0.606
	UA + CrO_4	24.8 ± 2.5		
Catalase (μmol O_2/mg protein/hr)	UA	131.6 ± 10.5	2.441	0.133
	UA + CrO_4	155.5 ± 11.0		
MDHAR (μmol NADH/mg protein/hr)	UA	2.6 ± 0.18	0.002	0.961
	UA + CrO_4	2.5 ± 0.18		
GTR (μmol GSSG/mg protein/hr)	UA	4.3 ± 0.6	1.402	0.250
	UA + CrO_4	5.2 ± 0.6		

DISCUSSION

Too often, laboratory UV-B studies fail to consider the solar UV-B spectral profile and/or natural UV-B: PAR ratios incident at the earth's surface. The main goals of this project were to clarify the role of the excessive UV-B wavebands transmitted by CA and propose an alternative UV-B lamp filtration technique, in which UV-B lamp emissions are altered to produce UV-B spectra nearly identical to solar flux. It was also an objective of this project to investigate the consequences of imbalanced UV-B: PAR ratios on the photobiology and oxidative stress responses of plant cells. Preliminary investigations were performed to select an "optimal" UV-B radiation intensity and exposure time to use during subsequent experiments. UV-B intensity range studies identified a range of UV-B intensities (5-8 μmol photons m^{-2} s^{-1}) that imposed physiological stress on *D. tertiolecta*, without lethal photobleaching. Previous reports have shown that *D. tertiolecta* maintains its photosynthetic integrity following 24-hour exposures to UV-B radiation at intensities as high as 30 μmol photons m^{-2} s^{-1} (12 Wm^{-2}) when lamp irradiance was filtered with 0.26 mM UA filters (Jahnke and Sampath-Wiley, 2009). Since comparisons between CA and UA filtration were proposed for the current study, it was essential to use a UV-B dose that *D. tertiolecta* could tolerate with either CA or UA filtration. Thus, a UV-B intensity of 6.0 - 6.9 μmol photons m^{-2} s^{-1} (2.4- 2.8 Wm^{-2}) was selected since at levels above this range, CA cultures were photobleached (Figure 1.5). This UV-B intensity was also selected because it represented UV-B levels reaching the earth's surface (Helbling *et al.*, 1992; Caldwell *et al.*, 1994; Whitehead *et al.*, 2000) and thus, any physiological effects resulting from this level of UV-B exposure could likely be used to make ecologically relevant projections.

Following the establishment of the experimental UV-B intensity, the duration of exposure needed to be determined. In addition to the fact that 24-hour exposures to UV-B radiation are unrepresentative of naturally occurring flux, it was unclear whether 24-hour exposures were ideal for assessing UV-B induced physiological responses. Thus, *D. tertiolecta* cultures receiving 6.0 – 6.9 μmol photons m^{-2} s^{-1} UV-B were evaluated at three hour intervals over a 12-hour period, and then again after 24 hours (Figures 1.6 & 1.7). Under both CA and UA treatment, F_v/F_m values declined significantly after three hours of UV-B exposure; where they remained consistent through 12 hours (Figure 1.6). Alternatively, APX activities of CA cultures climaxed after 9-12 hours and UA cultures were unaffected by UV-B treatment altogether (Figure 1.7A). Because peak escalations of APX were observed after 12 hours and F_v/F_m values also differed from control values after this exposure period, the UV-B treatment for subsequent experiments was selected to be 12-hour exposures to 6.0 – 6.9 μmol photons m^{-2} s^{-1} UV-B radiation (Figures 1.6 & 1.7). This period of time was also in accordance with the UV-B radiation exposures present in many "natural" phytoplankton communities.

UV-B Effects on Photosynthesis

It is recognized that PPFD plays a fundamental role in governing UV-B radiation sensitivity in plants. There are several hypotheses which may account for this mitigation: 1) that a high PPFD facilitates morphological and anatomical changes (e.g. leaf thickening) lessening a plant's sensitivity to UV-B radiation 2) that elevated PPFD stimulates the production of protective pigments (flavonoids) and other UV-B absorbing compounds (MAAs) and 3) that direct interactions between PPFD and UV-B radiation

initiate photorepair and photoreactivation processes (Warner and Caldwell, 1983; Mirecki and Teramura, 1984). In the current study, *D. tertiolecta* cultures were exposed to a constant UV-B flux under varying PPFDs. There have been many reports on the attenuation of photoinhibitory damages when a high PPFD is applied jointly with UV-B radiation (Adamse and Britz, 1992 Deckmyn *et al.*, 1994; Deckmyn and Impens 1997). For example, Allen *et al.* (1998) purposed that high PPFD provided protection against UV-B induced damage via increased photosynthesis, which produces the biochemical energy required for defense and/or repair processes. The work of Mackerness *et al.* (1996) supports this notion, as they reported that UV-B induced declines in PSII and RuBisCO mRNA transcripts at 150 μmol photons m^{-2} s^{-1} PAR were eliminated after the PAR was raised to 350 μmol photons m^{-2} s^{-1}.

Of additional significance were the dissimilarities in photosynthetic parameters between CA and UA treatments. Cultures using CA filtration suffered acute P_{LS} losses across all PPFDs, while those receiving identical UV-B intensities via UA filters maintained P_{LS} rates that were indistinguishable from controls (Figure 1.8A). This suggests that the excessive short-wave UV-B radiation transmitted by CA filters was the source driving P_{LS} decline (Figure 1.8A). Although under low PAR UV-B treatment caused P_{LL} declines within UA cultures, when PPFD was elevated, P_{LL} rates remained identical to controls (Figure 1.8B) suggesting that photoprotective mechanisms were also up-regulated by elevated PPFD (Allen *et al.*, 1998; Mackerness *et al.*, 1996).

From their work on soybean (*Glycine max* [L.] Merr.), Mirecki and Teramura (1984) proposed that high PPFD applied with UV-B radiation decreased cellular respiration and cell division, which provided energy for heightened dark repair of UV-B

induced photodamages. They further implied that such photoprotective processes worked cooperatively with photoreactivation processes, in which longer wavelengths (315-550 nm) activate specific enzymes to repair UV-B injuries. Photoprotection mechanisms involve the chloroplast-encoded protein synthesis of PSII complex components (Shelly *et al.*, 2002; Heraud and Beardall, 2000; Masi and Melis, 1997) and photoreactivation genes have been identified in *D. salina* (Cheng *et al.*, 2007; Lv *et al.*, 2008). Therefore, it is probable that photorepair to PSII was ongoing in UA cultures receiving PPFD above 200 μmol photons m^{-2} s^{-1}, but were inactive /hindered by low PPFD and/or the presence of excessive 290-320 nm radiation in the CA treatment (Figure 1.8).

The notion that *D. tertiolecta* repaired UV-B induced photodamage via PPFD photorepair/photoreactivation mechanisms was further supported by P_{LS}: P_{LL} ratio trends (Figure 1.9). In general, declines in P_{LL}: P_{LS} signify deterioration of electron transport efficiency, while increases are indicative of damage to RubisCO (or other enzymes) and stress on the carbon fixation reactions (White and Jahnke, 2002). The results of this study suggest that electron transport efficiency was compromised by UV-B radiation under low PPFD, but preserved at higher PPFDs (Figure 1.9).

Electron transport commences at the PSII complex, where water is oxidized and electrons are released. The ratio of variable to maximal fluorescence (F_v/F_m) is a direct measurement of the maximum efficiency of electron movement through PSII. The results of this study further suggest that the protective effects of high PPFD on electron transport efficiency could not compensate for the damages incurred by short-wave UV-B radiation transmitted by CA filters (Figure 1.10). This conclusion is supported by the fact that UA cultures suffered declines in F_v/F_m only under 100 PAR while, F_v/F_m ratios in CA

cultures remained significantly lower than both UA and control treatments even under the highest PPFD (Figure 1.10).

Photoinhibition is defined as the light-dependent inhibition of photosynthesis and is specifically caused by the light-induced damage of the PSII reaction center by both visible and UV irradiation (Osmond, 1994; Baker, 1996). The exact mechanism of photoinhibitory damage is still debated, as is whether visible and UV radiation cause damage at the same locations within PSII. A number of studies indicate that UVR impairs electron transfer between Mn and Tyr-Z^+ generating $^1O_2$ and subsequent PSII destruction (i.e. donor side inhibition; Tyystjärvi, 2008; Hakala, *et al.*, 2005; Vass *et al.*, 2002; Larkum *et al.*, 2001). Others insist that high irradiances launch a series of light-induced modifications at the acceptor side of PSII (Q_A and Q_B), causing disruptions in electron transport, generation of triplet state reaction centers ($^3P_{680}$) and $^1O_2$ (Durrant *et al.*, 1990; Fufezan *et al.*, 2007; Vass *et al.*, 2007). Evidence for distinct PAR and UV-B PSII inactivation pathways have been described. Using isolated spinach thylakoids and *Synechocystis* cultures, Sicora *et al.* (2003) showed that the inactivation of PSII by PAR and UV-B photons occurred discretely via non-interacting mechanisms that targeted different sites on PSII. Furthermore, they demonstrated that the inactivation of PSII was lessened if PAR and UV-B radiation were applied simultaneously. Sicora *et al.* (2003) concluded that amelioration of PSII damage occurred via PSII repair enhancement as a result of PAR and UV-B wavelength interactions. Acceptor side damage has been observed in *D. tertiolecta* (Beardall *et al.*, 2002), but the likelihood for donor side damages via CA filtered UV-B radiation cannot be ruled out.

Irrespective of the photoinhibitory pathway, inactivation of the PSII complex results in the destruction/damage of the D1 and D2 proteins, which must be removed and re-synthesized *de novo*. If the rate of repair/replacement keeps pace with the rate of damages incurred, a stable photosynthetic rate results (dynamic photoinhibition). If however, damages exceed the rate of PSII repair, both quantum efficiency and P_{max} suffer declines (chronic photoinhibition).

The re-synthesis and replacement of the D1 protein is slowed and/or eliminated during UV inhibition (Masi and Melis, 1997; Chaturvedi and Shyam, 2000; Heraud and Beardall, 2000; Xiong, 2001). Consequently, quantification of D1 protein has often been used to determine the effect of UV-B radiation on PSII; specifically the turnover rate of D1 protein (Melis *et al.*, 1992; Friso *et al.*, 1995; Masi and Melis, 1997). Immunoblotting of *D. tertiolecta* total proteins performed in the current study resulted in the visualization of a D1 doublet (Figure 1.11b). Several explanations are provided by Agrisera (Stockholm, Sweden) to explain why such a pattern was observed. Firstly, the precursor to PsbA has a 9 amino acid tail in higher plants (16 in cyanobacteria) that can be resolved by electrophoresis. Secondly, degradation products may have also been visualized, since the degradation of D1 is a complex set of events and the products can be influenced by both the extraction procedure and the physiology of the cells prior to harvest. Lastly, cross-linking between the D1 and cytochrome b559 may occur, shifting the protein higher in the gel. The results presented in the present study indicate that excessive radiation in the range of 290-320 nm was directly responsible for PSII damages in *D. tertiolecta* and was independent from PPFD (Figure 1.11).

Aro *et al.* (1993) demonstrated that D1 protein degradation increased with increasing incident light intensities only if PAR was applied at levels that did not cause photoinhibition *in vivo* (< 400 μmol photons m^{-2} s^{-1}). When PPFD was elevated to intensities high enough to elicit photoinhibition (≥ 1600 μmol photons m^{-2} s^{-1}), D1 protein degradation remained at levels consistent with those receiving non-photoinhibitory PPFD fluxes (Aro *et al.*, 1993). The results of the current study are consistent with the findings of Aro *et al.* (1993), in which all PPFD levels applied affected D1 protein turnover equally (Table 1.1; Figure 1.11). On the other hand, CA cultures suffered severe declines in D1 protein contents across all PAR levels, while UA cultures lost minimal protein (Figure 1.11A). These findings directly implicate the excessive short-wave UV-B radiation transmitted by CA in facilitating direct damage to the PSII complex. Furthermore, it can be inferred that the rate of PSII damage in CA cultures was higher and/or the PSII repair cycle was hindered by the presence of excessive UV-B radiation (Figure 1.11A).

In a study of natural phytoplankton communities, phytoplankton in which the PSII repair cycle was blocked showed similar D1 protein degradation rates following exposure to both natural ambient irradiance and natural ambient irradiance supplemented with a high dose of UV-B (Bouchard *et al.*, 2005). Bouchard *et al.* (2005) further demonstrated that repairs to the D1 protein declined faster under supplemental UV-B treatment compared to those receiving ambient irradiance. They (Bouchard *et al.*, 2005) concluded that UV-B inhibition of the PSII repair cycle was central to the photoinhibition response as opposed to the initial photodamage of D1 protein. That is, the main source of photodamage was sustained by accumulating unrepaired/damaged D1 proteins. Similarly,

Lesser *et al.* (2002) proposed that the ability of Antarctic *Scenedesmus* sp. to survive their environments high UVR irradiances was partly due to enhanced repair/replacement of damaged D1 proteins. Therefore, it is possible that the failure of CA cultures to maintain sufficient D1 protein contents was also the result of obstructed PSII repair mechanisms stemmed from excessive 290-320 nm wavelengths incident on cultures.

The destruction of the photosynthetic apparatus and the oxidation of chlorophyll are both consequences of chronic photoinhibition (Osmond, 1994). Increases in F_o values (i.e. dark adapted minimal fluorescence) indicate damage or loss of PSII reaction centers (Baker, 2008). Increased F_o following UV-B treatment at 100 μmol photons m^{-2} s^{-1} PAR (Figure 1.12A) implies that UV-B radiation applied under low PPFD failed to induce photorepair mechanisms and resulted in PSII destruction. When PPFD was increased to 200 or 600 μmol photons m^{-2} s^{-1}, F_o values increased significantly (Figure 1.12A). Interestingly, these trends were present regardless of whether CA or UA filtered UV-B was applied (Figure 1.12B). Similar increases in F_o values following photoinhibitory light treatment have also been reported in *Chlorella sorokiniana* (Xiong *et al.*, 1999), *Ulva rotundata* (Franklin *et al.*, 1992; Osmond *et al.*, 1993), *Ochromonas danica* (Chrysophyceae; Herrmann *et al.*, 1996) and red algae (Hanelt *et al.*, 1992).

It is worthwhile to note that presuming the photoinactivation of PSII based exclusively on F_o data should be done with caution. Fluorescence *in vivo* is determined by two factors: 1) the physicochemical properties of PSII and 2) the optical properties of the plant/cell (Baker, 2008). Often, optical properties of an organism change in response to an experimental treatment (Δ water content, Δ irradiance, etc.). As a result, the proportion of incident PPFD on the plant that is actually absorbed can fluctuate (Baker,

2008). Additionally, if the experimental treatment facilitates adjustments in thylakoid membrane structure and/or organization, the fraction of absorbed PPFD received by PSII complexes also changes (Baker, 2008). In either case, absolute differences in F_o cannot be used alone to designate PSII reaction center loss (Baker, 2008). However, in the present study, F_o trends were consistent with F_v/F_m ratios (Figure 1.10) and D1 protein data (Figure 1.11), suggesting that PSII photo-deactivation was occurring with CA filtered UV-B treatment.

It is well understood that the careful and precise application of Biological Weighting Functions (BWFs) is essential for comparing the effects of UV radiation exposures that differ from solar UV (Caldwell *et al.*, 1986; Cullen *et al.*, 1992; Cullen and Neale, 1997). However, even under the best conditions, BWFs remain cumbersome and very situation-dependent since they are specific for species, previous growth conditions, current growth conditions, exposure durations, enzyme and genetic responses (Caldwell and Flint, 1997; Neale, 2000; Banaszak and Neale 2001; Micheletti *et al.*, 2003; Krizek, 2004; Caldwell and Flint, 2006). Recently, three BWFs were developed for the inhibition of photosynthesis and growth in *D. tertiolecta* under defined conditions (Andreasson and Wängberg, 2006, 2007). When Andreasson and Wängberg's (2007) photosynthetic carbon fixation weighting function was applied to the 6.0 μmol photons m^{-2} s^{-1} *unweighted* UV-B radiation used in the current study, the presence of additional photons between 290 and 310 nm in the CA irradiance increased the *effective flux density* 59% compared to the UA filtered UV-B (i.e. the biologically effective UV-B radiation (BE_{UV-B}) of CA treatment = 9.54 μmol photons m^{-2} s^{-1} under Andreasson and Wängberg (2007)).

A BWF specific for comparing the effects of UV-B lamp emissions filtered with CA against solar radiation was developed by Behrenfeld *et al.* (1993) for the inhibition of carbon fixation in natural populations of marine phytoplankton. In this case, the excessive UV-B photons in CA filtered radiation increased the *effective flux density* 144% against UA filtered UV-B (i.e. the $BE_{UV\text{-}B}$ of CA treatment = 14.6 μmol photons m^{-2} s^{-1} using Behrenfeld *et al.* (1993) BWF). Therefore, *D. tertiolecta* cultures in the present study receiving 6 μmol photons m^{-2} s^{-1} *unweighted* UV-B through CA filters were essentially experiencing a $BE_{UV\text{-}B}$ of 9 -15 μmol photons m^{-2} s^{-1} solar UV-B flux, while due to the similarities between UA and solar spectra (Figure 1.2), UA cultures received $BE_{UV\text{-}B}$ of 6 μmol photons m^{-2} s^{-1} solar UV-B.

The limitations of BWFs have been recognized (Cullen and Neale, 1997; Deckmyn and Impens, 1997; Ghetti *et al.*, 1998; Ivanov *et al.*, 2000, Neale, 2000; Banaszak and Neale, 2001; Caldwell and Flint, 2006). The broad application of one BWF amongst different species under similar/identical experimental conditions and/or in the same species experiencing slightly altered environments may also lack precision (Caldwell and Flint, 1997). In a recent study, Jahnke and Sampath-Wiley (2009) compared P_{LS} rates of *D. tertiolecta* receiving a range of UV-B irradiances (0- 30 μmol photons m^{-2} s^{-1}) filtered by UA or CA filters. The results of their study determined that even after weighting CA filtered radiation using the BWFs of Andreasson and Wängberg (2007) and Behrenfeld *et al.* (1993), the significant differences between UA and weighted CA filter emissions was upheld. That is, photosynthetic declines with increasing UV-B irradiance were significantly greater in CA treated cultures. Furthermore, Jahnke and Sampath-Wiley (2009) noted that cultures receiving UA filtered radiation could tolerate 24-hour

exposures to UV-B intensities as high as 30 μmol photons m^{-2} s^{-1} (12 Wm^{-2}) without experiencing lethal photobleaching. Consequently, the application of BWFs to *unweighted* data did not fully compensate for the effects of the additional short-wave UV-B present with CA filtration (Jahnke and Sampath-Wiley, 2009).

It is recognized that the CA and UA filtered UV-B radiation used in the current study did not have identical $BE_{UV\text{-}B}$. It is was the fundamental purpose of this investigation to clarify the role of excessive 290-320 nm radiation transmitted by CA on the physiology of *D. tertiolecta*. It was also the intention to propose an alternative filtration technique, in which UV-B lamp emissions are altered to produce UV-B spectra identical to solar flux; thereby eliminating the necessity of BWFs. It was not an objective of this project to determine whether BWFs could realistically account for spectral differences between CA and UA filtration. This aspect of the problem has been addressed by Jahnke and Sampath-Wiley (2009). Here we have shown that the presence of excessive photons between 290-320 nm applied concomitantly with unbalanced UV-B: PAR ratios, contributed directly to the destruction of PSII complexes and is likely involved in hindering PSII repair cycle processes. It has also been demonstrated that when UV-B radiation is applied under a UV-B: PAR ratio of 1:100, photoinhibition is eliminated.

UV-B radiation effects on pigments

The ability of the chloroplast to adapt to changing irradiance is a fundamental growth-response associated with changes in leaf anatomy and morphology, chloroplast structure and the physiology and biochemistry of the plant (Lichtenthaler *et al.*, 1981). Typically, the concentration of total chlorophylls (Chl) and carotenoids are lower in "sun"

chloroplasts compared to "shade" plants (Boardman 1977; Anderson *et al.*, 1988; Lichtenthaler *et al.*, 2007). Moreover, because sun plants are limited by electron transport rather than light capture, they are also equipped with greater ratios of cytochrome *b/f* complexes, ATP synthases, plastoquinone, plastocyanin, ferredoxin and more carbon fixation enzymes (Anderson and Osmond, 1987). Shade plants have more Chl *b* and more of the light-harvesting chlorophyll proteins (PSII LHC and PSI LHC) and pigments for maximal light capture (Anderson *et al.*, 1995). Adjustments to LHC antennae sizes and thylakoid membrane ultra structure are also commonplace in response to changing PPFD (Lichtenthaler, 1981; Baroli and Melis, 1998). Typically, shade plant chloroplasts have a greater thylakoid area, many stacked thylakoids per granum and little stored starch while sun plants possess a smaller thylakoid area, few thylakoids per granum and large starch grains (Lichtenthaler, 1981; Anderson *et al.*, 1988). The results of this study are consistent with these concepts, as pigment contents decreased with increasing PPFD (Figure 1.13).

In general, PSII is more sensitive to UV-B damage than PSI, and because Chl *b* is primarily associated with PSII, any damage to PSII will ultimately yield decreases in Chl *b* contents (Deckmyn et al 1994; Adams and Britz, 1992). While the UV-B induced destruction of chlorophyll molecules has been described (Teramura 1980a,b; Iwanzik et al. 1983; Mirecki and Teramura 1984; Kulandaivelu et al 1989), there is no evidence that UV-B interferes with the chlorophyll biosynthetic pathway; but down regulation of genes crucial for chlorophyll binding proteins has been observed following UV-B treatment (Jordan et al. 1991; Strid and Porra 1992). However, in the present study, Chl *b* contents *increased* following UV-B treatment, with the most significant gains occurring in CA

cultures (Figure 1.14). Because elevated Chl *b* contents are a direct sign of increased pigments associated with PSII, and increased synthesis of PSII complexes typically occur in shaded plants, it could be hypothesized that CA cultures were inducing shade-like responses while undergoing stressful UV-B treatment.

In green algae, high irradiance levels typically elicit a reduction of LHC antenna while low irradiance levels facilitate LHC size increases (Anderson *et al.*, 1988). In experiments on *D. salina*, Baroli and Melis (1998) showed that cells with small PSII light-harvesting antenna (60 *Chl* molecules) experienced significantly less photodamage compared to those with "normal", larger antennae (500 *Chl* molecules). They concluded that increased PSII antenna size enhanced the rate of light absorption and thus, photodamage in the cells. In a separate study on barley, Cleland and Melis (1987) demonstrated that Chl *b*-less mutants with small antenna (50 Chl *a* molecules) had slower rates of photodamage compared to wild type plants that possessed larger antenna containing Chl *b* (Chl *a* + *b*; 250 molecules). The conclusions from these studies are that the mitigation of PSII photodamage by means of increased photosynthetic electron transport was counteracted by increased rates of light absorption.

Why would *D. tertiolecta* establish a shade-like morphology whilst experiencing photochemically damaging UV-B radiation and/or high PPFD? The variation between CA and UA UV-B spectra support the likelihood that the excessive photons between 290-320 nm incident on CA cultures "tricked" *D. tertiolecta* into establishing a ultrastructure and/or morphology indicative of shade plants. Fagerberg (2007) demonstrated that sunflower (*Helianthus annuus* L.) receiving below ambient amounts of CA filtered UV-B radiation (0.05 μmol photons m^{-2} s^{-1}/ 0.021 W/m^2) under both high (550-600 μmol

photons m^{-2} s^{-1}) and low (130-150 μmol photons m^{-2} s^{-1}) PPFD altered their thylakoids to that typical of shaded plants. In a related study, Fagerberg and Bornman (1997) demonstrated that *Brassica* elicits a chloroplast ultrastructure and biochemistry indicative of shading responses following exposure to above ambient levels of UV-B (13kJ m^{-2} day^{-1}). Fagerberg (2007) proposed that changes in chloroplast volume/structure following UV-B exposure could be facilitated by deceptive signaling responses in chloroplast osmoregulation. Hence, the curious increases in Chl *b* content observed in the current study (Figures 1.14A & C) could be an indication that *D. tertiolecta* cultures were fooled into establishing shade-like chloroplast ultrastructure during exposure to UV-B radiation with excessive short-wave UV-B. If this was the case, then increased PSII antenna size and/or increased thylakoid surface area would have exacerbated photoinhibitory damages and exacerbated photosynthetic inhibition; as seen in the present study (Figures 1.8 & 1.10).

Antioxidant Responses

Carotenoids are often regarded for their role as accessory pigments in photosynthesis, yet they do play a fundamental antioxidant role in the chloroplast. Photoinhibitory attacks on PSII generate $^1O_2$ and triplet state chlorophyll (Smirnoff, 1993), both of which are scavenged by carotenoids offering localized chloroplast protection against lipid peroxidation and blocking radical chain reactions. Further evidence that excessive short-wave UV-B radiation is responsible for indirectly inducing ROS formation in the chloroplast was demonstrated by the significant increase in total carotenoid contents of

CA cultures (Figure 1.14B) in addition to similar increases in both APX and SOD activities (Figure 1.15A & B).

UV-B induced photosynthetic damage with the indirect formation of ROS has been previously reported (Lesser and Shick, 1989; Malanga and Puntarulo, 1995; Vass 1997; Langebartels *et al.*, 2002). In experiments on the zooxanthellae *Symbiodinium* sp., Lesser and Shick (1989) showed a 40% increase in SOD activity following UVR treatment and concluded that ROS formation was an important consequence of UV photoinhibition. Correspondingly, Lesser (1996a, b) showed that elevations in SOD and APX activities were correlated with increased H_2O_2 and O_2^- production following exposure to UVR in the dinoflagellate *Prorocentrum micans*.

In contrast with the findings of CA cultures, the antioxidant enzymes activities of UA cultures were consistent with research suggesting that exposure to elevated solar UV-B will not cause heightened oxidative stress and ROS formation (White and Jahnke, 2002). In their study on *Dunaliella* sp., White and Jahnke (2002) exposed cultures growing at 35 or 150 μmol photons $m^{-2} s^{-1}$ PAR to 1.9 μmol photons $m^{-2} s^{-1}$ (0.76 Wm^{-2}) UV-B for 24 hours, after which cells did not exhibit any signs of photoinhibitory damages or increased ROS formation.

The sensitivity of catalase to high irradiance and UV-B radiation is well documented (Cheng *et al.*, 1981; Polidoros and Scandalios, 1997; Aubailly *et al.*, 2000). Therefore, it was not surprising to find that catalase activities decreased following UV-B treatment (for both UA and CA; Figure 1.15C) and at higher PAR levels (Figure 1.16B). Irreversible inactivation of catalase occurs directly *via* light absorption of the heme moieties and indirectly through the photooxidative processes occurring in the chloroplast

(Grotjohann *et al.*, 1997). Shang and Feierabend (1999) determined that chloroplast mediated catalase inactivation in the peroxisome occurs *in vivo* either directly or indirectly through ROS generated during chloroplast electron transport processes. Therefore, it is possible that the decreases in catalase activity observed in the present study were the result of the direct absorption of excessive short-wave UV-B radiation by heme in addition to the destruction of catalase protein by chloroplast generated ROS.

Interestingly, Heck *et al.* (2003) reported that keratinocytes (epidermal cells) over-expressing catalase harbored increased ROS production following UV-B treatment. They (Heck *et al.*, 2003) proposed that direct interactions between UV-B wavelengths and catalase facilitated heightened production of reactive chemical intermediates, which necessitated detoxification by other antioxidant enzymes. They also suggested that the accumulation of excessive ROS *via* catalase intensified the overall oxidative stress and DNA damage experienced by the cells. Heck *et al.* (2003) is obviously at odds with much of the literature, which portrays catalase as an *anti*oxidant enzyme. It is quite speculative to consider that catalase may be acting as some kind of screening pigment (e.g. flavonoids, MAAs, β-carotene, etc.) ameliorating the damaging effects of high-energy UV-B photons by defensively producing ROS. Although this hpothesis is controversial, it is feasible that direct absorption of light by catalase would generate ROS. Any protein that has a tryptophan (Trp), tyrosine (Tyr) or phenylalanine (Phe) residue is capable of absorbing UV-B photons ($\lambda_{max} \approx 280$nm). Absorbance of a photon, especially by a Trp, can lead to a single electron oxidation of the residue and the reduction of oxygen to superoxide (Walrant and Santus, 1974; Caldwell, 1993; Greenberg *et al.*, 1997). Yet, it is

doubtful that *D. tertiolecta* contains a high enough cellular catalase concentration to perform this type of screening.

Role of UV-A radiation emitted by UV-B lamps.

Photoreactivation requires UV-A and/or short wave visible light. Therefore, because UA filtered UV-B lamp emissions contain twice the UV-A flux of CA filtered lamp emissions when *equal fluxes* of UV-B are used (Jahnke and Sampath-Wiley, 2009), it could be hypothesized that the lack of UV-B induced photoinhibition in UA cultures was the result of heightened photoreactivation processes[1].

Consequently, in order to clarify whether the lack of observable photoinhibition in UA cultures was the result of excessive UV-B removal or due to the doubling of incident UV-A radiation, experiments in which UV-A radiation were removed from UV-B lamp emissions were performed (Figure 1.4). Photosynthesis and oxidative stress parameters of *D. tertiolecta* exposed to UA filtered UV-B lamp emissions with (UA) and without (UA + K_2CrO_4) UV-A radiation were performed (Table 1.3). The results clearly indicated that the added UV-A radiation incident on UA cultures did not impose any physiological benefits (or impairments; Table 1.3).

These findings support the idea that the deviations from UV-B solar flux present following CA filtration of UV-B lamp emissions are directly responsible for eliciting photoinhibitory and oxidative stresses on plant cells, which are eliminated following UA filtration. The fact that the photooxidative damages reported in studies using CA filtered

[1] In other words, cultures using UA filtration were receiving 6 μmol photons $m^{-2}s^{-1}$ UV-B + 12 μmol photons $m^{-2}s^{-1}$ UV-A while CA cultures received 6 μmol photons $m^{-2}s^{-1}$ UV-B + 6 μmol photons $m^{-2}s^{-1}$ UV-A.

UV-B radiation may be an exaggeration of the "true" effects of solar UV-B flux have been raised. Most importantly, this work highlighted that through the use of UA filters, UV-B lamp emissions can be modified into a spectrum nearly identical to solar flux thereby producing an accurate representation of "biological" UV-B radiation without the use of BWF.

CONCLUSIONS

The significance of seemingly small spectral divergences between CA and UA transmitted UV-B radiation were emphasized as was the importance of using more realistic UV-B: PAR ratios. The excessive short-wave UV-B radiation transmitted by CA filtration facilitated direct damage to the PSII complex and was likely responsible for hindering PSII repair processes. This problem was exacerbated when PPFD was applied at low levels distorting natural UV-B: PAR ratios and was compounded by the indirect generation of ROS. Moreover, the divergences between CA transmitted UV-B and solar flux necessitates the use of BWFs, which can be cumbersome and imprecise. These challenges were met by the use of a novel UA filter, which removes those portions of 290-320 nm radiation that differ from solar UV-B and yields a UV-B spectral profile nearly identical to that of solar flux. We have shown that the removal of these contaminating 290-320 nm wavelengths from lamp emissions, and not the presence of additional UV-A radiation, eliminates commonly described UV-B induced photodamages. The results of this study suggest that increased UV-B radiation incident at

the earth's surface (due to increased atmospheric ozone depletion) may not lead to decreased photosynthetic performance or heightened oxidative stress. Similar conclusions have also been reached in studies using different methodologies (Fiscus and Booker, 1995; Allen *et al.*, 1998; Searles *et al.*, 2001; Nogues *et al.*, 2006).

In conclusion, CA filtration of UV-B lamp emissions generate substantial physiological stresses that are not representative of effects likely to transpire with increasing UV-B irradiances reaching the Earth's surface. This oversight is common in laboratory and field based UV-B experiments that make use of fluorescent UV-B lamps and thus, caution should be used when inferring ecological trends from these data. To compensate for the shortcomings of CA and gather ecologically relevant data, we suggest using the novel UA filter and a UV-B: PAR ratio that is in accordance with solar flux.

CHAPTER II

ULTRAVIOLET-A (UV-A) RADIATION IS A MAJOR SOURCE OF UV-INDUCED PHOTOINHIBITON AND OXIDATIVE STRESS IN *DUNALIELLA TERTIOLECTA*

ABSTRACT

There is relatively little information known regarding the effects of ultraviolet-A (UV-A) radiation on primary producers like phytoplankton. Efforts to elucidate the role of UV-A flux on key processes like photosynthesis have been limited since the depletion of stratospheric ozone has been linked to increased transmittance of UV-B (but not UV-A) irradiance into the biosphere. To gain insight into the physiological impact of UV-A radiation, photosynthesis and oxidative stress responses in cultures of the unicellular green alga *Dunaliella tertiolecta* were monitored before and after treatment with UV-A flux. Cultures grown under low (100 μmol photons m^{-2} s^{-1}) and high (600 μmol photons m^{-2} s^{-1}) photosynthetically active radiation (PAR) were treated for 12 hours with 60 μmol photons m^{-2} s^{-1} (20.55 Wm^{-2}) UV-A with and without the presence of UV-B flux (6 μmol photons m^{-2} s^{-1}; 2.4 Wm^{-2}). UV-A radiation applied alone caused significant declines in photosynthesis and PSII efficiency, while dark-adapted minimal (F_o) and maximal (F_m) fluorescence parameters increased. The activities of the antioxidant enzymes superoxide dismutase (SOD), ascorbate peroxidase (APX) and monodehydroascorbate reductase (MDHAR) also increased following exposure to UV-A radiation. The incorporation of

UV-B flux did not yield further photosynthetic stress and surprisingly lead to reductions in SOD, APX and catalase. The relevance of the UV: PAR ratio is addressed, as are the interactive effects of UV-B + UV-A flux in mitigating UV-induced injuries.

INTRODUCTION

Since the realization of atmospheric ozone depletion, there has been intense effort to assess the biological impact of increased ultraviolet-B (UV-B) radiation penetrating the troposphere. Because ultraviolet-A (UV-A; 320- 400 nm) radiation is not attenuated by atmospheric ozone, experimental efforts to elucidate its photobiological roles have for the most part, been inadequate. Although a UV-B photon carries slightly more energy than a photon in the UV-A range, UV-A wavebands reach the Earth's surface at flux densities ten times that of UV-B. As a result, 40-50% of the photosynthetic inhibition occurring in natural phytoplankton communities is driven by UV-A, while only 10% is attributable to UV-B radiation (Cullen *et al.*, 1992; Helbling *et al.*, 1992; Holm-Hansen *et al.*, 1993).

Susceptibility to UV-A induced photoinhibitory damages has been shown in higher plants (Nayak *et al.*, 2003), phytoplankton (Cullen *et al.*, 1992; Helbling *et al.*, 1992; Holm-Hansen *et al.*, 1993; Cullen and Neale, 1994; Kim and Watanabe, 1993, 1994) and within isolated thylakoids (Turcàsanyi and Vass, 2000). However, the exact target(s) of UV-A damage are currently unresolved. Both the water oxidizing complex and the Q_B -binding site of PSII have shown vulnerability to UV-A (Joshi *et al.*, 1997; Turcàsanyi and Vass, 2000; Nayak *et al.*, 2003), while carbon fixation enzymes like

ribulose bisphosphate carboxylase/oxygenase (RuBisCO) are also suspected to sustain direct injury by UV-A flux (Figueroa *et al.*, 1997; Bischof *et al.*, 2000; Grzymski *et al.*, 2001).

In contrast to UV-B, which is absorbed directly by deoxyribonucleic acid (DNA) and proteins (Krizek, 2004), UV-A radiation is absorbed by non-DNA primary chromophores including photosensitizers. Ultimately, a photosensitizer electronically excited by an UV-A photon can produce reactive oxygen species (ROS) that are destructive to nucleic acids, proteins and lipids (Peak and Peak, 1986). Consequently, it is the indirect damage to DNA and protein molecules by way of ROS that allows UV-A radiation to be damaging to both plant and animal cells (Tyrrell, 1991; Jeffrey and Mitchell, 1997).

Interactions between UV/ROS and DNA molecules also generate cyclobutane pyrimidine (CPD) and pyrimidine (6-4) pyrimidione dimers (6-4 PP; Lesser, 2006). There are two mechanisms in plants that repair CPD and 6-4 PP DNA mutations (1) photoenzymatic repair requiring a photolyase enzyme and (2) nucleotide excision repair (e.g. dark repair; Krizek, 2004). DNA damaged by UV radiation is repaired using near UV/blue light and photolyase enzymes in process called photoreactivation (Britt, 2004). Photolyase is energized exclusively by 320-500 nm wavebands and restores damaged DNA by reversing pyrimidine dimer bonds (Kimura *et al.*, 2004). Dark repair includes nucleotide excision repair in which damaged DNA is recognized, removed and a newly synthesized DNA segment is ligated into the strand (Kimura *et al.*, 2004). Dark repairs do not require light activation and are therefore independent of photoreactivation processes.

It is known that elevated levels of photosynthetically active radiation (PAR) can lessen damages sustained by UV-B radiation (Warner and Caldwell, 1983; Mirecki and Teramura, 1984). UV-A radiation has also been shown to provide similar protection (Caldwell *et al.*, 1994; Krizek, 2004; Joshi *et al.*, 2007). Although the protective properties of both PAR and UV-A against UV-B induced injuries are well described, only a handful of studies have addressed the individual and interactive effects of UV-A with PAR and/or UV-B (Caldwell *et al.*, 1994; Deckmyn *et al.*, 1994; Middleton and Teramura, 1994; Shelly *et al.*, 2003). It was therefore the goal of this project to (1) investigate the direct effect of UV-A radiation whilst examining variations in the UV-A: PAR ratio, (2) produce an irradiance environment in a laboratory setting representative of solar UV-B: UV-A: PAR ratios (i.e. 1:10:100; Döhler *et al.*, 1997; West *et al.*, 1999; Zudaire and Roy, 2001) and (3) compare and contrast the effects of UV-A and UV-B + UV-A radiations on plant cell physiology. Specifically, this research sought to determine the individual and interactive effects of UV-A + PAR with and without the presence of UV-B radiation on photosynthesis and oxidative stress responses using the unicellular green alga *Dunaliella tertiolecta* Butcher as an experimental model.

MATERIALS AND METHODS

Cultures of *Dunaliella tertiolecta* (Chlorophyta) were grown and maintained as described in Chapter I Materials and Methods. PAR was provided by two high output cool-white fluorescent lamps (100 μmol photons m^{-2} s^{-1} PAR; 100 PAR) or by eight Commercial

Electric 42W compact fluorescent white light bulbs (600 μmol photons m^{-2} s^{-1} PAR; 600 PAR). All experiments began using cultures acclimated to experimental PAR treatment levels without UV exposure and a chlorophyll density between 1.0-1.5 μg chl ml^{-1}. All experiments were conducted using cell suspensions within 28 x 200 mm quartz tubes. Because fluorescent lamps are known to emit a small flux of UV radiation, a layer of UV-blocking plastic film that absorbs all radiation below 395nm was placed between the water bath and the fluorescent light bank to remove any extraneous UV radiation (Edmund Scientific, Barrington, NJ type G39, 426).

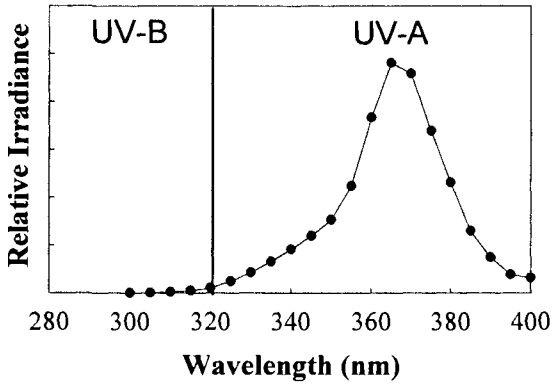

Figure 2.1.Wavelength distribution of radiation emitted by UV-A lamps. UV-A radiation was produced using one Sylvania (18") F15T8/350BL lamp and one GE (18") BLB lamp. Radiation was measured with a spectroradiometer fiber optics probe placed within culture tubes *in situ* as described in Materials and Methods.

UV-A flux was produced using one 18" Sylvania F15T8/350BL and one 18" GE F15T8/BLB lamp placed on the side of the water bath opposite the cool-white lamps so that manipulation could occur independently of PAR. The employment of two different UV-A lamps broadened the emission spectrum as compared to using only a single lamp

type (Figure 2.1). In experiments requiring the use of both UV-A and UV-B radiation, two National Biological Corporation 24" UV-B lamps were incorporated into the UV-A light bank so that all ultraviolet (UV) radiation was applied simultaneously from one side of the water bath (Figure 2.2). UV flux densities were altered by changing the distance of the lamps to the cultures and/or by inserting stainless steel screens between the UV lamps and the culture tubes. All UV-B + UV-A radiation was filtered through a 0.26 mM UA liquid filter as detailed in Chapter I Material and Methods. Cultures receiving no UV radiation (i.e. controls) were produced using UV-blocking film (Edmund Scientific). All experiments were performed using 12-hour UV radiation exposures under continuous PAR. Solar UV radiation data was measured by Michael P. Lesser during May at the Isle of Shoals in the Gulf of Maine (latitude N42.98925) under less than 10% cloud cover and a standard ozone (0.327 cm-ATM; personal communication).

The total UV irradiance incident on experimental cells was determined *in situ* using the potassium ferrioxalate chemical actinometer of Hatchard and Parker (1956). The actinometer measurements of total radiation intercepted were partitioned into UV-B, UV-A and blue wavebands based on previously described fractional distributions (Jahnke and Sampath-Wiley, 2009; White and Jahnke, 2004). The spectral distribution of the UV radiation was determined using a spectroradiometer (International Light model 1700/760D/783, Newburyport, MA) with a 2 nm bandpass and a fiber-optics probe calibrated by International Light. PAR density (400-700nm) was measured with a Li-Cor LI-185 D quantum radiometer. Photosynthesis rates, pigment contents, fluorescent parameters, antioxidant enzyme activity rates and western blotting procedures were conducted as detailed within Chapter I Material and Methods.

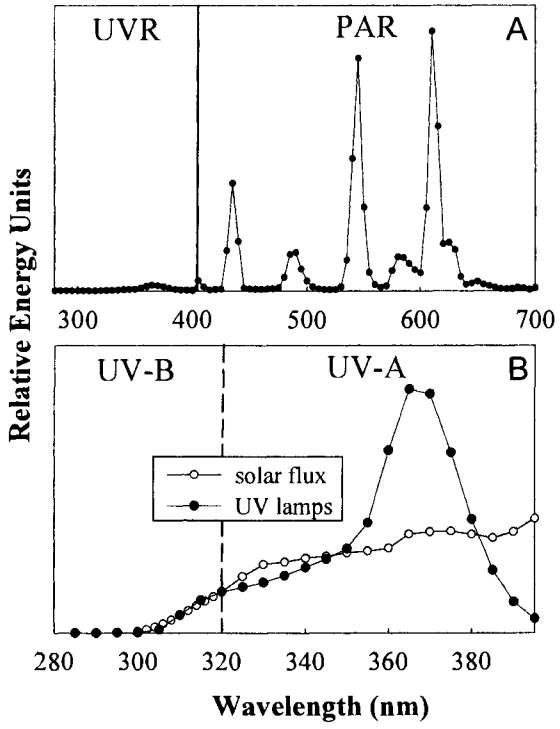

Figure 2.2. Wavelength distribution of irradiance flux incident on cultures. A) Relative energy from 290-700 nm experienced by cultures. Visible radiation was provided by eight Commercial Electric (42 Watt) white lamps. UV-B was supplied by two NBC (24") lamps. UV-A radiation was produced by one Sylavania (18") F15T8/350BL and one GE F15T8 BLB lamp. Wavelengths were normalized at 610 nm. B) Comparison between UV-B and UV-A spectra applied against solar flux as measured by M.P. Lesser. Radiation was measured using a spectroradiometer fiber optics probe placed within culture tube *in situ*. Wavelengths normalized at 320nm.

The effects of UV-A and UV-B + UV-A radiations on photosynthesis were tested separately for each PAR level (100 or 600 PAR) as one-way ANOVAs with UV treatment as the experimental factor (i.e. control *vs.* UVR). Individual and interactive effects of UV and PAR treatments on D1 protein, pigment contents and antioxidants were tested as 2 x 2 factorial ANOVAs with PAR level (100 or 600 PAR) and UV treatment (i.e. control *vs.* UVR) as experimental factors. Western blot quantifications were performed by initially

$\log_{10}$ transforming ImageJ optical density data prior to ANOVA analysis. Graphical data are representative of back-transformed mean values and standard errors. Tukey's pairwise comparisons were made where applicable. All calculations were done using SYSTAT v. 12 (Systat, Inc.).

RESULTS

UV-A radiation effects on photosynthesis and antioxidants

UV-A flux densities were applied at 60 μmol photons $m^{-2}s^{-1}$ (20.55 Wm^{-2}; see Appendix A for flux density and cumulative dose values) and coupled with either 100 or 600 μmol photons $m^{-2}s^{-1}$ PAR so that the UV-A: PAR ratios were 1: 1.7 and 1:10, respectively. As a result, the low PAR cultures experienced an irradiance environment very dissimilar to solar flux (but common in much laboratory research), while the high PAR cultures were subjected to irradiance densities comparable to natural radiation.

Following UV-A treatment, photosynthetic rates (P_{LS} and P_{LL}) decreased regardless of which PAR level was applied (Table 2.1). The light-limited: light saturated photosynthetic ratio (P_{LL}: P_{LS}) and the ratio of variable to maximal fluorescence (F_v/F_m) also dropped 22-27%, at both PAR densities (Table 2.1). UV-A radiation generated a 91% and 52% increase in the dark adapted fluorescence (F_o) in 100PAR and 600PAR cultures, respectively. Dark adapted maximal fluorescence (F_m) values increased significantly only in cells growing under 100PAR (Table 2.1). F_m values in 600APR cultures were not affected by UV-A treatment (Table 2.1). The relative quantities of D1

protein in 100 PAR cultures decreased 67% after UV-A treatment ($p = 0.001$), yet remained unchanged under 600PAR ($p = 0.999$; Figure 2.3).

Table 2.1. Effect of UV-A radiation on photosynthesis. *D. tertiolecta* cultures growing at 100 or 600 μmol photons m^{-2} s^{-1} PAR were treated for 12 hours with 60 μmol photons m^{-2} s^{-1} UV-A radiation (20.55 Wm^{-2}). Control cultures were maintained using UV-blocking film. P_{LS} (light-saturated) and P_{LL} (light-limited) photosynthetic rates (μmol O_2 mg chl^{-1} h^{-1}); F_v/F_m (variable to maximal fluorescence ratio); F_o (dark adapted minimal fluorescence); F_m (dark adapted maximal fluorescence). Data represent means of at least n = 10 samples per treatment ± one standard error. P-values are results from one-way ANOVAs. Bolded values represent statistical significance.

Response	PAR (μmol photons $m^{-2}s^{-1}$)	Mean ± SE	% control	p-value
P_{LS} (μmol O_2 mg $chl^{-1}h^{-1}$)	100	207.8 ± 8	77	**< 0.001**
	600	271.2 ± 19	68	**< 0.001**
P_{LL} (μmol O_2 mg $chl^{-1}h^{-1}$)	100	72.8 ± 6	58	**< 0.001**
	600	63.8 ± 10	52	**0.001**
P_{LL}: P_{LS}	100	0.346 ± 0.02	75	**< 0.001**
	600	0.232 ± 0.02	78	**0.023**
Fv/Fm	100	0.527 ± 0.01	76	**< 0.001**
	600	0.492 ± 0.02	73	**< 0.001**
F_o	100	70.75 ± 2.4	191	**< 0.001**
	600	62.7 ± 2.7	152	**< 0.001**
F_m	100	149.7 ± 2.8	122	**< 0.001**
	600	123.4 ± 3.2	98	0.974

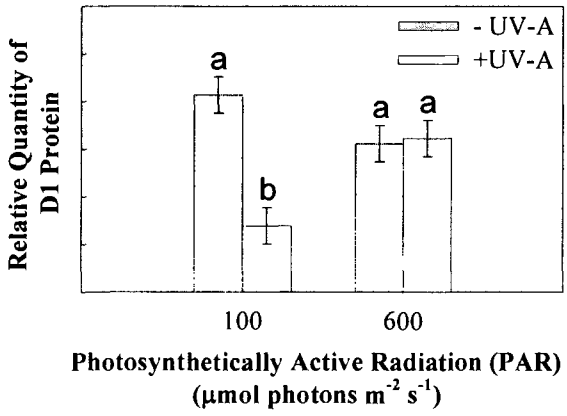

Figure 2.3. Relative quantity of D1 protein following exposure to UV-A radiation. *D. tertiolecta* cultures growing at 100 and 600 μmol photons m^{-2} s^{-1} PAR were treated for 12 hours to 60 μmol photons m^{-2} s^{-1} (20.55 Wm^{-2}) UV-A radiation (+ UV-A). Control cultures (- UV-A) were established using UV-blocking film. Data are representative of n = 5 mean values per treatment ± one standard error.

In all cases, cultures grown at 600 PAR possessed significantly less pigment content than those growing at 100 PAR and were not affected by treatment with UV-A radiation (Figure 2.4). In contrast, the pigment profile of 100 PAR cultures was sensitive to UV-A radiation, with these cells losing 18% of their total chlorophyll (total chl) and chlorophyll *a* (chl *a*) contents (Figure 2.4). UV-A did not produce significant alterations in carotenoids or chlorophyll *b* (chl *b*) at either PAR level.

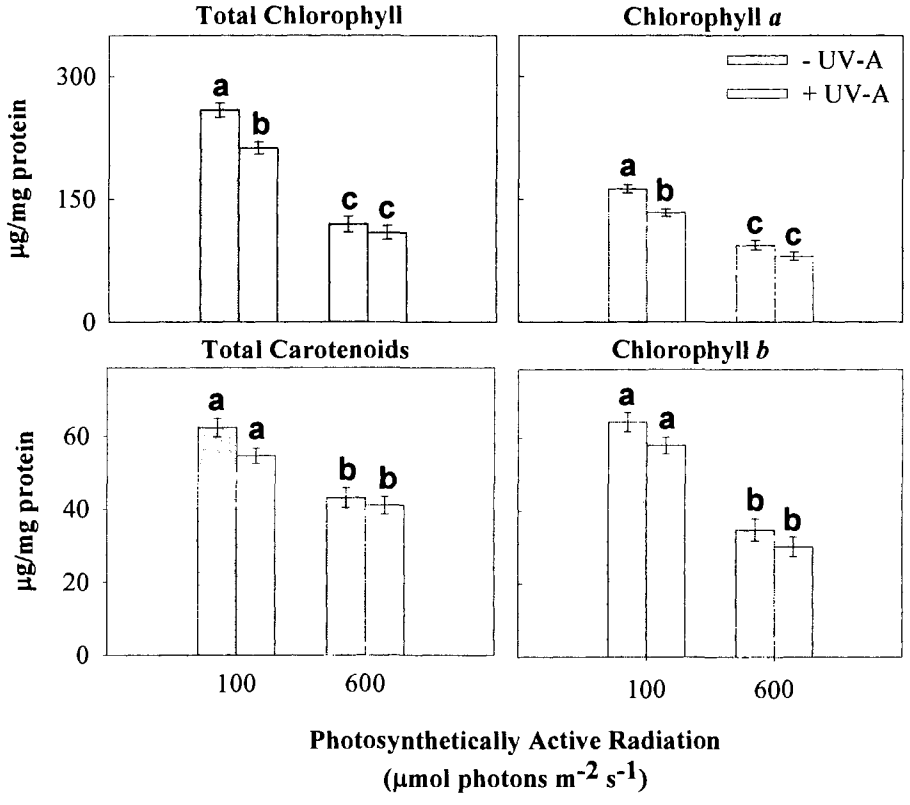

Figure 2.4 Photosynthetic pigment contents following treatment with UV-A radiation. *D. tertiolecta* growing under 100 and 600 µmol photons $m^{-2}s^{-1}$ PAR were treated for 12 hours to 60 µmol photons $m^{-2}s^{-1}$ (20.55 Wm^{-2}) UV-A radiation unfiltered (+ UV-A) or filtered by UV-blocking film (- UV-A). Data represent mean of at least n = 10 samples per treatment. Error bars are ± one standard error. For a particular pigment, means with the same letter are not statistically different ($\alpha = 0.05$).

The effect of UV-A radiation on APX activity was dependent on the PAR level applied (Table 2.2). At both PAR densities, exposure to UV-A yielded increased APX activity however, the rates of 100 PAR cultures were 88% higher compared to 600 PAR cultures ($p = 0.002$; Figure 2.5). Catalase activity rates dropped 32% between 100 and 600PAR (Figure 2.6) and were also negatively affected by UV-A treatment (Figure 2.7c). Conversely, superoxide dismutase (SOD) and monodehydroascorbate reductase

(MDHAR) activities increased 17% and 42%, respectively, after treatment with UV-A, regardless of whether 100 or 600 PAR was applied (Table 2.2; Figure 2.7).

Table 2.2. ANOVA results (p-values) for antioxidant enzymes following exposure to UV-A radiation. *D. tertiolecta* cultures were treated for 12 hours with 60 μmol $m^{-2}s^{-1}$ (20.55 Wm^{-2}) UV-A radiation. Experimental factors were PAR level (100 or 600 μmol m^{-2} s^{-1}) and UV-A radiation level (0 or 60 μmol m^{-2} s^{-1}). P-values are results from 2 x 2 factorial ANOVAs. Bolded values represent statistical significance. Values < 0.05 that are not bolded indicate that a significant interaction with another experimental factor is present.

Response	Main Effects		Interactive Effect
	PAR level	UV-A level	PAR x UV-A
APX	0.033	<0.001	**0.005**
GTR	0.103	0.131	0.477
SOD	0.069	**0.022**	0.115
MDHAR	0.96	**<0.001**	0.068
Catalase	**<0.001**	**<0.001**	0.944

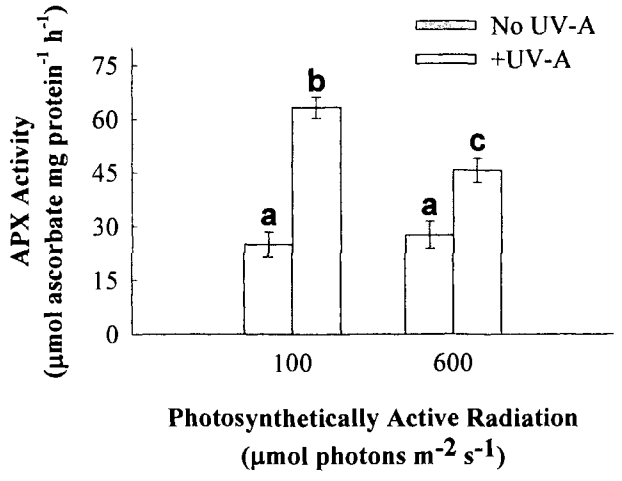

Figure 2.5. Ascorbate peroxidase activity following UV-A radiation treatment. *D. tertiolecta* cultures growing under 100 or 600 µmol m^{-2} s^{-1} PAR were exposed to 60 µmol m^{-2} s^{-1} (20.55 Wm^{-2}) UV-A radiation (+ UV-A) for 12 hours. Control cultures were established using UV-blocking film (- UV-A). Data represent mean of n = 10 samples per treatment ± one standard error. Means with the same letter are not statistically different ($\alpha = 0.05$).

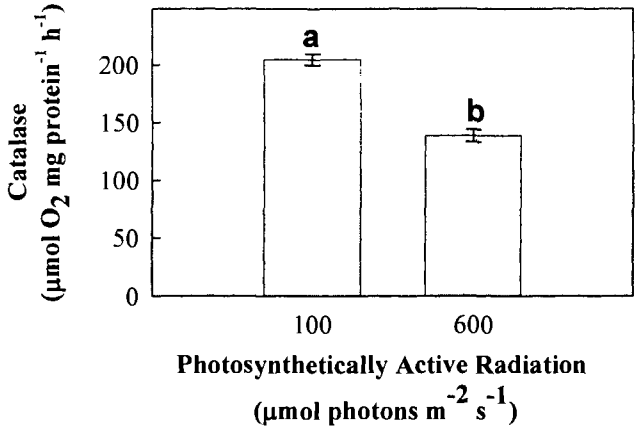

Figure 2.6. Effect of photosynthetically active radiation (PAR) level on catalase activity. *D. tertiolecta* cultures growing under 100 or 600 µmol m^{-2} s^{-1} PAR were exposed to 60 µmol m^{-2} s^{-1} (20.55 Wm^{-2}) UV-A radiation (+ UV-A) for 12 hours. Data represent mean of n = 25 samples per treatment ± one standard error. Means with the same letter are not statistically different ($\alpha = 0.05$).

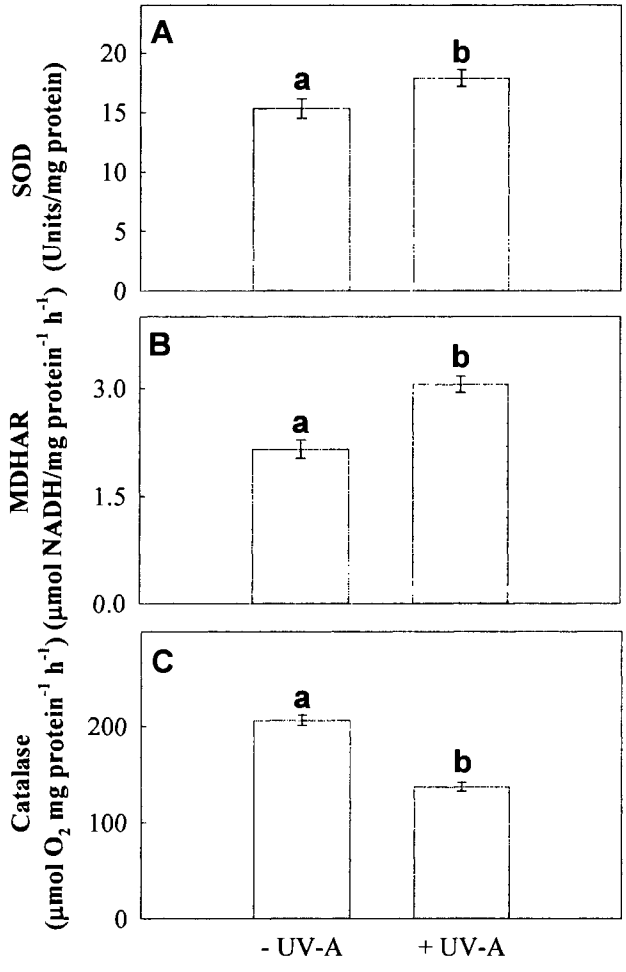

Figure 2.7. Enzyme activities of SOD, MDHAR and catalase in response to UV-A radiation. Enzyme activities of A) superoxide dismutase (SOD) B) monodehydro-ascorbate reductase (MDHAR) and C) catalase were recorded after 12-hour exposures to 60 μmol m^{-2} s^{-1} (20 Wm^{-2}) UV-A radiation (+ UV-A). Control cultures were established using UV-blocking film (- UV-A). Experiments were performed at 100 and 600 μmol m^{-2} s^{-1} PAR. Data represent mean of at least n = 10 samples per treatment. Error bars are ± one standard error. For a particular enzyme, means with the same letter are not statistically different ($\alpha = 0.05$).

Production of simulated solar radiation in the laboratory

To simulate a solar-like UV spectrum (290- 400 nm), 6 μmol photons $m^{-2}s^{-1}$ (2.4 Wm^{-2}) UV-B radiation was added to 60 μmol photons m^{-2} s^{-1} (20.55 Wm^{-2}) UV-A flux (Figure 2.2). Under these conditions, all cultures treated with UV radiation experienced a UV-B: UV-A intensity consistent with natural flux ratios (i.e. 1: 10). However, the addition of 100 or 600 PAR produced an irradiance environment with a UV-B: UV-A: PAR flux ratio of either 1: 10: 17 or 1:10:100, respectively. Consequently, 100PAR cultures received an imbalanced UV: PAR ratio, while the 600PAR cultures experienced an irradiance environment comparable to solar flux.

For all of the photosynthetic parameters measured, the addition of UV-B flux caused no further damage. That is, the application of UV-B + UV-A radiation generated photosynthesis rates and fluorescence measurements that were statistically identical to those obtained following treatment with UV-A radiation alone (Table 2.3). The addition of UV-B radiation caused significant declines in all measured photosynthetic pigments in cultures growing at 100PAR ($\alpha = 0.5$), with total chl, chl *a*, chl *b* and carotenoid contents decreasing 33%, 28%, 48% and 29%, respectively (Figure 2.8). Pigment contents of 600PAR cultures were unaffected by the addition of UV-B radiation (Figure 2.8).

Table 2.3. Comparison of UV-A and UV-B + UV-A radiation on photosynthesis. *D. tertiolecta* cultures growing under 100 or 600 μmol photons m^{-2} s^{-1} PAR were treated for 12 hours with 60 μmol photons $m^{-2}s^{-1}$ (20.55 Wm^{-2}) UV-A radiation (UV-A) or 6 μmol photons $m^{-2}s^{-1}$ (2.4 Wm^{-2}) UV-B + 60 μmol photons $m^{-2}s^{-1}$ UV-A radiation (UV-B +UV-A). P_{LS} (light-saturated) and P_{LL} (light-limited) photosynthetic rates (μmol O_2 mg chl^{-1} h^{-1}); F_v/F_m (variable to maximal fluorescence ratio); F_o (dark adapted minimal fluorescence); F_m (dark adapted maximal fluorescence). Data represent means of n = 10-18 samples per treatment ± one standard error. Percent change between UV-A and UV-B + UV-A values are given (% Δ). P-values are results from one-way ANOVAs. Bolded values represent statistical significance.

Response	PAR (μmol photons $m^{-2}s^{-1}$)	UVR	Mean ± SE	% Δ	p-value
P_{LS}	100	UV-A	207.8 ± 13	1.7	0.997
		UV-A + UV-B	211.4 ± 12		
	600	UV-A	271.2 ± 14	2.5	0.984
		UV-A + UV-B	264.5 ± 12		
P_{LL}	100	UV-A	72.8 ± 6	16.1	0.501
		UV-A + UV-B	61.1 ± 6		
	600	UV-A	63.8 ± 7	16.9	0.616
		UV-A + UV-B	74.6 ± 6		
P_{LL}/P_{LS}	100	UV-A	0.353 ± 0.02	18.1	0.055
		UV-A + UV-B	0.289 ± 0.02		
	600	UV-A	0.232 ± 0.02	17.6	0.435
		UV-A + UV-B	0.273 ± 0.02		
Fv/Fm	100	UV-A	0.527 ± 0.02	7.8	0.494
		UV-A + UV-B	0.486 ± 0.02		
	600	UV-A	0.492 ± 0.02	2.2	0.984
		UV-A + UV-B	0.503 ± 0.02		
F_o	100	UV-A	70.8 ± 5.6	26.1	0.094
		UV-A + UV-B	89.3 ± 5.3		
	600	UV-A	62.7 ± 6.6	8.1	0.930
		UV-A + UV-B	57.6 ± 5.4		
F_m	100	UV-A	149.7 ± 8.4	16.2	0.165
		UV-A + UV-B	174.1 ± 8.0		
	600	UV-A	123.41 ± 9.7	0.5	1.000
		UV-A + UV-B	122.8 ± 8.0		

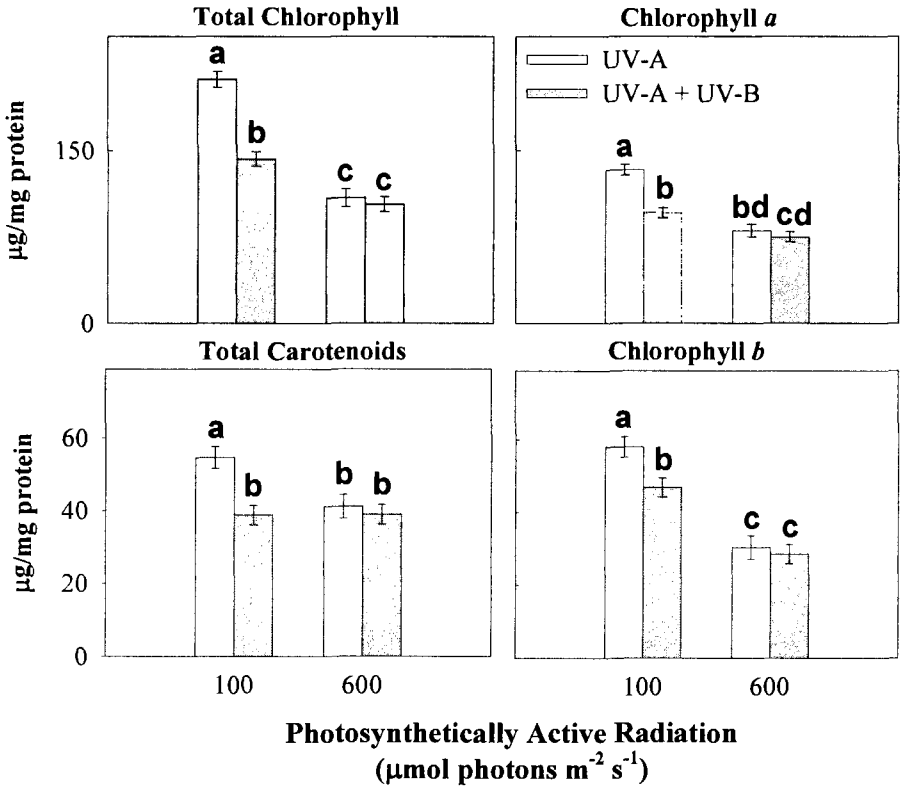

Figure 2.8 Photosynthetic pigment contents between UV-A and UV-B + UV-A radiation environments. *D. tertiolecta* cultures growing at 100 or 600 µmol photons $m^{-2}s^{-1}$ PAR were treated for 12 hours with 60 µmol photons $m^{-2}s^{-1}$ (20.55 Wm^{-2}) UV-A (UV-A) or 60 µmol photons $m^{-2}s^{-1}$ UV-A + 6 µmol photons $m^{-2}s^{-1}$ (2.4 Wm^{-2}) UV-B (UV-A +UV-B) radiation filtered by a 0.26 mM urate solution. Data represent mean of n = 12-18 samples per treatment. Error bars are ± one standard error. For a particular pigment, means with the same letter are not statistically different ($\alpha = 0.05$).

The application of UV-B +UV-A flux caused a 53% decline in APX activity (Table 2.4; Figure 2.9). Elevating PAR from 100 to 600 μmol photons m^{-2} s^{-1} also prompted a 33% drop in APX activities (Table 2.4; Figure 2.10). Differences in the activities of SOD and catalase between the UV-A and UV-B + UV-A irradiation environments were contingent on whether low or high PAR was applied (Table 2.4). Under 100PAR, SOD activities did not differ between UV-A and UV-B + UV-A treatments ($p = 0.269$), but declined 27% in 600PAR, cultures after UV-B flux was incorporated ($p = 0.023$; Figure 2.11a). Alternatively, the addition of UV-B radiation generated significant declines in catalase activity, regardless of whether low or high PAR was applied ($p \leq 0.001$), with catalase rates dropping 45% and 32% within 100 and 600PAR cultures, respectively (Figure 2.11b). The activity rates of glutathione reductase (GTR) remained consistent for all experimental treatments (Table 2.2).

Table 2.4. ANOVA results (p-values) for antioxidant enzyme activities following UV exposure. *D. tertiolecta* were treated for 12 hours with 60 μmol m^{-2} s^{-1} (20.55 Wm^{-2}) UV-A or 60 μmol m^{-2} s^{-1} UV-A + 6 μmol m^{-2} s^{-1} (2.4 Wm^{-2}) UV-B radiation. Experimental factors were PAR (100 or 600 μmol m^{-2} s^{-1}) and UV treatment (UV-A or UV-A + UV-B). P-values are results from 2 x 2 factorial ANOVAs. Bolded values represent statistical significance. Values < 0.05 that are not bolded indicate that a significant interaction with another experimental factor is present.

Response	Main Effects		Interactive Effect
	PAR	UVR	PAR x UVR
APX	**< 0.001**	**< 0.001**	0.624
GTR	0.065	0.228	0.437
SOD	0.582	0.564	**0.002**
Catalase	< 0.001	< 0.001	**0.002**

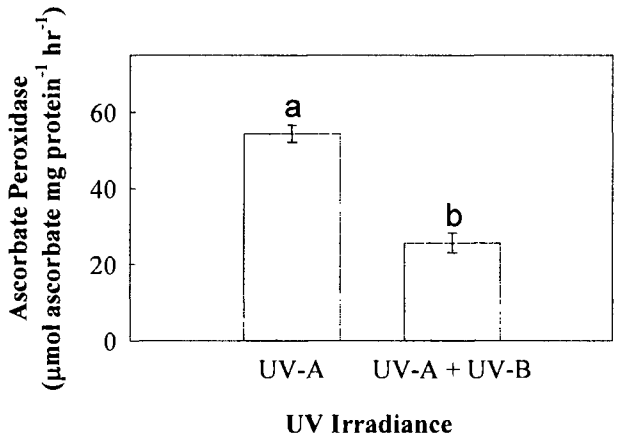

Figure 2.9. Effect of UV radiation on ascorbate peroxidase activity. *D. tertiolecta* growing at 100 or 600 μmol photons $m^{-2}s^{-1}$ PAR were treated for 12 hours with 60 μmol photons $m^{-2}s^{-1}$ (20.55 Wm^{-2}) UV-A (UV-A) or 6 μmol photons $m^{-2}s^{-1}$ (2.4 Wm^{-2}) UV-B + 60 μmol photons $m^{-2}s^{-1}$ UV-A radiation (UV-B + UV-A). Data represent mean of n = 25 samples per treatment ± one standard error. Means with the same letter are not statistically different ($\alpha = 0.05$).

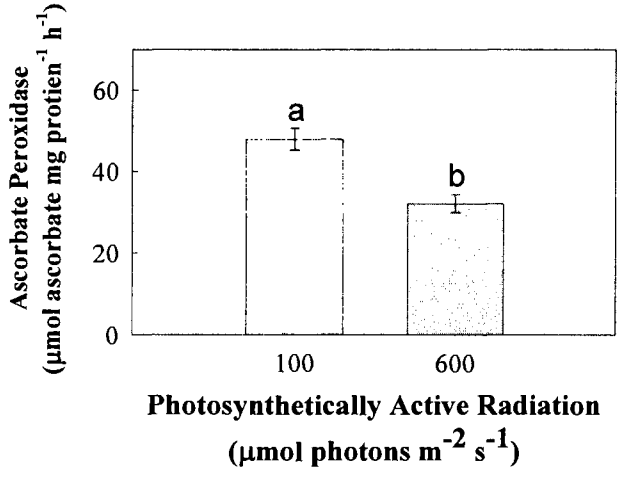

Figure 2.10. Effect of PAR on ascorbate peroxidase activity. *D. tertiolecta* growing at 100 or 600 μmol photons $m^{-2}s^{-1}$ PAR were treated for 12 hours with 60 μmol photons $m^{-2}s^{-1}$ (20.55 Wm^{-2}) UV-A (UV-A) or 6 μmol photons $m^{-2}s^{-1}$ (2.4 Wm^{-2}) UV-B + 60 μmol photons $m^{-2}s^{-1}$ UV-A radiation (UV-B + UV-A). Data represent mean of n = 25 samples per treatment ± one standard error. Means with the same letter are not statistically different ($\alpha = 0.05$).

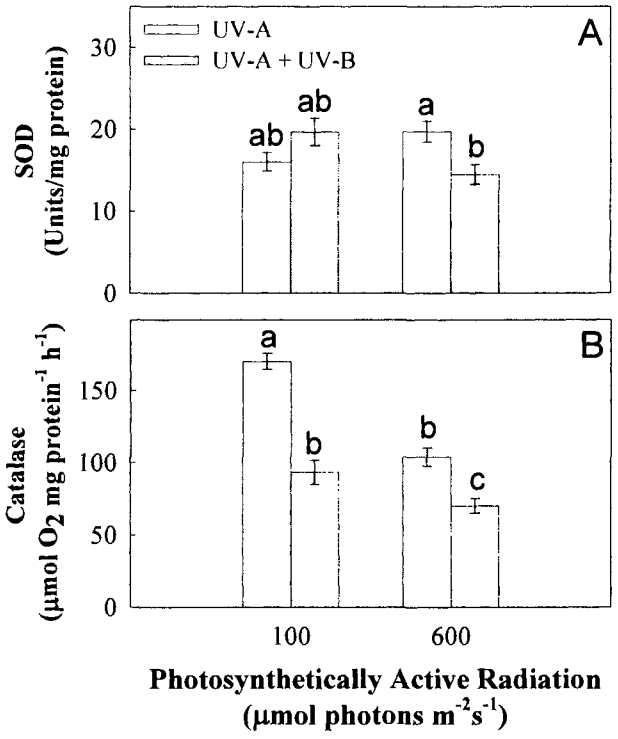

Figure 2.11. SOD and catalase activities following UV exposure. Enzyme activities of A) superoxide dismutase (SOD) and B) catalase in *D. tertiolecta* growing at 100 or 600 μmol photons $m^{-2}s^{-1}$ PAR following 12-hour exposures to 60 μmol photons $m^{-2}s^{-1}$ (20.55 Wm^{-2}) UV-A (UV-A) or 6 μmol photons $m^{-2}s^{-1}$ (2.4 Wm^{-2}) UV-B + 60 μmol photons $m^{-2}s^{-1}$ UV-A radiation (UV-B + UV-A). Data are mean of n = 7-17 samples per treatment ± one standard error. For a particular pigment, means with the same letter are not statistically different ($\alpha = 0.05$).

DISCUSSION

Depending on the season and latitude, solar flux will contain between 20 - 125 μmol photons m^{-2} s^{-1} (6.8-42.8 Wm^{-2}) UV-A at the Earth's surface (Holm-Hansen *et al.*, 1993; Whitehead *et al.*, 2000). Here, we applied an UV-A irradiance flux of 60 μmol photons m^{-2} s^{-1} (20.55 Wm^{-2}) to cultures of *D. tertiolecta* growing at 100 or 600 μmol photons m^{-2} s^{-1} PAR. The purpose was to apply ambient levels of UV-A together with low or high

PAR flux. As a result, the irradiance environment under 100 PAR diverged from solar flux, but was characteristic of much UV research (i.e. UV-A: PAR ratio = 1: 1.7), while the cultures growing at 600 PAR received a UV + PAR flux density representative of solar ratios (i.e. 1:10). This experimental approach was focused on manipulating the UV-A and PAR *flux densities*, not centered on controlling the *wavelength distribution* of the UV-A spectrum. Indeed, UV-A radiation generated in a laboratory setting deviates somewhat from the solar spectrum (Figure 2.2).

UV-A induced photoinhibition

The declines in photosynthesis (P_{LS} and P_{LL}) following exposure to UV-A radiation under both low and high PAR indicated that manipulating the UV-A: PAR ratio could not alleviate UV-A induced photoinhibition (Table 2.1). This was in stark contrast to the previously observed UV-B radiation effects, in which photoinhibition was lessened by elevating the PAR intensity (see Figure 1.8 of Chapter I). The contrasting effects of UV-B and UV-A fluxes suggested that unlike the photoinhibitory damages induced by UV-B, the injuries sustained from UV-A could not be mitigated through PAR mediated photorepair processes. Declining F_v/F_m and P_{LL}: P_{LS} ratios in conjunction with increased F_o values further implied that UV-A wavebands were impairing PSII electron transport (Table 2.1).

Direct damage to the water oxidation Mn cluster and the D1/D2 reaction center proteins has been observed following UV-A treatment (Turcsányi and Vass, 2000; Vass *et al.*, 2002). Fragmentation of the D1 protein by UV-A wavebands occurs under a mechanism similar to that induced by UV-B radiation (Turcsányi and Vass, 2000; Vass *et*

al., 2002). Therefore, one would expect to see similar effects of UV-A and UV-B radiation on PSII integrity. Yet, in the current study, total D1 protein contents declined in response to UV-A treatment only under low PAR (Figure 2.3), indicating that higher PAR densities offered some protection against PSII photoinactivation. This was not the case following treatment with UV-B, in which similar D1 protein losses were experienced across all PAR levels (see Figure 1.11 of Chapter I).

In a study on the green alga *Chlorella*, Kim and Watanabe (1994) demonstrated that short-term (0-2h) exposures to UV-A radiation (44-73 μmol photons m^{-2} s^{-1} [15-25 Wm^{-2}]) under moderate PAR intensities (300 μmol photons m^{-2} s^{-1}) resulted in the severe inhibition of photosynthesis, while prolonged exposures (4- 5h) to the same UV-A + PAR doses yielded photosynthetic rates identical to controls. Apparently, the longer UV-A exposure times permitted the cells to recover from their initial photoinhibitory damages to rates equal to that of cells never receiving any UV radiation (Kim and Watanabe, 1994). Similar photosynthetic recovery patterns following prolonged UV (UV-B + UV-A) exposure have also been reported for marine diatoms (Hazzard *et al.*, 1997) and Antarctic green algae (Lesser *et al.*, 2002).

It was not evident from these data whether 600 PAR cultures suffered immediate PS II injury and recovered, or if the high PAR intensity promoted photoprotective processes to shield against UV-A damage. One other possibility could be that the D1 proteins were more vulnerable to UV-B photons than UV-A photons. This could explain why *D. tertiolecta* suffered to UV-B induced damages under all PAR levels (see Chapter I), but avoided D1 degradation when the UV-A: PAR ratio represented solar irradiance intensities.

Only a handful of researchers have examined the photoinhibitory effects of UV-A radiation on *Dunaliella* (Jahnke, 1995; Herrmann *et al.*, 1996, 1997; White and Jahnke, 2002). Jahnke (1995) reported a 50% decline in F_v/F_m in *D. parva* cultures exposed to UV-A radiation. Similarly, White and Jahnke (2002) found comparable losses in F_v/F_m in *D. bardawil* and *D. salina* after exposures to UV-A. In contrast, Herrmann *et al.* (1996) reported negligible changes in *D. salina* F_v/F_m following 30 minutes of UV-A treatment (18.5-22 Wm^{-2}; 54-64 μmol photons $m^{-2}s^{-1}$) using a short-wave deficient UV-A spectrum ($\lambda > 338$) and a UV-A: PAR ratio of 1:15.

There are at least two flaws with the experimental design employed by Herrmann *et al.* (1996). (1) *D. salina* is one of two *Dunaliella* species capable of accumulating massive amounts of carotenoids (particularly β-carotene) during exposure to high irradiances and UV radiation (Jahnke, 1999). Accumulation of β-carotene has been shown to offer protection against photooxidative damages caused by singlet oxygen and triplet state chlorophyll (Niyogi, 1999), both of which are likely to form following UV-A exposure (Turcsányi and Vass, 2000). Thus, one cannot rule out the possibility that the lack of response in F_v/F_m ratios reported by Herrmann *et al.* (1996) could have been the result of protective screening by carotenoids, which were not evaluated. (2) The application of wavelengths > 338 nm, would have avoided physiological damages resultant from short-wave UV-A. These wavebands (320-338 nm) possess the greatest amount of energy per photon within the UV-A range and removing them from the incident spectral profile thereby fails to simulate ecologically relevant UV-A flux. Furthermore, applying a PAR intensity above that typically present in solar environments (1:10 ratio UV-A: PAR), may have avoided UV-A induced effects. The results of the

present study correspond with the findings of Jahnke (1995) and White and Jahnke (2002) that UV-A radiation causes decreased PSII electron transfer efficiency in *Dunaliella* (Table 2.1; Figure 2.3). Our data further suggest that when a UV-A treatment is applied under UV-A: PAR ratio comparable to solar flux, the integrity of PSII protein subunits is maintained (Figure 2.3).

Because the photosynthetic rates measured as O_2 evolution declined under both PAR levels, treatment with UV-A radiation not only affected PSII, but also likely disrupted the carbon fixation reactions. Key components of carbon fixation such as RuBisCO are directly impaired by UV-B radiation (Gerhardt *et al.*, 1999; Andreasson and Wängberg, 2006). Yet, the direct effects of UV-A on this system are currently unknown. RuBisCO is a Type I 560 kDa protein consisting of eight large (56 kDa) and eight small (14 kDa) subunits and is responsible for catalyzing the initial carboxylation reaction of 1, 5-bisphosphate (RuBP) of the Calvin Cycle (Buchanan *et al.*, 2000). Both subunits of RuBisCO contain tryptophan (Trp) residues susceptible to direct photomodification *in vitro* by UV-B (Greenberg *et al.*, 1996) and UV-A radiation (Tyrell, 1991). Photolysis of Trp with subsequent inactivation of RuBisCO enzyme activity has been shown following UV-B treatment *in vivo* (Gerhardt *et al.*, 1999). However, it is unclear whether UV-A interacts with RuBisCO in a similar manner.

In 2001, Savitch *et al.* examined the effects of UV-A radiation on CO_2 assimilation, carbon partitioning and PSII photochemistry in *Brassica napus*. Plants treated with UV-A showed decreased RuBP regeneration, a decline in light- and CO_2-saturated CO_2 assimilation rates and a down-regulation of sucrose-starch biosynthesis (Savitch *et al.*, 2001). Interestingly, they (Savitch *et al.*, 2001) did not observe any

differences in RuBisCO activity, total quantities of RuBisCO protein or PSII photochemistry between control and UV-A exposed plants. It was concluded that UV-A radiation did not affect PSII operation, but was responsible for causing feedback effects on photosynthesis *via* CO_2 assimilation and carbon partitioning mechanisms (e.g. starch and sucrose catabolism; Savitch *et al.*, 2001). In a related field study, 20-22% declines in RuBisCO contents and P_{LS} rates in Antarctic phytoplankton exposed to UV radiation (UV-B + UV-A) were reported without any net effects on PSII (e.g. F_v/F_m; Lesser *et al.*, 1996). The authors (Lesser et al., 1996) showed that decreased RuBisCO was a consequence of UV radiation was central to mechanisms involved in photosynthetic inhibition.

Similar studies have suggested that declines in carbon fixation efficiency and net photosynthesis, along with the direct impairment of RuBisCO within phytoplankton communities, occurs primarily in response to UV-A not UV-B flux (Helbling *et al.*, 1992; Boucher and Prezélin, 1996; Figueroa *et al.*, 1997; Bischof *et al.*, 2000). However, quantitative data confirming these hypotheses have not been gathered. Nevertheless, in the present study, decreases in PSII electron transport efficiency were likely occurring in tandem with impaired CO_2 assimilation processes in response to UV-A exposure. Whether decreased rates of carbon fixation were the result of direct or indirect interactions with UV-A wavebands cannot be determined from these data. It would be worthwhile to investigate whether the UV-A treatments applied here were affecting the contents/ activities of RuBisCO and its associative enzymes to clarify such ambiguities.

Oxidative stress responses following UV-A exposure

UV-A radiation excites a variety of photosensitizers within plant cells including porphyrins, flavins, pyridine nucleotides and quinones (Jahnke *et al.*, 2009). The enhanced production of superoxide radicals and the accelerated breakage of DNA are both consequences of interactions between NADH/NADPH coenzymes and UV wavebands (Peak *et al.*, 1984; Cunningham *et al.*, 1985; Jahnke *et al.*, 2009). Heightened levels of lipid peroxidation and ROS production in response to UV-A treatment have been observed in cultures of the marine diatoms *Thalassiosira pseudonana* and *Ditylum brightwellii* (Rijstenbil, 2001, 2002) as well as in the freshwater cladoceran *Daphnia longispina* (Vega and Pizarro, 2000). Unfortunately, the current understanding of how antioxidant enzyme action mitigates UV-A induced oxidative stress is ambiguous.

In a series of experiments, Rijstenbil (2001, 2002, 2003) examined whether UV-A radiation altered the antioxidant enzyme response in marine diatoms. After exposure to similar UV-A radiation treatments, cultures of *Cylindrotheca closterium* and *T. pseudonana* failed to exhibit increased APX, SOD or GTR activities (Rijstenbil, 2002, 2003) while increased SOD activities and elevated glutathione (GSH) contents were found in cultures of *D. brightwellii* (Rijstenbil, 2001). The responses of the antioxidant enzymes reported in the present work, suggest that UV-A radiation generates increased oxidative stress in *D. tertiolecta* (Figure 2.4 & 2.5). The reported increases in SOD, APX and MDHAR activities are of particular interest, as no other phytoplankton study has reported similar increases in all three enzymes as a consequence of treatment with UV-A radiation.

Balancing key constituents within the SOD-APX-GTR metabolic pathway is crucial for mitigating oxidative stress in plants (Polle, 2001; see Figure 1 in Introduction). The simultaneous increase in SOD, APX and MDHAR observed here supports the hypothesis that UV-A radiation caused excessive $O_2^{\cdot -}$ and H_2O_2 formation in the cell. The uniformity of GTR rates under all experimental conditions was initially surprising, but several supportive theories exist to explain this anomaly.

First and foremost, constant GTR rates signify that the enzyme activity variations of SOD, APX and MDHAR were likely an accurate reflection of metabolic adjustments and not the result of fluctuating total protein contents. Secondly, the glutathione redox system functions independently from the APX redox system (Polle, 2001). Using a metabolic model to elucidate the mechanisms of chloroplast ROS detoxification, Polle (2001) demonstrated that the primary function of GTR was to recycle glutathione oxidized by non-enzymatic reactions (e.g. GSSG) *not* support the regeneration of reduced ascorbate required for APX functionality. Recycling of oxidized ascorbate is predominantly performed through the actions of ferredoxin and dehydroascorbate reductase (DHAR; see Figure 2 of Introduction; Asada, 1999). The current data suggest that *D. tertiolecta* experienced little to no loss of GSH following UV-A treatment, yet sustained significant depletion of the reduced ascorbate pool. This would justify a steady GTR rate in conjunction with elevated APX and MDHAR activities (Figure 2.5; Figure 2.7).

Electron transfer from PSI to molecular oxygen is also intended to safely release excessive excitation energy from the system and is commonly referred to as the water-water cycle (see Introduction Figure 2; Asada, 1999). Plants utilize this pathway with the

subsequent formation and immediate detoxification of $O_2^{\cdot -}$ into H_2O_2 (*via* SOD). Ultimately, H_2O_2 produced by SOD is metabolized by APX into water. It seems probable that in the current study, UV-A radiation contributed to elevated H_2O_2 concentrations through the enhancement of the water-water cycle. This hypothesis is supported not only by elevated SOD and APX activities (Figure 2.5, 2.7), but also by increases in MDHAR, which would have been required to keep the ascorbate pool in a reduced state (Figure 2.7).

UV-A+ UV-B effects on photosynthesis and pigments

The addition of 6 μmol photons $m^{-2}s^{-1}$ (2.4 Wm^{-2}) UV-B to the UV-A flux was intended to create a balanced irradiance environment consistent with natural UV radiation (1:10 ratio UV-B: UV-A). Variations in PAR intensity were used to produce a complete irradiance profile characteristic of solar conditions (600 PAR) and an environment with an unrealistically high UV: PAR ratio (100 PAR). Direct comparisons between UV-A and UV-B + UV-A treatments were designed to clarify the role of UV-B in promoting photoinhibition and oxidative stress in plants. Specifically, it was our intention to determine whether UV-B radiation exacerbated the physiological damages incurred by UV-A radiation or if the UV-B flux would have no further influence on the total sustained UV-induced injuries.

Following the addition of UV-B radiation, cultures of *D. tertiolecta* did not encounter any additional photosynthetic stress (Table 2.3). This strongly suggested that UV-A radiation was the primary source of sustained photoinhibitory damages. These findings are in accordance with solar exclusion (Helbling *et al.*, 1992; Holm-Hansen *et*

al., 1993) and laboratory based studies (Callieri *et al.*, 2001; Zudaire and Roy, 2001) that have previously compared the effects of UV-B, UV-A and UV-A + UV-B irradiances on various species of phytoplankton. In particular, the work of Helbing *et al.* (1992) demonstrated that within natural Antarctic and tropical phytoplankton populations, the UV-A portion of the spectrum was responsible for over 50% of the total photosynthetic inhibition experienced, and that radiation below 305 nm was responsible for only 15-20% of the UV-B induced photodamages. Likewise, the work of Cullen *et al.* (1992) supported the idea that UV-A radiation is a significant source of photoinhibition within natural phytoplankton communities.

Additional research has shown that UV-A wavebands can mitigate UV-B induced damages via photoreactivation repair of UV-B damaged DNA molecules (Caldwell *et al.*, 1994; Quesada *et al.*, 1995; Krizek, 2004; Joshi *et al.*, 2007). If this had occurred in the present study, UV-A radiation would have ameliorated UV-B induced injuries using photoreactivation and/or photorepair processes. Although photoreactivation is a well-documented phenomenon in plants, the absence of UV-B induced photoinhibition in cultures exposed to urate filtered UV-B lamp emissions ruled out the likelihood that UV-B would contribute significantly to the impairment of photosynthesis (see Chapter I). The results of this study seem to indicate that the UV-A wavebands were responsible for reductions in photosynthesis and photosynthetic efficiency (Table 2.1 and 2.3).

It was not surprising to find that 600 PAR cultures contained less pigment than 100 PAR cultures, as lower pigment contents are usually associated with higher irradiances (Figure 2.4 & 2.8; Lichtenthaler, 1981; Anderson *et al.*, 1995). It was interesting to discover that the addition of UV-B flux only affected pigment contents of

cells growing under low PAR (Figure 2.8). Previous reports using cellulose acetate filtered UV-B radiation have linked UV-B wavebands with direct PSII LHC damage and adjustments to LHC antennae size (Cleland and Melis, 1987; Baroli and Melis, 1998). Here, pigment contents in cultures exposed to UV-B + UV-A remained steady as long as high PAR (600 PAR) was also applied. Therefore, balancing the UV-B: PAR ratio (along with using urate filtered UV-B lamp emissions) maintained the structure and composition of photosynthetic pigments throughout the UV exposure. Conversely, the significant declines of all measured pigments in the low PAR treatment depict the vulnerability of photosynthetic pigment molecules to UV-B induced degradation when the spectral balance of UV and PAR are not upheld.

The present findings support the view that UV-B is not the major contributor to photoinhibition in phytoplankton and land based photosynthetic communities under ozone replete conditions (Fiscus and Booker, 1995; Allen *et al.*, 1998; Searles *et al.*, 2001; Nogues *et al.*, 2006). In fact, it appeared that UV-A was the principal source of UV-induced photoinhibition in *D. tertiolecta*. This was particularly evident as all of the photosynthetic parameters remained unchanged following the addition of UV-B flux to the UV-A + PAR regime (Table 2.1). Furthermore, when a UV: PAR ratio representative of solar flux was applied, pigment contents were also unaffected (Figure 2.3 & 2.4).

UV-B + UV-A effects on oxidative stress responses

With the exception of GTR, all of the antioxidant enzyme activities examined *decreased* following the inclusion of UV-B (Figure 2.9 & 2.11), indicating that either oxidative stress levels in the cells had declined or that UV-B wavebands were damaging the

enzymes. The latter idea seemed unlikely since previous findings have shown that with the exception of catalase, UV-B radiation with a spectral profile comparable to that of solar flux (i.e. urate filtered lamp emissions) does not adversely affect the antioxidant enzymes examined in this study (see Chapter I). Furthermore, if the UV-B wavebands were altering protein structure, GTR activity rates would have also changed with incident UV-B flux. Yet, GTR activities were consistent across all experimental parameters suggesting that the observed enzyme rate changes are reflecting metabolic responses.

Inquiries into the effects of monochromatic UV wavebands (290- 390 nm) on ROS production have indicated that impairments to photosynthesis by $O_2 \cdot^-$ are predominantly caused in response to UV-B wavebands (and not UV-A; Barta *et al.*, 2004). Rijstenbil (2003) reported no change in the activities of SOD, APX, MDHAR and GTR in C. *closterium* exposed to UV-A, but observed escalations in SOD after cultures were treated with UV-B + UV-A. These findings contradict the results of the current study in which urate filtered UV-B (applied +/- UV-A) did not elicit ROS production (Figure 2.11; Figure 1.15 Chapter 1). In fact, cultures exposed to UV-B + UV-A exhibited *reduced* activities in enzymes responsible for scavenging ROS (Figure 2.9 & 2.11). This discovery differs greatly with previous reports that UV-B plays a fundamental role in the exacerbation of oxidative stress in plants (Greenberg *et al.*, 1997; Hideg, 2006). This study supports the idea that ROS levels in *D. tertiolecta* cells declined with UV-B + UV-A flux treatment because the irradiance environment was properly balanced (UV-B: UV-A: PAR).

He *et al.* (2002) exposed cultures of the cyanobacteria *Anabaena* to UV-B + UV-A radiation (0.018 + 0.107 $mWcm^{-2}$, respectively) for a period of two weeks. Initially,

cultures exhibited acute signs of oxidative stress including lipid peroxidation, DNA strand breakage and photosynthetic quantum yield (F_v/F_m and photochemical/non-photochemical quenching). However, after 4-7 days of irradiance treatment, all signs of oxidative damage had vanished and the cell cultures had acclimated to the UV-B flux, survived and grown. He *et al.* (2002) speculated that one or more of the following may have been occurring to allow cultures to adapt to moderately stressful levels of UV-B irradiance: (1) that upon the production of UV-B-induced photosynthetic and DNA injuries, highly efficient repair and *de novo* synthesis processes for the UV-damaged molecules [proteins (D1/D2), lipids and DNA] were up regulated (2) that the recovery/adaptation was mediated by rapid genetic mechanisms associated with ROS damage to lipids, proteins and DNA (3) that the H_2O_2, $O_2\cdot^-$ and lipid hydroperoxides generated as a result of UV-B radiation acted as signaling species for the induction/ activation of antioxidant defense systems (e.g. ROS scavenging enzymes). Ultimately, He *et al.* (2002) concluded that the ability of *Anabaena* to acclimate to prolonged UV-B exposure was contingent on the occurrence of signaling/ repair/ adaptation processes initiated by UV-B induced oxidative injuries.

Comparable antioxidant enzyme responses have also been reported in the freshwater green alga *Chlorella vulgaris* (Malanga *et al.*, 1997) and the marine diatom *Cylindrotheca closteruim* (Roncarati *et al.*, 2008). SOD activities in chloroplasts of *C. vulgaris* exposed to UV-B radiation [11.5 μmol photons $m^{-2}s^{-1}$ (4.58 Wm^{-2})] for 12 hours decreased by 50% while, APX, ascorbic acid and β-carotene contents were unaffected altogether (Malanga *et al.*, 1997). Similarly, Roncarati *et al.* (2008) reported identical

SOD activities and GSH contents in cultures of *C. closterium* grown both with and without UV-B radiation (~0.7 μmol photons $m^{-2}s^{-1}$ [0.24 Wm^{-2}]).

In study on Arctic marine macroalgae, Aguilera *et al.* (2002) reported that prolonged exposure (8 days) to UV radiation (UV-B [1.05 μmol photons $m^{-2}s^{-1}$/0.36 Wm^{-2}] + UV-A [23 μmol photons $m^{-2}s^{-1}$/ 8 Wm^{-2}]) had no significant effect on SOD, CAT or APX enzyme activities in the green alga *Acrosiphonia penicilliformis* (Foslie) Kjellman and the red alga species *Palmaria palmata* (L.) Grev. and *Devaleraea ramentacea* (L.) Guiry. Adaptation to photooxidative stress is multifaceted and involves the regulation of both protein repair/synthesis and the upregulation of antioxidants. Here, exposure to UV-B + UV-A radiation under a spectral profile comparable to that of solar flux *decreased* antioxidant activities compared to when only UV-A radiation was used. It appeared as if the UV-B flux might have contributed to heightened UV-protective mechanisms that were not activated with UV-A radiation alone. More specifically, it is likely that physiological damages induced by UV-B served to initiate rapid and efficient metabolic responses that curbed and/or lessened oxidative stress levels within the cell. However, such speculations cannot be confirmed without further investigation.

CONCLUSIONS

The view that UV-A and *not* UV-B radiation imposes the majority of photosynthetic and oxidative stress on phototrophs has been supported by the present study. The significant declines in both oxygenic photosynthesis and PSII operational efficiency indicated that exposure UV-A radiation not only impaired light-mediated electron transport, but may also be directly inflicting damage to the carbon fixation processes. Although oxidative stress responses in *D. tertiolecta* increased dramatically in response to UV-A treatment, the addition of UV-B flux dampened this response suggesting that balanced UV-B: UV-A: PAR ratios do not elicit excessive ROS production in *D. tertiolecta*. These findings also hinted towards the presence of UV acclimation/adaption mechanisms that may serve to heighten the resistance against UV-induced physiological damages in phytoplankton. This report combined with the findings of Chapter I, signify that ecologically meaningful inquiries into the "real" effects of UV radiation can be achieved within a laboratory settings with important proviso that the details regarding the irradiance profile are taken into careful consideration.

CHAPTER III

CHARACTERIZATION OF CHLOROPLASTIC AND CYTOSOLIC ASCORBATE PEROXIDASE ISOFORMS IN THE UNICELLULAR GREEN ALGA *DUNALIELLA TERTIOLECTA*

ABSTRACT

In higher plants, isoforms of the H_2O_2 scavenging enzyme ascorbate peroxidase (APX) have been characterized from the chloroplast, cytosol, microbody and mitochondria. In contrast, only chloroplastic APXs have been described in unicellular green algae. When total protein extracts from the halotolerant green alga *Dunaliella tertiolecta* were separated by polyacrylamide gel electrophoresis (PAGE) under non-denaturing/non-reducing conditions (i.e. Native gels) and subjected to an APX activity assay, four distinct bands of activity were resolved. Immunodetection using cytosolic (cAPX) and stromal (sAPX) polyclonal antibodies raised against tea and maize APX respectively, confirmed that three of the bands were APX protein. Two of the proteins cross-reacted with the sAPX-specific antibodies and are likely localized in the chloroplast, while the third protein was identified as cAPX. SDS-PAGE followed by immunodetection with cAPX specific antibodies identified the presence of two APX proteins with molecular masses of 59kDa and 19kDa. Using cDNA APX sequences from green algae, degenerate oligonucleotide primers were designed and used to amplify a 546 base pair *D. tertiolecta* segment that exhibited high homology to APXs from *Chlamydomonas reinhardtii* and

higher plants. Phylogenetic analysis suggests that this newly characterized *D. tertiolecta* cDNA sequence falls in the chloroplastic APX lineage. This is the first report to propose the presence of APX isoforms in eukaryotic green algae.

INTRODUCTION

Hydrogen peroxide (H_2O_2) is a common metabolic by-product produced throughout the cell (Buchanan *et al.* 2002). In plants, the water-water cycle (see Figure 2 in Introduction) and respiratory electron transport chains are responsible for H_2O_2 generation in the chloroplast and mitochondria, respectively (Braidot *et al.*, 1999; Asada, 2006). Photorespiratory C_2 processes occurring in the peroxisome also contribute considerable quantities of H_2O_2 as a consequence of RuBP oxygenation in the chloroplast of C_3 plants lacking a CO_2-concentration mechanism (CCM). Yet, many unicellular green algae like *Dunaliella* possess CCMs that substantially reduce and/or eliminate photorespiration by maintaining high CO_2/O_2 ratios at the site of carbon fixation. Apoplastic production of H_2O_2 is primarily associated with cell wall lignification and NADPH-oxidase enzyme action, but has also been linked to the metabolic regulation of growth, programmed cell death and cell signaling (Apel and Hirt, 2004; Mittler *et al.*, 2004; Desikan *et al.*, 2005).

At low concentrations (~10 μM), H_2O_2 is a weak oxidizing agent interfering with the function of a variety of enzymes including those involved in carbon fixation (Ishikawa and Shigeoka, 2008). Yet, in the presence of transition metals such as iron, H_2O_2 becomes considerably more toxic, rapidly oxidizing into the highly reactive

hydroxyl radical (Queval *et al.*, 2008). It is therefore essential for all aerobic organisms to possess various detoxification mechanisms to rapidly quench H_2O_2 from the cell and prevent its conversion into more reactive species.

Ascorbate peroxidase (APX; EC 1.11.1.11) is a heme-containing enzyme that catalyzes the conversion of H_2O_2 into water using ascorbate as a reducing substrate (see Figure 3 of Introduction). It is widely distributed in plants and eukaryotic algae and belongs to the Class I category of plant-type heme peroxidases, which also includes cytochrome c peroxidase (from yeast) and catalase-peroxidase (from cyanobacteria; Ishikawa and Shigeoka, 2008).

The APX gene family of higher plants is complex and diverse. Presently, there are nine nuclear encoded APX genes characterized in *Arabidopsis*, eight in rice and seven in tomato (Mittler and Poulos, 2005; Teixeira *et al.*, 2006; Najami *et al.*, 2008). Based on their subcellular locations and biochemical properties, isoenzymes of APX have been classified into chloroplastic, cytosolic and microbody subfamilies (Ishikawa and Shigeoka, 2008). In the chloroplast, APX exists as a stromal-soluble (sAPX) and thylakoid membrane-bound (tAPX) form. A third isoenzyme has recently been identified from the thylakoid lumen of *Arabidopsis*, however its specific function has yet to be established (Ishikawa and Shigeoka, 2008). In *Arabidopsis* (Mittler and Poulos, 2005) and rice (Teixeira *et al.*, 2006), cytosolic APX (cAPX) apparently scavenges H_2O_2 diffusing from the chloroplast and is believed to play a central role in the quenching of reactive oxygen species in higher plants (Davletova *et al.*, 2005). More specifically, cAPX regulates the concentration of H_2O_2 in the cytosol and influences the activities of secondary messengers responsible for redox gene expression (Ishikawa and Shigeoka,

2008). The regulatory role of cAPX has been supported by studies involving cAPX (APX1)-knockout *Arabidopsis* plants, in which genes involved with stress related proteins and transcription factors were upregulated after H_2O_2 accumulated in the cytosol (Pnueli *et al.*, 2003). The microbody APX isoform is transported to either the glyoxysome or peroxisome (pAPX) depending on the target peptides and transmembrane domains located within the N- and COOH-terminal regions (Mittler and Poulos, 2005; Dabrowska *et al.*, 2007). Although not completely characterized, a mitochondiral APX (mAPX) subfamily has also been proposed. In *Arabidopsis* and rice, mAPX and sAPX isoforms are believed to arise from the same protein that is dually targeted to both the mitochondria and plastids (Chew *et al.*, 2003; Teixeira *et al.*, 2006). But, this is not the case in tobacco and tomato, which are thought to possess distinct genes for each isoform (Madhusudhan *et al.*, 2003; Mittova *et al.*, 2004).

Distinguishing between the APX isoforms biochemically is largely dependent on their varying responses to ascorbate concentration. Chloroplastic (tAPX and sAPX) and mAPXs are inactivated in seconds following ascorbate depletion (≤ 20 μM), while cAPX and pAPXs are much less sensitive to ascorbate loss; maintaining half-inactivation rates of about 1 hour (Shigeoka *et al.*, 2002). Reduced sensitivity to low concentrations of ascorbate may be due to fact that some APX isoforms are capable of using alternative electron donors. The inactivation of APX occurs when H_2O_2 molecules attack the heme moiety of Compound I (Miyake and Asada, 1996; see Figure 3 Introduction). Therefore, because cAPXs can also oxidize aromatic phenols like pyrogallol and guaiacol, they function for substantially longer periods under ascorbate-depleted conditions (Chen and Asada, 1989; Asada, 1997).

In contrast to the depth of information available on higher plant APXs, there has been minimal effort to elucidate the role(s) of APX in eukaryotic algae. The current understanding is that green algae utilize APX in the chloroplast and draw on additional H_2O_2-scavenging enzymes to purge H_2O_2 generated within other parts of the cell (Takeda *et al.*, 1993; Ishikawa and Shigeoka, 2008). Indeed, this is the case for *Chlamydomonas reinhardtii*, which possesses APX in the chloroplast, but relies on catalase (EC1.11.1.6) and glutathione peroxidase (GPX; EC 1.11.1.9) to reduce H_2O_2 concentration (Takeda *et al.*, 1993). Comparable findings in *Chlorella vulgaris* and the halotolerant *Chlamydomonas* sp. W80 have provided addition evidence that green algae only possess chloroplastic APXs (Takeda *et al.*, 1998, 2000). Nonetheless, all of the APXs currently described from green algae exhibit a reduced sensitivity to ascorbate depletion comparable to that described for cAPX from higher plants and *Euglena* (Takeda *et al.*, 1997, 1998, 2000). *Euglena* is unique with respect to its H_2O_2 scavenging system since it does not contain catalase. Instead, H_2O_2 is removed from the cell *via* a APX-GTR cycle located in the cytosol, not the chloroplast (Ishikawa *et al.*, 1996).

In contrast to green algae, two cAPX isoenzymes have been purified from the unicellular red algae *Galdieria partita* (Sano *et al.*, 2001; Ishikawa and Shigeoka, 2008). Both of these APX isozymes possess a comparable biochemistry to sAPX of higher plants, yet only one of the two isoforms cross-reacts with monoclonal antibodies raised against *Euglena* (Sano *et al.*, 2001). In the red macroalga *Porphyra*, chloroplastic APXs have not yet been characterized, however cAPXs transcripts (mRNAs) have also been identified (*P. haitanensis* (EU807991), *P. yezoensis* (AY282755)). Such discrepancies among algal groups, in addition to the limited scope of available data, have made it

difficult to characterize the specific subcellular role(s), distribution and evolutionary relationships of APXs in the eukaryotic algae. It was deemed important to elucidate where in a green algal cell APX was localized and to determine whether multiple isoforms exist. To achieve these objectives, a combination of biochemical and molecular techniques were employed using the halotolerant green alga *Dunaliella tertiolecta* as a model organism.

MATERIALS AND METHODS

Culture and radiation procedures

Dunaliella tertiolecta (Chlorophyta) cultures were grown in medium TK containing 0.5M NaCl as described by Jahnke and White (2003). Air was bubbled through the cultures at a rate of approximately 150-200 ml min^{-1} for a 150 ml culture. Cultures were grown in 38 x 300 mm Pyrex tubes maintained at 24°C in a water bath constructed of UV-transmitting plastic (Acrylite OP-4; Cadillac Plastics, Manchester, NH) according to the methods of White and Jahnke (2004). Photosynthetic photon flux density (PPFD) was provided by two cool-white fluorescent lamps on one side of the water bath producing light intensities in the range of 50-100 μmol photons m^{-2} s^{-1}. All analyses were conducted using cultures maintained at 100 μmol photons $m^{-2}s^{-1}$ without exposure to UV radiation and with a chlorophyll density between 1.5-2.0 mg chl ml^{-1} as detailed in Chapter I Materials and Methods.

Native PAGE

Polyacrylamide gel electrophoretic (PAGE) separation of proteins under non-denaturing and non-reducing conditions (i.e. Native gels) was performed as described by Mittler and Zilinskas (1993). Total protein extracts were prepared by centrifuging 150 mL cell culture at 1000 x g for 5 minutes, and re-suspending pellets in 2 mL 0.1 M sodium phosphate buffer (pH 7.0) and 5mM ascorbate. Samples were sonicated at room temperature and centrifuged three times for 3 minutes at 12,000 x g to thoroughly remove course cellular debris remaining in the extract. For each sample, 100 μg total protein was loaded into a 10-well 7.3% polyacrylamide gel that had been equilibrated by pre-running the gel in running buffer (6 mM Tris, pH 8.0, 38 mM glycine, 2mM ascorbate) for at least one hour. Equilibrating the gels prior to sample separation ensured that the ascorbate in the running buffer entered the gel. Electrophoresis of protein samples was conducted with fresh running buffer at 4°C and 32mA for 2-4 hours until loading dye ran through the gel. The electrophoresis unit was maintained at ~0°C in ice. In cases where APX was to be visualized through immunodetection, the gels were equilibrated in 25 mM Tris + 192 mM glycine immediately following PAGE and prior to protein transfer.

APX, catalase and SOD activity staining

Immediately following native PAGE, gels were sliced vertically with a clean razor to isolate individual sample lanes. Each lane therefore contained an identical protein sample separated in tandem. Individual lanes were subjected to either APX, catalase or superoxide dismutase (SOD) activity assays. APX activity staining was conducted as per Mittler and Zilinskas (1993) and begun by equilibrating gels at room temperature for 30

minutes in buffer A (50 mM sodium phosphate pH 7.0, 2 mM ascorbate) on a gentle shake; changing the buffer every 10 minutes. Gels were transferred into freshly made buffer B (50 mM sodium phosphate (pH 7.0), 4mM ascorbate, 2mM H_2O_2) for 20 minutes. Following a brief rinse (~ 1 minute) in 50mM sodium phosphate (pH 7.0), gels were submersed in activity stain (50 mM sodium phosphate (pH 7.8), 28 mM TEMED, 2.45 mM NBT) for 15-30 minutes with gentle shaking. APX isoforms were visualized as achromatic activity bands on a dark purple background. Submersing the stained gels in deionized water stopped the APX reaction, after which gels were dried and preserved in cellophane plastic.

Catalase was detected using the method of Woodbury *et al.* (1971). Gels were washed in deionized water for 45 minutes on a gentle shake, replacing the water every 15 minutes. Following a 10 minute wash in 0.0007% H_2O_2 and a brief rinse (~1minute) with deionized water, gels were incubated with 1% ferrichloride, 1% ferricyanide for 10-15 minutes. Catalase was visualized as an achromatic activity band on a dark orange/brown background.

The method of Beauchamp and Fridovich (1971) was used to detect superoxide dismutase (SOD) activity. Immediately following electrophoresis, gels were washed for 45 minutes in deionized water on a gentle shake; changing the water every 15 minutes. Thereafter, gels were incubated for 20 minutes with 2.5mM NBT, rinsed with deionized water and submersed for 15 minutes in 0.28M EDTA, 0.0028mM riboflavin, 0.36M sodium phosphate (pH 7.8). After exposing the gel to visible light for 10-15 minutes, SOD was visualized as an achromatic activity band on a light purple background.

SDS PAGE

Total protein extracts were prepared by centrifuging ~50 mL cell suspensions at 1000 x g for 5 minutes, washing the cell pellet with 1M glycerol in 50 mM phosphate buffer and re-centrifuging the samples. Cell pellets were suspended in 1 mL 0.5M sorbitol, 50 mM phosphate (pH 7.0), sonicated and centrifuged 3 minutes at 12,000 x g. Centrifugation was repeated twice more to completely remove cellular debris, after which, total protein extracts were diluted at least 1: 4 with sample buffer (0.625M TRIS pH 6.8, 10% glycerol, 2% sodium dodecylsulfate (SDS), 0.05% bromophenol blue, 0.05% (w/v) β-mercapoethanol) and heated for 5-10 minutes at 95°C. For each sample, 15μg total protein was loaded into a 4-12% gradient polyacrylamide gel (BioRad) and separated by SDS-PAGE as detailed by Laemmli (1970). Gels were processed at 200V for ~ 50 minutes until loading dye ran through. Gels were equilibrated in 25 mM Tris, 192 mM glycine prior to immunoblotting and western detection.

Immunoblotting

Electroblot transfer of proteins onto polyvinylidene difluoride (PVDF; BioRad) membranes was conducted at 100V for 1 hour followed by membrane blocking with 5% BLOTTO: 5% w/v powered milk in TBS-T (20mM Tris pH 7.6, 137 mM NaCl, 0.1% Tween-20) overnight at 4°C (or at room temperature for 1 hour). Blocked membranes were incubated with either sAPX or cAPX primary antibodies for one hour at room temperature. Polyclonal IgG anti-sAPX (from tea leaf tissue) were generously donated by Dr. Michael P. Lesser (*via* Chen and Asada, 1989) and used at a 1:2000 dilution. Polyclonal rabbit anti-cAPX antibodies (Agrisera AS06180) were used at a 1:3000

dilution and were synthesized using N-terminal peptide protein from maize cAPX as the antigen. Following incubation with primary antibody, membranes were washed three times for 15 minutes in 5% BLOTTO and incubated for one hour with goat anti-Rabbit IgG(Fc) HRP conjugated secondary antibodies (Pierce 31463) at a dilution of 1:62,500. Three additional 10-15 minutes washes in 5% BLOTTO were followed by exposure to Super Signal® West Pico chemiluminescent substrate (Pierce 34080) for five minutes. APX proteins were visualized using Kodak™Biomax® XAR film and Kodak™ processing chemicals under standard darkroom procedures. In some cases, stripping the PVDF membranes was necessary to re-probe with same/different antibodies. In these situations, membranes were exposed to Restore™ Western Blot Stripping Buffer (Pierce 21059) for 20 minutes and washed thoroughly with TBS-T washing buffer (25 mM Tris (pH 7.6), 150 mM NaCl, 0.05% Tween-20) before re-blocking with 5% BLOTTO.

RNA extraction and cDNA synthesis

Total RNA was isolated from ~ 8 x 10^6 *D. tertiolecta* cells using RNeasy® Mini Kit and QIA shredder™ spin columns (Qiagen). Although the Qiagen RNeasy kit is specifically designed to remove the vast majority of cellular DNA, to ensure that any residual genomic DNA was eliminated, cDNA synthesis using a SMART™ cDNA Library Construction Kit (Clontech Laboratories, Inc. Mountain View, CA) was performed. During this procedure, full-length cDNAs were generated using a modified oligo(dT) primer (CDSIII/3' PCR primer) to prime the first strand synthesis reaction, while a short SMART IV™ Oligonucleotide (SMART IV™ Oligo) served as an extended template to the 5' end of the mRNA. When reverse transcriptase reached the 5'end, the enzymes terminal

transferase activity attached the SMART IV™ Oligo creating an extended template at the 5' end. This reaction generated full-length single strand (ss) cDNA containing the complete 5' end of the mRNA as well as a sequence complementary to the SMART IV™ Oligo; which then served as the universal priming site in the subsequent PCR amplifications. Only ss cDNAs containing a SMART IV™ Oligo anchor sequence at the 5' end could have served as a template for PCR amplification. Incomplete cDNAs and ployA RNAs lacked the SMART IV™ Oligo anchor and were not amplified. Therefore, contamination of isolated RNA by genomic DNA and polyA RNA was eluded.

Approximately 1.0 μg total RNA was used to synthesize full length, double stranded (ds) cDNA with the SMART™ cDNA Library Construction Kit (Clontech Laboratories, Inc. Mountain View, CA) and Clontech GeneAmp 2400/9600 thermal cycling program [95°C 20s; 95°C 5s, 68°C 6 min (19 cycles); 4°C hold]. Quantification of total RNA and cDNA were conducted using a nanodrop spectrophotometer (Thermo Scientific) at 260 nm. Degenerate oligonucleotides were designed from conserved amino acid sequences of NCBI published APX sequences (Table 3.1) and synthesized by Integrated DNA Technologies, Inc. to use as primers (Table 3.2a). Estimated PCR product sizes for each forward and reverse primer pair were based on ClustalW alignments of Table 3.1 NCBI APX sequences and are given in Table 3.2b. PCR was performed using *D. tertiolecta* cDNA template and Dynazyme™ EXT DNA Polymerase kit/reagents (New England Biolabs, Inc.) with the following program: 4 minutes at 95 °C, followed by 35 cycles of 1 minute at 95 °C, 1 minute at 47-67 °C and 2 minutes at 72°C, 72°C for 10 minutes with a final hold at 4°C. Amplified cDNA was separated at 95 V/cm in a 1.2% (w/v) SeaPlaque agrose gel containing 0.5 μg/ml ethidium bromide in 1X TAE buffer

and visualized under UV light. Bands corresponding to estimated fragment sizes (Table 3.2b) were excised with a razor and gel purified using agarase enzyme. The University of New Hampshire Hubbard Center of Genomic Studies performed direct sequencing of PCR products. A *D. tertiolecta* APX contig was deduced from several 400bp and 600bp fragment sequences using the sequence analysis program SeqMan (DNASTAR Lasergene®). Alignment of the newly described *D. tertiolecta* cDNA sequence with uncharacterized *D. salina* expressed sequence tags (ESTs) was accomplished using Sequencher™ DNA sequence assembly software.

Table 3.1. APX enzyme sequences used to design degenerate oligonucleotide primers. The conserved amino acid regions of known eukaryotic green algae APX were used as templates to design degenerate oligonucleotides primers. Sequences are identified by their NCBI Accession number.

Accession #	Organism
AJ223325	*Chlamydomonas reinhardtii*
AB009084	*Chlamydomonas reinhardtii*
AY973821	*Chlorella vulgaris*
AY951933	*Chlorella* symbiont of *Hydra viridis*
DQ286543	*Ulva fasciata*

Table 3.2. Degenerate oligonucleotide primer characteristics. A) Forward and reverse degenerate primer sequences were used to amplify *D. tertiolecta* cDNA corresponding to ascorbate peroxidase enzyme. Oligonucleotide length, percent GC content and fold degeneracy are given. B) Estimated PCR product size in base pairs (bp) for each degenerate primer pair.

A.

Forward Primers	Sequence (5'→3')	Length	% GC	Fold Degenerate
1A	CGCCTGGGMTGGCACGA	17	73.5	2
1B	MGSCTGGSVTGGCACGA	17	71.6	24
1C	CGCCTSGSMTGGCACGA	17	73.5	8

Reverse Primers	Sequence (5'→3')	Length	% GC	Fold Degenerate
5D	GCSTKGTCSKYYGCGTACTTCTC	23	60.9	64
7A	CTCAGCACCACAATGTCCT	19	52.6	0
7E	CCRCTCAGCACCACAATGTCCT	22	56.8	2

B.

Primer Pair	Estimated product size (bp)
1A + 5D	600
1A + 7A/E	400
1B + 5D	600
1B + 7A/E	400
1C + 5D	600
1C + 7A/E	400

Phylogenetic analysis

Phylogenetic analyses were performed using two different approaches using members of the green algal genera *Dunaliella*, *Chlamydomonas*, *Chlorella* and *Ulva*, as well as a select group of higher plant taxa including cytosolic, peroxisomal and chloroplastic APX isoforms (Table 3.3). Analysis of cDNA sequences was executed using Maximum-likelihood (ML) algorithms with bootstrap replicates (n=500) in the PhyML v. 2.4.4 (Guindon and Gascuel, 2003) program under a general time reversible (GTR) + I + Γ

model with four substitution rate categories. The transition transversion ratio, gamma distribution parameters and proportion of invariable sites were estimated during the analysis.

To better resolve the interspecific relationships among the deeply rooted APX isoform phylogenies, a second alignment was created using the translated amino acid sequences. This alignment was trimmed to incorporate only those positions overlapping the *D. tertiolecta* contig. The protein analysis was performed in attempt to resolve the variability existing within the algae and higher plant chloroplastic APX clade following phylogenetic analysis using cDNA sequences. The translated amino acid sequences were analyzed *via* ML using PhyML v. 2.4.4 (Guindon and Gascuel, 2003) under a WAG model and 100 bootstrap replicates (n=100). Topology, branch lengths and rate parameters were optimized during the run and the Ti/Tv ratio, proportion of invariable sites and Gamma distribution were estimated with 4 substitution rate categories. In addition, translated amino acid sequences were also compared with a neighbor joining (NJ) analysis under a JTT model matrix with 2000 bootstrap replicates (n= 2000). NJ algorithms were run using the MEGA v. 4 program with a heuristic search option and six substitution sites under the GTR +I + Γ model. Four substitution rate categories and invariable sites were estimated during the NJ analysis.

RESULTS

Total protein extracts from *D. tertiolecta* were separated by Native-PAGE and subjected to APX, catalase or SOD activity assays. Of the four APX achromatic bands resolved (APX1, APX2, APX3 and APX4; Figure 3.1a), only three were distinct from catalase and SOD activity bands (Figure 3.1b & c). The catalase assay visualized a single band that did not align with any APX isoforms (Figure 3.1b), while the SOD activity band was highly correlated with APX1 (Figure 3.1c).

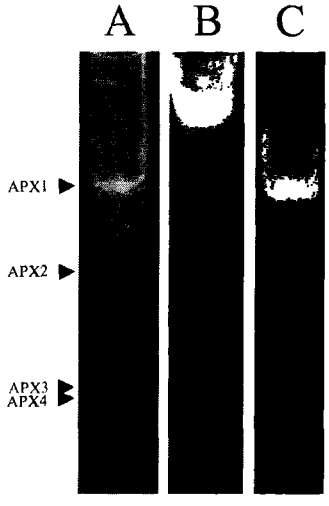

Figure 3.1 APX, catalase and SOD activity staining. Total proteins extracted from *D. tertiolecta* were separated in a 7.3% resolving gel under non-denaturing and non-reducing conditions and subjected to either an A) APX activity assay B) catalase activity assay or C) superoxide dismutase (SOD) activity assay.

To resolve which of the APX activity bands corresponded to APX protein, immunoblotting with either sAPX or cAPX specific antibodies was conducted (Figure 3.2b and c, respectively). Incubation with sAPX antibodies visualized a band that corresponded to both APX3 and APX4 (Figure 3.2b), while cAPX antibodies were consistent with APX2 (Figure 3.2c). Neither sAPX nor cAPX specific antibodies reacted with APX1proteins. Thus, only three of the four observed APX activity bands were confirmed using available APX specific antibodies. SDS-PAGE followed by immunodetection with cAPX antibodies revealed the presence of two APX proteins with molecular masses of 58.9 kDa and 18.9 kDa, respectively (Figure 3.2d).

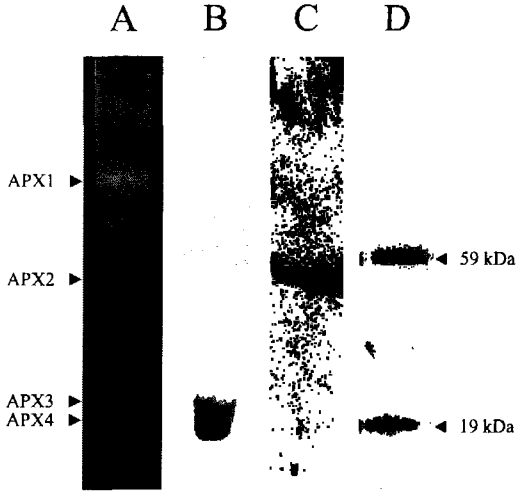

Figure 3.2 APX activity assay, immunoblotting and SDS-PAGE of *D. tertiolecta* total protein extracts. Separation of total proteins in a 7.3% resolving gel by Native-PAGE was followed by A) APX activity in-gel assay B) immunoblot using sAPX antibody or C) immunoblot using cAPX antibody. D) SDS-PAGE separation of total proteins on a 4-12% resolving gel and immunodetection with cAPX specific antibodies revealed the presence of 59 kDa and 19 kDa APX proteins.

APX amplification and sequencing

Using an annealing temperature of 54.6°C, the following degenerate primer pair combinations generated PCR products of the expected size (Table 3.2b): 1B+7A, 1B+7E, 1A+5D, 1A+7A, 1A+7E, 1C+7A and 1C+7E (Figure 3.3). The 400 and 600bp products were aligned to produce a single 546bp contig that when used as a NCBI BLAST query against only *Dunaliella* sp. nucleotide sequences, revealed high homologies with five uncharacterized ESTs from *D. salina*. Alignment of the *D. salina* ESTs with the newly described *D. tertiolecta* cDNA produced a second contig containing a complete open reading frame (Figure 3.4). The *D. tertiolecta* and *D. salina* sequences, their alignment and the resultant open reading frame amino acid translation are given in Appendix B.

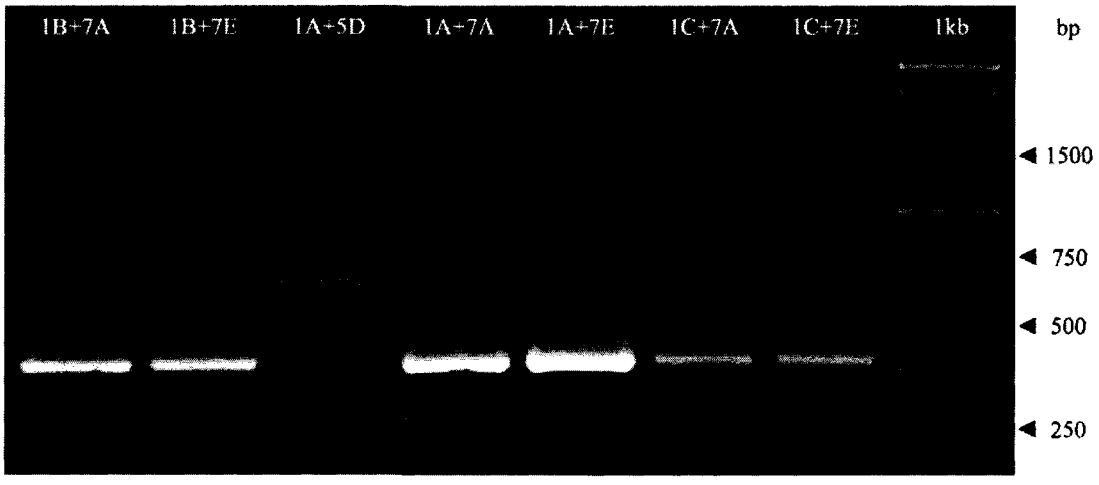

Figure 3.3. PCR amplified fragments generated using degenerate oligonucleotide primers. DNA fragments resulting from PCR with 1B + 7A (lane 1), 1B + 7E (lane 2), 1A +5D (lane 3), 1A +7A (lane 4), 1A +7E (lane 5), 1C + 7A (lane 6) and 1C + 7E (lane 7) degenerate primer pairs after agarose gel electrophoresis and ethidium bromide staining. A 1Kb DNA ladder standard is represented in the last lane (lane 8).

To characterize the *D. tertiolecta* 546bp product, NCBI blastx (searches protein database using the translated cDNA sequence) and tblastx (searches translated nucleotide database using the translated cDNA sequence) analyses were performed. The blastx search yielded high homology to APX based on low e-value probability, high score value, percent identification and percent positives (Table 3.3). The validity of classifying the *D. tertiolecta* PCR product as APX was further strengthened after tblastx searches produced similar results (Table 3.4). The 546bp sequence from *D. tertiolecta* in the current report was registered at NCBI as a partial APX sequence under the Accession #s FJ769282 and ACN86309.

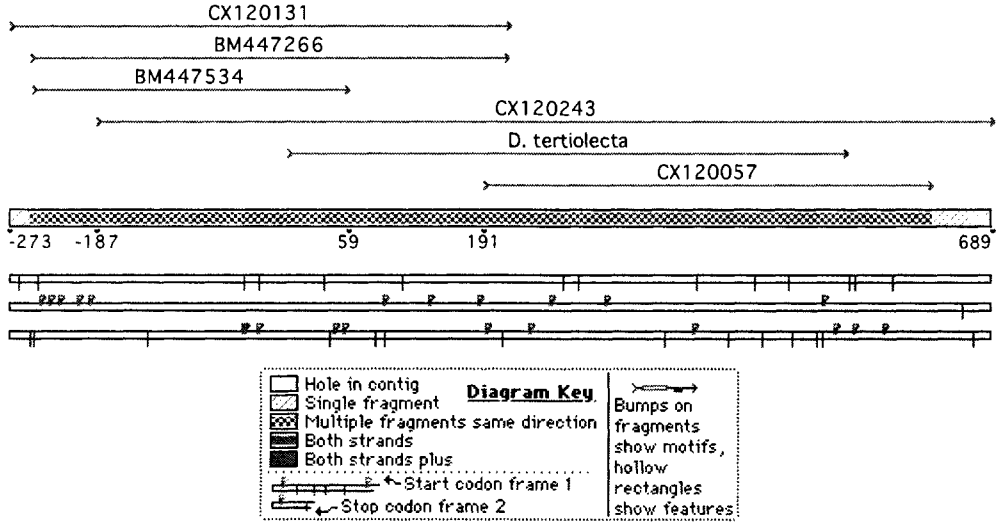

Figure 3.4. APX contig constructed with *D. tertiolecta* and *D. salina* sequences. The newly characterized *D. tertiolecta* sequence was used in a NCBI BLAST against only *Dunaliella* nucleotide sequences and yielded high homology to five uncharacterized *D. salina* expressed sequence tags (ESTs). When aligned using Sequencher™ DNA sequence assembly software, these cDNA fragments generated a contig with a continuous open reading frame.

Table 3.3. NCBI blastx results for the newly characterized *D. tertiolecta* APX. High homology based on e-value, score, percent identification (%ID) and percent positives (% +). Hypothetical protein (HP), Predicted protein (PP), Cytochrome C peroxidase (CCP).

Accession #	Homology	Organism	E-value	Score	% ID	% +
XP_001701947	APX	*Chlamydomonas reinhardtii*	3.E-56	221	57	70
EEC77311	HP	*Oryza sativa* Indica	6.E-54	213	63	76
XP_001784801	PP	*Physcomitrella patens*	6.E-54	213	61	75
AAC19394	sAPX	*Mesembryanthemum crystallinum*	1.E-53	212	62	73
AAC19393	tAPX	*Mesembryanthemum crystallinum*	1.E-53	212	62	73
NP_001132683	HP	*Zea mays*	4.E-53	210	60	75
AAN77158	tAPX	*Triticum aestivum*	1.E-52	209	59	75
BAD33296	Putative tAPX	*Oryza sativa* Japonica	1.E-52	209	60	74
EEF42139	CCP	*Ricinus communis*	3.E-52	207	60	75
AAN60069	sAPX	*Retama raetam*	3.E-52	207	59	72
BAD14931	tAPX	*Brassica oleracea*	4.E-52	207	59	74
BAA22196	sAPX	*Cucurbita cv. K. A.*	4.E-52	207	60	73
BAA12029	tAPX	*Cucurbita cv. K. A.*	4.E-52	207	60	73
AAS80158	tAPX	*Triticum aestivum*	6.E-52	206	58	74
AAS55852	tAPX	*Vigna unguiculata*	6.E-52	206	58	73

Table 3.4. NCBI tblastx results for the newly characterized *D. tertiolecta* APX. High homology based on percent identification (%ID), overlap and e-value. Predicted protein (PP).

Accession #	Homology	Organism	E-value	Score	%ID	% +
AJ223325	APX	*Chlamydomonas reinhardtii*	1.E-63	126	66	79
XM_001701895	APX	*Chlamydomonas reinhardtii*	1.E-63	126	66	79
XM_001784749	PP	*Physcomitrella patens*	2.E-61	158	68	82
AB114855	sAPX	*Oryza sativa Japonica*	6.E-61	153	67	80
AF069316	sAPX	*Mesembryanthemum crystallinum*	9.E-61	151	67	76
AF069315	tAPX	*Mesembryanthemum crystallinum*	9.E-61	151	67	76
AB090956	sAPX	*Nicotiana tabacum*	9.E-61	151	67	76
AK287337	cDNA clone	*Glycine max*	3.E-60	153	67	78
BT036621	cDNA clone	*Zea mays*	6.E-60	150	63	79
AF532973	tAPX	*Triticum aestivum*	8.E-60	147	64	79
AY148471	sAPX	*Retama raetam*	5.E-59	152	66	78
AB125634	tAPX	*Brassica oleracea*	7.E-59	148	66	77
D83656	tAPX	*Cucurbita cv. K. A.*	7.E-59	149	66	77
D88420	sAPX	*Cucurbita cv. K. A.*	7.E-59	149	66	77
AY484493	sAPX	*Vigna unguiculata*	1.E-58	152	65	78

A phylogenetic analysis of available eukaryotic algae and higher plant APX nucleotide sequences (Table 3.5) produced three APX lineages (Figure 3.5). cAPXs and pAPXs segregated to form two distinct clades with high homologies in each group. The third and largest assemblage contained the eukaryotic green algae, *Porphyra* and higher plant chloroplast sequences. Although members of the higher plant chloroplastic APX (sAPX/ tAPX) group maintained high homologies with each other (i.e. bootstrap values >50%), the algal clade was distinguished using low bootstrap values and long branch lengths. So much variability within the algal cluster made it difficult to resolve relationships among the taxa (Figure 3.5), and warranted a second phylogenetic analysis with translated amino acid sequences.

The interspecific relationships of the algal clade were further resolved using translated amino acid APX sequences, in which a distinct eukaryotic algal cluster segregated from the higher plant chloroplast group (Figure 3.6). Although there was weak support in the algae group itself (e.g. bootstrap values below 50%), all of the algae sequences clearly separated from the higher plant chloroplastic clade. The *D. tertiolecta* APX (ACN86309) grouped with the other algae and higher plant chloroplast APX isoforms, corroborating with the NCBI blastx and tblastx results (Table 3.3 and 3.4).

Table 3.5. Classification of APX sequences used in phylogenetic analyses. All sequences are registered with the National Center for Biotechnology Information (NCBI) by their Accession number. Isoforms of APX types are designated: C (cytosolic) APX; T (thylakoid bound) APX; S (stromal) APX; P (peroxisomal) APX.

Group	Species	NCBI Accession #		APX type	Sequence type
		cDNA	protein		
Higher Plants	*Arabidopsis thaliana*	X98926		T	complete
	Arabidopsis thaliana	AY056319		S	complete
	Brassica oleracea	AB078599	BAB84008	C	complete
	Brassica oleracea	AB125635	BAD14931	T	complete
	Brassica oleracea	AB125634	BAD14932	S	complete
	Capsicum annum	X81376	CAA57140	C	complete
	Cucurbita sp. cv Kurokawa Amakuri	AB070626	BAB64351	P	complete
	Cucurbita sp. cv Kurokawa Amakuri	D88420	BAA22196	S	complete
	Cucurbita sp. cv Kurokawa Amakuri	D83656	BAA12029	T	complete
	Glycine max	AB082931	BAC92739	C	complete
	Hordeum vulgare	AB063117	BAB62533	P	complete
	Ipomoea batatas	AY206407		C	complete
	Nicotiana tabacum	U15933		C	complete
	Nicotiana tabacum	AB090956	BAA78553	S	partial
	Nicotiana tabacum	AB022273	BAA78552	T	complete
	Oryza sativa	AB053297	BAB20889	C	complete
	Pisum sativa	X62077	CAA43992	C	complete
	Raphanus sativus	X78452	CAA55209	C	complete
	Spinacia oleracea	D85864	BAA12890	C	complete
	Spinacia oleracea	D83669	BAA12039	S	complete
	Spinacia oleracea	D77997	BAA24609	T	complete
	Vigna unguiculata	U61379	AAB03844	C	complete
	Vigna unguiculata	AY466858	AAS46016	P	complete
	Vigna unguiculata	AY484493	AAS55853	S	complete
	Vigna unguiculata	AY484492	AAS55852	T	complete
Red Algae	*Galdieria partita*	AB037537			complete
	Galdieria sulphuraria	EF589721			complete
	Porphyra haitanensis	EU807991		C	complete
	Porphyra yezoensis	AY282755		C	complete
Green Algae	*Dunaliella tertiolecta*	FJ69282	ACN86309		partial
	Dunaliella salina	CX120243			partial
	Chlamydomonas reinhardtii	AJ223325	XP_001701947		complete
	Chlamydomonas sp. W80	AB009084	BAA83595		complete
	Chlorella vulgaris	AY973821	AAY51484		partial
	Chlorella symbiont of *Hydra viridis*	AY951933	AAY26385		partial
	Ulva fasciata	DQ286543	ABB88581		complete

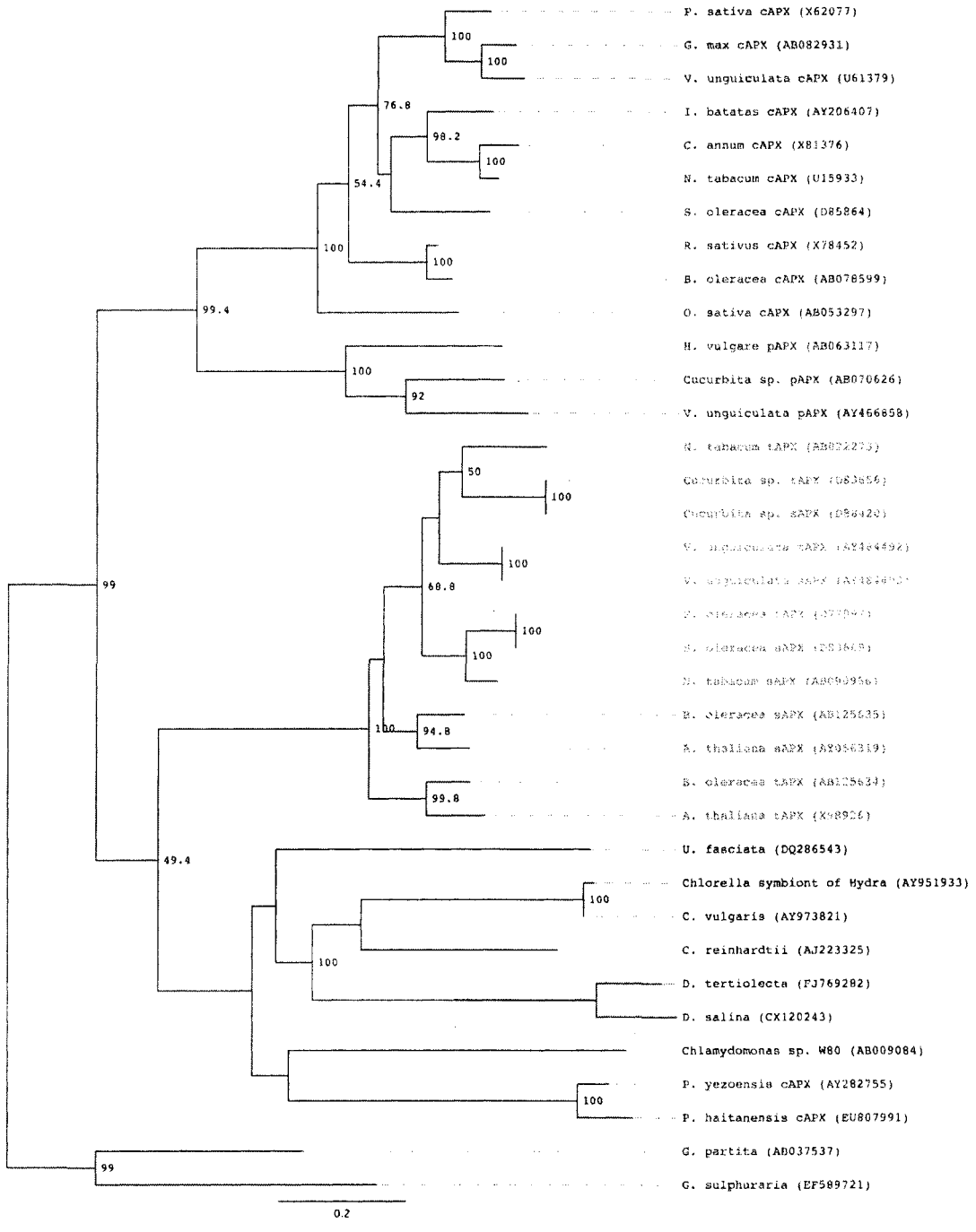

Figure 3.5. Phylogenetic analysis of ascorbate peroxidase APX. Phylogenetic tree represents results from an unrooted maximum likelihood (ML) analysis. APX cDNA sequences from higher plant chloroplast (green), peroxisome (blue) and cytosol (purple) were compared with eukaryotic green (black) and red (red) algal sequences. *D. tertiolecta* FJ769282 is a new sequence obtained in this study. Scale bar inferred number of nucleotide substitutions per site. Grey box denotes the *Dunaliella* clade.

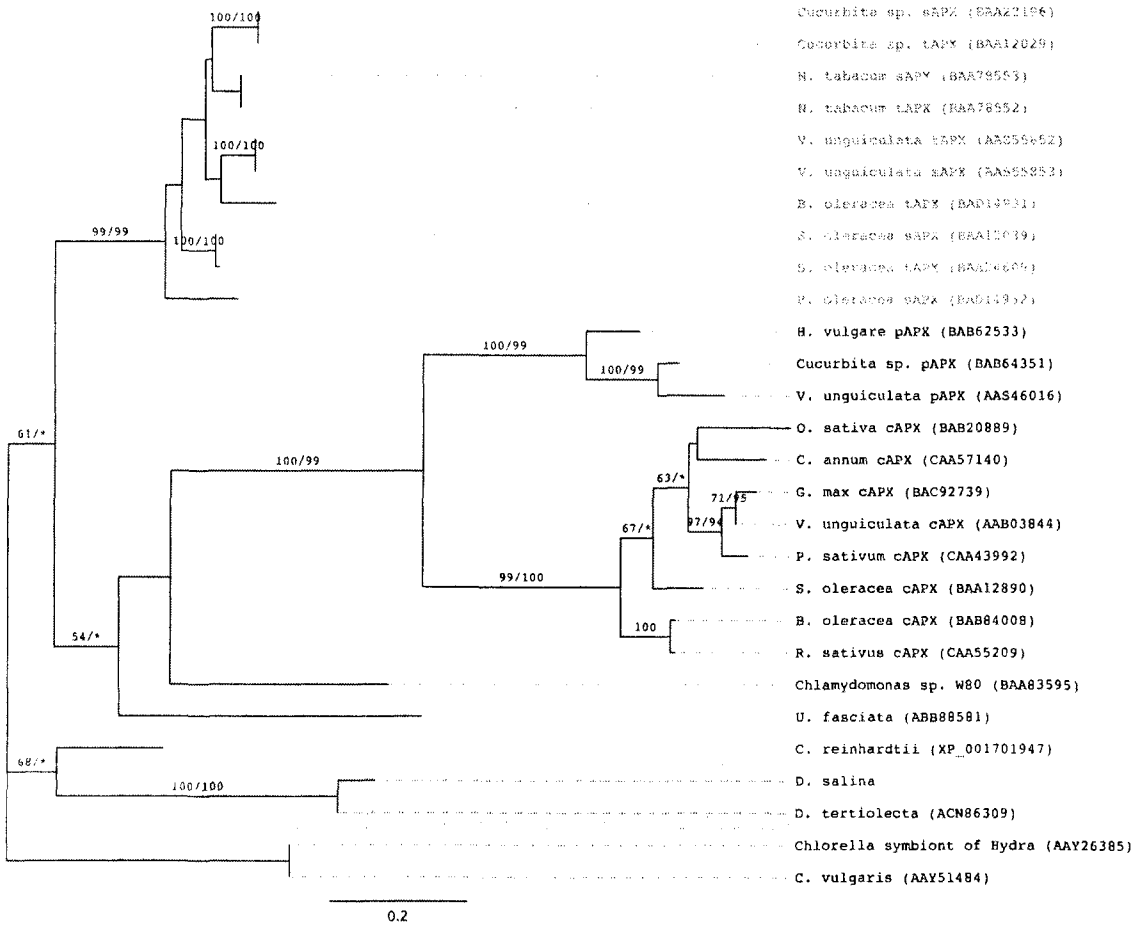

Figure 3.6. Phylogenetic analysis of ascorbate peroxidase APX protein sequences. Phylogenetic tree represents the results from unrooted maximum likelihood (ML) and a neighbor joining (NL) analyses. APX translated amino acid sequences from higher plant chloroplast (green), peroxisome (blue) and cytosol (purple) were compared with eukaryotic green algae (black) sequences. Bootstrap values represent results from ML/NJ analyses, respectively. Asterisks (*) indicate values below 50%. All sequences were aligned and trimmed to *D. tertiolecta* (ACN86309) prior to analyses. Grey box denotes the *Dunaliella* clade.

DISCUSSION

Biochemical characterization of APX

The generation of H_2O_2 as a metabolic by-product has necessitated the need for rapid and efficient ROS scavenging and detoxification systems. APX is a major contributor to redox regulation, and in higher plants is present as isoforms in various subcellular compartments. In the present study, four APX isoenzymes from the unicellular green alga *Dunaliella tertiolecta* were detected using an APX activity assay, contradicting previous claims that green algae only possess a single APX isoform (Figure 3.1; Takeda *et al.*, 1997, 1998; Ishikawa and Shigeoka, 2008).

The APX activity assay relies on the ascorbate-dependent reduction of nitroblue tetrazolium (NBT) in the presence of H_2O_2 (Mittler and Zilinskas, 1993). When ascorbate is oxidized, NBT reduction does not take place and an achromatic band is generated as evidence of APX activity. Because the presence of H_2O_2 is also required to drive this response, any enzyme that consumes H_2O_2 theoretically has the ability to form an achromatic band. Mittler and Zilinskas (1993) claimed to have vetted this technique against all enzymatic reactions capable of H_2O_2-dependent/independent ascorbate oxidation (e.g. APX, horseradish peroxidase and ascorbate oxidase). Yet, the intricacy of the assay combined with the heightened sensitivity of APX to ascorbate-deplete inactivation, generated uncertainty whether all four achromatic bands visualized actually represented APX isoforms. As a result, catalase and SOD in-gel activity assays were used to determine if achromatic bands formed as a result of non-APX enzyme action.

The close proximity between APX1 and SOD band suggests that this assay may not have been APX specific (Figure 3.1). Proteins in a native PAGE do not separate according to size, but are instead distributed by their charge density and hydrodynamic size. Charge density is based on a proteins amino acid composition and post-translational modifications (mass: charge ratio), while hydrodynamic size is centered on a proteins conformation (i.e. compact vs. relaxed). It is probable that APX1 and SOD possess similar charge densities and therefore migrated to similar locations in the gel column (of a 7.3% PAGE gel). It was also possible that an enzyme other than APX or SOD produced the achromatic bands.

To date, there are no previous reports characterizing multiple APX isoforms from a unicellular green alga. However, in the current study, immunoblotting of natively separated proteins confirmed the presence of cAPX (APX2) and at least one putative chloroplastic APX (APX3 and APX4) in *D. tertiolecta* (Figure 3.2). Virtually identical APX activity assay band patterns to those observed in the current study (i.e. one top band + lower doublet) have been reported for species in the monocot order Poales including *Triticum aestovi* L. (wheat), *Tricicum dicoccum* Schr., *Zea mays* (maize), *Zea Mexicana* (Schrad.) Iltis (Paciolla *et al.*, 1996) and *Triticum durum* (De Gara *et al.*, 2003), as well as in the archaic seed bearing plant *Ginkgo biloba* (Tommasi *et al.*, 1999). Paciolla *et al.* (1996) also examined a variety of dicot species, and while the majority (>50 species) produced only a single APX band, APX doublets were observed from extracts of *Liriodendron tulipifera* L. (tulip poplar), *Ranunculus* sp. L. (buttercup) and *Paeonia suffruticosa* Andrè (tree peony). Similar studies on *Arabidopsis thaliana* (Murgia *et al.*,

2004) and cultured tobacco cells (*Nicotiana tabacum*; de Pinto *et al.*, 2000) have also indicated the presence of an APX doublet from in-gel assays.

Confirmation that both cAPX and sAPXs existed in *D. tertiolecta* established that like higher plants, unicellular green algae also possess APX isoenzymes. The fact that the the APX1 activity band was not identified by native immunodetection does not necessarily imply that an enzyme other than APX was responsible for the in-gel reaction (Figure 3.2). Although APX proteins from various isoforms do maintain certain levels of homology, the sAPX and cAPX antibodies used in this study were made using APX isolated from tea leaf extracts and maize APX peptides, respectively. They were not specifically synthesized from *D. tertiolecta* APX protein or APX isolated from a closely related Chlorophyta species. Furthermore, the presence of at least three APX isoenzymes strongly suggests that like higher plants, unicellular green alga maintain isoforms of APX in multiple subcellular compartments. Therefore, immunodetection with only cytosolic and stromal specific APX antibodies neglected to account for isoforms potentially localized elsewhere in the cell (i.e. mitochondria). Consequently, the failure to identify APX1 activity bands as APX protein *via* immunodetection in the current study may have been the result of antibody-protein incompatibilities and/or the presence of a third APX isoform.

The idea that *D. tertiolecta* possesses isoforms of APX was further supported by the discovery of two proteins following SDS-PAGE (Figure 3.2d). The visualization of 59kDa and 19kDa proteins signifies that APX likely exists as a monomer and a homodimer. In *Euglena gracilis*, APX presumably functions in the cytosol as a 58kDa monomer and possess a similar biochemistry to that of cAPXs from higher plants

(Ishikawa *et al.*, 1996). Cross-reaction of *E. gracilis* monoclonal APX antibodies with cAPXs from *Brassica rapa*, *Arabidopsis* and spinach as well as sAPXs from *Chlamydomonas*, tea and spinach suggest that this enzyme retains high homologies to APX isoforms from various species and subcellular compartments (Ishikawa *et al.*, 1996). Therefore, the finding of an APX protein of similar size to that of the *Euglena* cAPX, may be one indication that *D. tertiolecta* possess a similar type of cAPX to that of *Euglena.*

In pea, tea, spinach and legume root nodules cAPX exists as a homodimer with a molecular weight of 57kDa, 57kDa, 48kDa and 47kDa, respectively (Dalton *et al.*, 1987; Nakano and Asada, 1987; Chen and Asada, 1989; Mittler and Zilinskas, 1991). In contrast to the cAPX isoform, chloroplastic APXs (sAPX/tAPX) from spinach, tea and *Arabidopsis* are smaller with molecular weights of 30/31, 34 and 40/46kDa, respectively (Chen and Asada, 1989; Nakano and Asada, 1987; Miyake *et al.*, 1993; Mittler and Poulos, 2005). Perhaps, the *D. tertiolecta* 18.9kDa protein described in the present study is representative of a homodimer APX isoform with a native molecular weight of 37.8kDa (Figure 3.2d). This hypothesis is highly speculative since all of the eukaryotic algal APXs characterized to date have been monomers localized in the chloroplast. APX monomers from *Chlorella vulgaris* (Takeda *et al.*, 1998) and the halotolerant *Chlamydomonas* sp. W80 (Takeda *et al.*, 2000) possess molecular masses of 32 and 30kDa, respectively while, both APX isoforms in the red alga *Galdieria partita* are monomers with a molecular weight of 28kDa (Sano *et al.*, 2001). Nonetheless, small APX proteins comparable to the 19kDa protein observed in the current study have been characterized. In *Arabidopsis*, the chloroplastic APX6 and the mitochondrial APX7

isoforms possess molecular weights of 18.2kDa and 11.7kDa, respectively (Mittler and Poulos, 2005). It is therefore hypothesized that *D. tertiolecta* contains at least two APX isoforms: (1) a 59kDa monomer APX enzyme that functions in the cytosol and (2) a 38kDa homodimer APX isoform that could be localized in either the cytosol or chloroplast.

The ambiguity regarding the characterization of the 18kDa APX protein stems from the fact that only cAPX-specific antibodies were used to determine the molecular weight of all APX proteins present in *D. tertiolecta*. Antibodies specific for sAPX were not available during these analyses, and as a consequence, it could not be determined whether APX proteins of identical sizes would have materialized if sAPX-specific antibodies were used. However, since proteins separated by SDS-PAGE are fully reduced and denatured it is plausible that the polyclonal cAPX antibodies recognized regions conserved in both cAPX and s/tAPXs.

Molecular characterization of APX

Amplification of *D. tertiolecta* cDNA using degenerate oligonucleotide primers designed using APX sequences from green algae (Table 3.1 and 3.2) produced a single 546bp fragment with high homology to APXs from *Chlamydomonas* and higher plants (Table 3.3 and 3.4). Alignment of the *D. tertiolecta* cDNA fragment with five uncharacterized ESTs from *D. salina* resulted in the resolution of a complete open reading frame, likely representative of an APX enzyme transcript (Figure 3.4). It was the occurrence of only one stop codon in the second reading frame of the the *D. tertiolecta* /*D. salina* alignment

(at the 5'end) which strongly suggested that this particular amino acid translation could correspond to a complete APX protein transcript (Figure 3.4).

Establishing which of the APX isoforms the *D. tertiolecta* cDNA associated with was determined by phylogenetic analyses of green algal APXs plus cAPX, pAPX and chloroplastic APXs from higher plants (Figure 3.5 and 3.6). The initial cDNA analysis, revealed two strongly supported cAPX and pAPX clades plus a third, highly variable group that contained both the algae and higher plant chloroplastic APXs (Figure 3.5). It was apparent that the higher plant chloroplastic sequences possessed high homologies with each other, yet their divergence from the algae cluster was poorly supported (bootstraps below 50%; Figure 3.5). A second analysis using translated amino acid sequences suggested that the algal strains were in fact divergent from the higher plant chloroplast APXs (Figure 3.6).

A clear definition of cAPX and pAPX groups was provided by robust branch separation from the chloroplastic APX/algae clade (Figure 3.6). The strong support of the higher plant chloroplast group (99% bootstrap value) suggests that although the algae group maintained weak associations, they are unambiguously discrete from the higher plant chloroplast clade. The placement of the newly described *D. tertiolecta* APX in the algal clade supports the hypothesis that this transcript represents an APX isoform localized in the chloroplast.

APPENDICES

APPENDIX A

FLUX DENSITIES AND CUMULATIVE DOSE OF UV-B AND UV-A RADIATION

Table A1. Flux densities and cumulative dose of UV-B and UV-A radiation. Cumulative dose values are representative of 12-hour exposures.

	μmol photons $m^{-2}s^{-1}$	Wm^{-2}	kJ m^{-2} day^{-1}
UV-B	5	2.0	86.4
	6	2.4	103.7
	7	2.8	120.9
	8	3.2	138.24
UV-A	60	20.55	887.76

APPENDIX B

ALIGNMENT AND AMINO ACID TRANSLATION OF FIVE *D. SALINA* EST SEQUENCES AND A *D. TERTIOLECTA* cDNA CONTIG

```
CX120131          #-158  TCCCACCCGC GTGCAGGCTG TGAACAAGGA GCAACTGGCG
BM447266          #-158  TCCCACCCGC GTGCAGGCTG TGAACAAGGA GCAACTGGCG
BM447534          #-158  TCCCACCCGC GTGCAGGCTG TGAACAAGGA GCAACTGGCG
CX120243          #-158  TCTAGAACTA GTGGATCCCC CGGGC:TGCA GGAA:T:TCG

                  #-158  TCCCACCCGC GTGCAGGCTG TGAACAAGGA GCAACTGGCG
                          P  T  R     V  Q  A  V     N  K  E     Q  L  A

CX120131          #-118  GGAGCATACA CCGAGCTCAA GAACTACATC CAGAGCAAAT
BM447266          #-118  GGAGCATACA CCGAGCTCAA GAACTACATC CAGAGCAAAT
BM447534          #-118  GGAGCATACA CCGAGCTCAA GAACTACATC CAGAGCAAAT
CX120243          #-118  GCA:C:GAGG CCGAGCTCAA GAACTACATC CAGAGCAAAT

                  #-118  GGAGCATACA CCGAGCTCAA GAACTACATC CAGAGCAAAT
                         G  A  Y  T     E  L  K     N  Y  I     Q  S  K  Y

CX120131           #-78  ACTGCAACCC CATCATCATC CGCCTGGCCT GGCATGATGC
BM447266           #-78  ACTGCAACCC CATCATCATC CGCCTGGCCT GGCATGATGC
BM447534           #-78  ACTGCAACCC CATCATCATC CGCCTGGCCT GGCATGATGC
CX120243           #-78  ACTGCAACCC CATCATCATC CGCCTGGCCT GGCATGATGC

                   #-78  ACTGCAACCC CATCATCATC CGCCTGGCCT GGCATGATGC
                           C  N  P     I  I  I     R  L  A  W     H  D  A

CX120131           #-38  CGGCACGTAT GACTGCACCA AAACCGAATT TCCCCAGCGC
BM447266           #-38  CGGCACGTAT GACTGCACCA AAACCGAATT TCCCCAGCGC
BM447534           #-38  CGGCACGTAT GACTGCACCA AAACCGAATT TCCCCAGCGC
CX120243           #-38  CGGCACGTAT GACTGCACCA AAACCGAATT TCCCCAGCGC
D. tertiolecta     >#1>                                          GC

                   #-38  CGGCACGTAT GACTGCACCA AAACCGAATT TCCCCAGCGC
                          G  T  Y     D  C  T  K     T  E  F     P  Q  R

CX120131             #3  GGAGGTGCCA ACGGTGCCAT CCGATTCCAG CCTGAGCTGA
BM447266             #3  GGAGGTGCCA ACGGTGCCAT CCGATTCCAG CCTGAGCTGA
BM447534             #3  GGAGGTGCCA ACGGTGCCAT CCGATTCCAG CCTGAGCTGA
CX120243             #3  GGAGGTGCCA ACGGTGCCAT CCGATTCCAG CCTGAGCTGA
D. tertiolecta       #3  GGAGGTGCCA ACGGTGCCAT CCGATTCCAG CCTGAGCTGA

                     #3  GGAGGTGCCA ACGGTGCCAT CCGATTCCAG CCTGAGCTGA
                         G  G  A  N     G  A  I     R  F  Q     P  E  L  S
```

```
CX120131          #43  GCCATGGTCA CAATGCAGGT CTGCAGGTGG CACTGGCCCT
BM447266          #43  GCCATGGTCA CAATGCAGGT CTGCAGGTGG CACTGGCCCT
BM447534          #43  GCCATGGTCA CAATGCA
CX120243          #43  GCCATGGTCA CAATGCAGGT CTGCAGGTGG CACTGGCCCT
D. tertiolecta    #43  GCCATGGTCA CAATGCAGGT CTGCAGGTGG CACTGGCCCT

                  #43  GCCATGGTCA CAATGCAGGT CTGCAGGTGG CACTGGCCCT
                         H  G  H   N  A  G   L  Q  V  A   L  A  L


CX120131          #83  GCTGAAGCCC ATGAAGGCCA AGTACCCTGA CGTCTCCCAC
BM447266          #83  GCTGAAGCCC ATGAAGGCCA AGTACCCTGA CGTCTCCCAC
CX120243          #83  GCTGAAGCCC ATGAAGGCCA AGTACCCTGA CGTCTCCCAC
D. tertiolecta    #83  GCTGAAGCCC ATGAAGGCCA AGTACCCTGA CGTCTCCCAC

                  #83  GCTGAAGCCC ATGAAGGCCA AGTACCCTGA CGTCTCCCAC
                        L  K  P   M  K  A  K   Y  P  D   V  S  H


CX120131         #123  GCAGACCTGT TTCAGATGGC CTCTGCTGCA GCCATCGAAG
BM447266         #123  GCAGACCTGT TTCAGATGGC CTCTGCTGCA GCCATCGAAG
CX120243         #123  GCAGACCTGT TTCAGATGGC CTCTGCTGCA GCCATCGAAG
D. tertiolecta   #123  GCAGACCTGT TTCAGATGGC CTCTGCTGCA GCCATCGAAG

                 #123  GCAGACCTGT TTCAGATGGC CTCTGCTGCA GCCATCGAAG
                       A  D  L  F   Q  M  A   S  A  A   A  I  E  A


CX120131         #163  CCGCGGGTGG GCCCAAGATC GACATGCAGT ATG:GTCGCA
BM447266         #163  CCGCGGGTGG GCCCAAGATC GACATGCAGT ATG:GTCGCA
CX120243         #163  CCGCGGGTGG GCCCAAGATC GACATGCAGT ATG:GTCGCA
D. tertiolecta   #163  CCGCGGGTGG GCCCAAGATC GACATGCAGT ATG:GTCGCA
CX120057        >#191>                                 GC ACGAGGCGCA

                 #163  CCGCGGGTGG GCCCAAGATC GACATGCAGT ATG:GTCGCA
                        A  G  G   P  K  I   D  M  Q  Y   G   R  K


CX120131         #202  AGGACGTGAC AGAC
BM447266         #202  AGGACGTGAC AG
CX120243         #202  AGGACGTGAC AGACGAACAA GGCTGTGCTC AAGATGGCCT
D. tertiolecta   #202  AGGACGTGAC AGACGAACAA GGCTGTGCTC AAGATGGCCT
CX120057         #202  AGGACGTGAC AGACGAACAA GGCTGTGCTC AAGATGGCCT

                 #202  AGGACGTGAC AGACGAACAA GGCTGTGCTC AAGATGGCCT
                        D  V  T   D  E  Q   G  C  A  Q   D  G  L


CX120243         #242  GCTCCCAGCT CCCATGCACG GAAGTAGCGC CACAGCGGCT
D. tertiolecta   #242  GCTCCCAGCT CCCATGCACG GAAGTAGCGC CACAGCGGCT
CX120057         #242  GCTCCCAGCT CCCATGCACG GAAGTAGCGC CACAGCGGCT

                 #242  GCTCCCAGCT CCCATGCACG GAAGTAGCGC CACAGCGGCT
                        L  P  A   P  M  H  G   S  S  A   T  A  A
```

```
CX120243          #282  GACCACATCC GCAAGGTGTT CAACCGCATG GGCTTCAACG
D. tertiolecta    #282  GACCACATCC GCAAGGTGTT CAACCGCATG GGCTTCAACG
CX120057          #282  GACCACATCC GCAAGGTGTT CAACCGCATG GGCTTCAACG

                  #282  GACCACATCC GCAAGGTGTT CAACCGCATG GGCTTCAACG
                        D  H  I  R   K  V  F   N  R  M   G  F  N  D


CX120243          #322  ACCAGGAGAT TGTGGTGCTG TCTGGCGCCC ACACCCTGGG
D. tertiolecta    #322  ACCAGGAGAT TGTGGTGCTG TCTGGCGCCC ACACCCTGGG
CX120057          #322  ACCAGGAGAT TGTGGTGCTG TCTGGCGCCC ACACCCTGGG

                  #322  ACCAGGAGAT TGTGGTGCTG TCTGGCGCCC ACACCCTGGG
                          Q  E  I   V  V  L   S  G  A  H   T  L  G


CX120243          #362  CCGCGTGAGG AAGGATCGCT CTGGCCTTGG TGTGGATGAG
D. tertiolecta    #362  CCGCGTGAGG AAGGATCGCT CTGGCCTTGG TGTGGATGAG
CX120057          #362  CCGCGTGAGG AAGGATCGCT CTGGCCTTGG TGTGGATGAG

                  #362  CCGCGTGAGG AAGGATCGCT CTGGCCTTGG TGTGGATGAG
                         R  V  R   K  D  R  S   G  L  G   V  D  E


CX120243          #402  ACCNAGTACA CCAAGGACGG CCCCGGCCTG AAGGGCGGGA
D. tertiolecta    #402  ACCAAGTACA CCAAGGACGG CCCCGGCCTG AAGGGCGGGA
CX120057          #402  ACCAAGTACA CCAAGGACGG CCCCGGCCTG AAGGGCGGGA

                  #402  ACCAAGTACA CCAAGGACGG CCCCGGCCTG AAGGGCGGGA
                        T  K  Y  T   K  D  G   P  G  L   K  G  G  T
                           +

CX120243          #442  CCTCCTGGAC CC:TGACTGG CTGA:CTTCA :CA:CAGCTA
D. tertiolecta    #442  CCTCCTGGAC CCCTGACTGG CTGAACTTCA ACAACAGCTA
CX120057          #442  CCTCCTGGAC CCCTGACTGG CTGAACTTCA ACAACAGCTA

                  #442  CCTCCTGGAC CCCTGACTGG CTGAACTTCA ACAACAGCTA
                          S  W  T   P  D  W   L  N  F  N   N  S  Y
                                       .           .      .  .

CX120243          #482  CT:C:NTGA: TTGAAG:CCA GG:GCGAC:C CGAC:TGAT:
D. tertiolecta    #482  CTTCACTGAA TTGAAGGCCA GGCGCGACGC CGACCTGATT
CX120057          #482  CTTCACTGAA TTGAAGGCCA GGCGCGACGC CGACCTGATT

                  #482  CTTCACTGAA TTGAAGGCCA GGCGCGACGC CGACCTGATT
                         F  T  E   L  K  A  R   R  D  A   D  L  I
                          .  .+   .      .      .     .      .    .

CX120243          #522  G:GATGNA:A C:GATGC:TG C:T:NTTGAG :AT:A:
D. tertiolecta    #522  GTGATGGACA CCGATGCCTG CATCT
CX120057          #522  GTGATGGACA CCGATGCCTG CATCTTTGAG GATGAG

                  #522  GTGATGGACA CCGATGCCTG CATCTTTGAG GATGAG
                        V  M  D  T   D  A  C   I  F  E   D  E
                         .    +  .   .     .    .  .+      .  .  .
```

LITERATURE CITED

Adams, P. and Britz, S.J. 1992. Spectral quality of two fluorescent UV sources during long-term use. *Photochem. Photobiol.* 56, 641-644.

Aguilera, J., Dummermuth, A., Karsten, U., Schriek, R. and Wiencke, C. 2002. Enzymatic defences against photooxidative stress induced by ultraviolet radiation in Arctic marine macroalgae. *Polar Biol.* 25: 432-441.

Allen, D.J., Nogues, S. and Baker, N.R. 1998. Ozone depletion and increased UV-B radiation: is there a real threat to photosynthesis? *J. Exp. Bot.* 49: 1775-1788.

Alscher, R.G., Erturk, N. and Heath, L.S. 2002. Role of superoxide dismutases (SODs) in controlling oxidative stress in plants. *J. Exp. Bot.* 53 (372): 1331-1341.

Anderson, J.M., Chow, W.S. and Goodchild, D.J. 1988. Thylakoid membrane organization in sun/shade acclimation. *In:* Evans, J.R., Caemmerer, S. von, Adams, W.W. III. (eds.) *Ecology of Photosynthesis in Sun and Shade.* Pp. 11-26. CSIRO, Melbourne.

Anderson, J.M., Chow, W.S. and Park, Y-I. 1995. The grand design of photosynthesis: acclimation of the photosynthetic apparatus to environmental cues. *Photosynth. Res.* 46: 129-139.

Anderson, J.M and Osmond, C.B. 1987. Shade-sun responses: Compromises between acclimation and photoinhibition. In: Kyle, D.J., Osmond, C.B. and Arntzen, C.J. (*eds.*) *Photoinhibition.* Elsevier, Amsterdam. pp. 1-38.

Andreasson, K.I.M. and Wängberg, S.-Å. 2006. Biological weighting functions as a tool for evaluating two ways to measure UVB radiation inhibition on photosynthesis. *J. Photochem. Photobiol. B: Biol.* 84: 111-118.

Andreasson, K.I.M. and Wängberg, S.-Å. 2007. Reduction in growth rate in *Phaeodactylum tricornutum* (Bacillariophyceae) and *Dunaliella tertiolecta* (Chlorophyceae) induced by UV-B radiation. *J. Photochem. Photobiol.* B. 86: 227-233.

Apel, K. and Hirt, H. 2004. Reactive oxygen species: metabolism, oxidative stress, and signal transduction. *Annu. Rev. Plant Biol.* 55: 373-399.

Aro, E-M., McCaffery, S. and Anderson , J.M. 1993. Photoinhibition and D1 Protein Degradation in Peas Acclimated to Different Growth Irradiances. *Plant Physiol.* 103: 835-843

Asada, K and Takahashi, M. 1987. Production and scavenging of active oxygen in photosynthesis. In: Kyle, D. J., Osmond, C. B. and Arntzen, C. J. (*eds.*) *Photoinhibition.* Elsevier Science Publishers, Amsterdam, New York, Oxford. pp.227- 289

Asada, K. 1999. The water-water cycle as alternative photon and electron sinks. *Philos. Trans. R. Soc. Lond. B Biol. Sci.* 355:1419-1431.

Asada, K. 2006. Production and scavenging of reactive oxygen species in chloroplasts and their functions. *Plant Physiol.* 141: 391-396.

Aubailly, M., Haigle, J., Giordani, A., Morliere, P. and Santus, R. 2000. UV photolysis of catalase revisited: a spectral study of photolytic intermediates. *J. Photochem Photobiol B: Biol.* 56: 61-67.

Baker, N.R. 1996. Photoinhibition of photosynthesis. *In*: Jennings, R.C., Zucchelli, G., Ghetti, F. and Colombetti, G. (*eds.*) *Light as an Energy Source and Information Carrier in Plant Physiology*. Plenum Press, New York. pp. 89-97.

Baker, N.R. 2008. Chlorophyll fluorescence: A probe of photosynthesis in vivo. *Annu. Rev. Plant Biol.* 59; 89-113.

Bari, R., Kebeish, R., Kalamajka, R., Rademacher, T. and Peterhänsel, C. 2004. A glycolate dehydrogenase in the mitochondria of *Arabidopsis thaliana*. *J. Exp. Bot.* 55 (397): 623-630.

Baroli, I. and Melis, A. 1998. Photoinhibitory damage is modulated by the rate of photosynthesis and by the photosystem II light-harvesting chlorophyll antenna size. *Planta* 205: 288-296

Barta, C., Kálai, T., Hideg, K., Vass, I. and Hideg, E. 2004. Differences in the ROS-generating efficiency of various ultraviolet wavelengths in detached spinach leaves. *Funct. Plant Biol.* 31: 23-28.

Banaszak, A. T. and Neale, P. J. 2001. Ultraviolet radiation sensitivity of photosynthesis in phytoplankton from an estuarine environment. *Limol. Oceangr.* 46, 592-603.

Beardall, J., Heraud, P., Roberts, S., Shelly, K. and Stojkovic, S. 2002. Effects of UV-B radiation on inorganic carbon acquisition by the marine microalga *D. tertiolecta* (Chlorophyceae). *Phycologia* 41: 269-272.

Beauchamp. C. and Fridovich, I. 1971. Superoxide dismutase: improved assays and an assay applicable to acrylamide gels. *Anal. Biochem.* 44(1): 276-287.

Behrenfeld, M. J., Chapman, J. W., Hardy J. T. and Lee, H. 1993 Is there a common response to ultraviolet-B radiation by marine phytoplankton? *Mar. Ecol. Progr. Series* 102: 59-68.

Ben-Amotz, A., A Lers, M. Avron, 1988. Stereoisomers of ß-carotene and phytoene in the alga *Dunaliella bardawil*. Plant Physiol. 86 (1988) 1286-1291

Bischof, K., Hanelt, D. and Wiencke, C. 2000. Effects of ultraviolet radiation on photosynthesis and related enzyme reactions of marine macroalgae. *Planta* 211: 555-562.

Blankenship, R.E. 2002. *Molecular mechanisms of photosynthesis*. Blackwell Science Ltd. Malden, MA, USA. pp. 321.

Boardman, N.K. 1977. Comparative Photosynthesis of Sun and Shade Plants. *Ann. Rev. Plant Physiol.* 28: 355-377.

Bouchard, J.N., Campbell, D.A. and Roy, S. 2005. Effects of UV-B radiation on the D1 protein repair cycle of natural phytoplankton communities from three latitudes (Canada, Brazil and Argentina). *J. Phycol.* 41: 273-286.

Boucher, N.P. and Prezélin, B.B. 1996. An *in situ* biological weighting function for UV inhibition of phytoplankton carbon fixation in the Southern Ocean. *Mar. Ecol. Prog. Ser.* 144: 223-236.

Bowen, E.J. 1932. Light filters for the mercury lamp. *J. Chem. Soc.* 1932: 2236-2239.

Bowen, E. J. 1946. *The Chemical Aspects of Light.* Clarendon Press, Oxford. 300pp.

Braidot, E., Petrussa, E., Vianello, A. and Macri, F. 1999. Hydrogen peroxide generation by higher plant mitochondria oxidizing complex I or complex II substrates. *FEBS Letters* 451: 347-350.

Britt, A.B. 2004 Repair of DNA damage induced by solar UV. *Photosynth. Res.* 81:105-112.

Buchanan, B.B., Gruissem, W. and Jones, R.L. 2000. *Biochemistry and Molecular Biology of Plants*. p. 1367. American Society of Plant Physiologists, Maryland, USA.

Bühlmann, B., Bossard, P. and Uehlinger, U. 1987. The influence of longwave ultraviolet radiation (u.v.-A) on the photosynthetic activity (14C-assimilation) of phytoplankton. *J. Plankton. Res.* 9: 935-943.

Caldwell, M.M. 1971. Solar UV irradiation and the growth and development of higher plants In: A.C. Giese (*ed.*) *Photophysiology v1: Current topics in photobiology and photochemistry*. pp.131-177.

Caldwell, M.M., Gold, W.G., Harris, G. and Ashurst, C. W.1983. A modulated lamp system for solar UV-B (280-320). Supplementation studies in the field. *Photochem. Photobiol.* 37:479-485.

Caldwell, M.M., Camp, L.B., Warner, C.W. and Flint, S.D. 1986. Action spectra and their key role in assessing biological consequences of solar UV-B radiation change. In: *Stratospheric Ozone Reduction, Solar Ultraviolet Radiation and Plant Life.* Worrest, R. and Caldwell, M. (eds.) pp. 87-111. Springer-Verlag, New York.

Caldwell, M.M., Flint, S.D. and Searles, P.S. 1994. Spectral balance and UV-B sensitivity of soybean: a field experiment. *Plant, Cell and Environ.* 17:267-276.

Caldwell, M.M., and Flint, S.D. 1997. Uses of biological spectral weighting functions and the need of scaling for the ozone reduction problem. *Plant Ecology* 128, 66-76.

Caldwell, M.M., and Flint, S.D. 2006. Use and evaluation of biological spectral UV weighting functions for the ozone reduction issue. In: Ghetti, F., Checcucci, G. and Bornman, J.F. (eds.) *Environmental UV Radiation Impact on Ecosystems and Human Health and Predictive Models*. Springer, The Netherlands. pp. 71-84.

Callieri, C., Morabito, G., Huot, Y., Neale, P.J. and Litchman, E. 2001. Photosynthetic response of pico- and nanoplanktonic algae to UVB, UVA and PAR in a high mountain lake. *Aquat. Sci.* 63: 286-293.

Chen, G-X. and Asada, K. 1989. Ascorbate peroxidase in tea leaves: occurrence of two isozymes and the difference in their enzymatic and molecular properties. *Plant Cell Physiol.* 30 (7): 987-998.

Chen, H. and Jiang, J-G. 2009. Osmotic responses of *Dunaliella* to the changes of salinity. *J. Cell. Physiol.* 219: 251-258.

Cheng, L., Kellogg, E.W. and Packer, L. 1981. Photoinactivation of catalase. *Photochem Photobiol.* 34:125-129.

Cheng, L., Qiao, D.R. Lu, X.Y., Xiong, Y., Bai, L.H., Xu, H., Yang, Y. and Cao, Y. 2007. Identification and expression of the gene product encoding a CPD photolyase from *Dunaliella salina*. *J. Photochem. Photobiol. B: Biology* 87: 137-143.

Chew, O., Whelan, J. and Miller, A.H. 2003. Molecular definition of the ascorbate-glutathione cycle in Arabidopsis mitochondria reveals dual targeting of antioxidant defenses in plants. *J. Biol. Chem.* 278: 46869-46877.

Cleland, R.E. and Melis, A. 1987. Probing the events of photoinhibition by altering electron-transport activity and light-harvesting capacity in chloroplast thylakoids. *Plant Cell Environ.* 10: 747-752.

Cullen, J.J and Lesser, M.P. 1991. Inhibition of photosynthesis by ultraviolet radiation as a function of dose and dosage rate: results for a marine diatom. *Mar. Biol.* 111:183-190.

Cullen, J.J. and Neale, P.J. 1994. Ultraviolet radiation, ozone depletion and marine photosynthesis. *Photosynth. Res.* 39: 303-320.

Cullen, J.J. and Neale, P.J. 1997. Biological weighting functions for describing the effects of ultraviolet radiation on aquatic systems. In *The Effects of Ozone Depletion on Aquatic Ecosystems.* Häder, D.-P. (*ed.*) pp. 97-118 Academic. Press, NY.

Cullen, J.J., Neale, P.J. and Lesser, M.P. 1992. Biological weighting function for the inhibition of phytoplankton photosynthesis by ultraviolet radiation. *Science* 258: 646-650.

Cunningham. M.L., Johnson, J.S., Giovanazzi, S.M. and Peak, M.J. 1985. Photosensitized production of superoxide anion by monochromatic (290 -405 nm) ultraviolet irradiation of NADH and NADPH coenzymes. *Photochem. Photobiol.* 42: 125-128.

Czochralska, B., Bojarska, E., Pawlicki, K. and Shugar, D. 1990. Photochemical and enzymatic redox transformations of reduced forms of coenzyme NADP+. *Photochem. Photobiol.* 51(4): 401-410.

Dabrowska, G., Kata, A., Goc, A., Szechynska-Hebda, M. and Skrzypek, E. 2007. Characteristics of the plant ascorbate peroxidase family. *Acta Biol. Cracov. Bot.* 49(1): 7-17.

Day, T. A. and Neale, P. J. 2002. Effects of UV-B radiation on terrestrial and aquatic primary producers. *Ann. Rev. Ecol. Syst.* 33:371-96.

Dalton, D.A., Hanus, F.J., Russell, S.A and Evans, H.J. 1987. Purification, properties and distribution of ascorbate peroxidase in legume root nodules. *Plant Physiol.* 83: 789-794.

Davletova, S., Rizhsky, L., Liang, H., Shengqiang, Z., Oliver, D.J., Coutu, J., Shulaev, V., Schlauch, K. and Mittler, R. 2005. Cytosolic ascorbate peroxidase is a central component of the reactive oxygen gene network of *Arabidopsis. Plant Cell* 17: 268-281.

Deckmyn, G. and Impens, I. 1997. The ratio of UV-B/photosynthetic active radiation (PAR) determines the sensitivity of rye to increased UV-B radiation. *Env. Exp. Botany* 37:3-12.

Deckmyn, G., Martens, C. and Impens, I. 1994 The importance of the ratio UV-B/photosynthetic active radiation (PAR) during leaf development as determining factor of plant sensitivity to increased UV-B irradiance: effects on growth, gas exchange and pigmentation of bean plants (*Phaseolus vulgaris* cv. Label) *Plant, Cell and Environ.* 17: 295-301.

De Gara, L., de Pinto, M.C. and Arrigoni, O. 1997. Ascorbate synthesis and ascorbate peroxidase activity during the early stage of wheat germination. *Physiol. Plant.* 100: 894-900.

De Gara, L., de Pinto, M.C., Moliterni, V.M.C.and D'Egidio, M.G. 2003. Redox regulation and storage processes during maturation in kernels of *Triticum durum. J. Exp. Bot.* 54(381): 249-258.

Delieu, T. and Walker, D. 1972. An improved cathode for the measurement of photosynthetic oxygen evolution by isolated chloroplasts. *New Phytol.* 71: 210-225.

Del Rio, L., Ortega, G. M., Lopez, L. A. and Lopez, G.J.1977. A more sensitive modification of the catalase assay with the clark oxygen electrode. *Anal. Biochem.* 80: 409-415.

Demmig-Adams, B. 1990. Carotenoids and photoprotection in plants: a role for the xanthophyll zeaxanthin. *Biochim. Biophys. Acta* 1020: 1-24.

Demmig-Adams, B. and Adams, W.W. 2006. Photoprotection in an ecological context: the remarkable complexity of thermal energy dissipation. *New Phytol.* 172: 11-21.

Desikan, R., Hancock, J. and Neill, S. 2005. Reactive oxygen species as signaling molecules. In: Smirnoff, N, *(ed.) Antioxidants and Reactive Oxygen Species in Plants*. Blackwell Publishing Ltd. Oxford, UK. Pp. 169-196.

Döhler, G., Drebes, G. and Lohmann, M. 1997. Effect of UV-A and UV-B radiation on pigments, free amino acids and adenylate content of *Dunaliella tertiolecta* Butcher (Chlorophyta). *J. Photochem. Photobiol. B: Biol.* 40 (2): 126-131.

Döhring, T., Köfferlein, M., Thiel, S. and Seidlitz, J. K. 1996. Spectral shaping of artificial UV-B irradiation for vegetation research. *J. Plant Physiol.* 148: 115-119.

Dring, M.J., Wagner, A., Boeskov, J. and Luning, K. 1996. Sensitivity of intertidal and subtidal red algae to UVA and UVB radiation, as monitored by chlorophyll fluorescence measurements: influence of collection depth and season and length of irradiation. *Eur. J. Phycol.* 31: 293-302.

Durrant, J.R., Giorgi, L.B., Barber, J., Klug, D.R. and Porter, G. 1990. Characterization of triplet states in isolated photosystem II reaction centres: oxygen quenching as a mechanism for photodamage. *Biochimica et Biophysica Acta* (BBA) *Bioenergetics* 1017 (2,1): 167–175.

Estevez, M.S., Malanga, G. and Puntarulo, S. 2001. UV-B effects on Antarctic *Chlorella* sp cells. *J Photochem. and Photobiol. B: Biology* 62: 19-25.

Fagerberg, W.R. 2007. Below-ambient levels of UV indce chloroplast structural change and alter starch metabolism. *Protoplasma* 230: 51-59.

Fagerberg, W.R. and Bornman, J.F. 1997. Ultraviolet-B radiation causes shade-type ultrastructural changes in *Brassica napus*. *Physiol. Plant.* 101:833-844.

Feierabend, J. and Engel, S. 1986. Photoinactivation of catalase in vitro and in leaves. *Arch. Biochem. Biophys.* 251(2): 567-576.

Figueroa, F.L., Bianco, J.M., Jimenez-Gomez, F and Rodriguez, J. 1997. Effects of ultraviolet radiation on carbon fixation in Antarctic nanophytoflagellates. *Photochem. Photobiol.* 66(2): 185-189.

Fiscus, E.L. and Booker, F.L. 1995. Is increased UVB a threat to crop photosynthesis and productivity? *Photosynth. Res.* 43: 81-92.

Flint, S.D. and Caldwell, M.M. 2003. Field testing of UV biological spectral weighting functions for higher plants. *Physiol. Plant.* 117: 145-153.

Franklin, L.A., Levavasseur, G., Osmond, C.B. Henley, W.J. and Rasmus, J. 1992. Two components of onset and recovery during photoinhibition of *Ulva rotundata*. *Planta* 186: 399-408.

Frederick, S.E., Gruber, P.J. and Tolbert, N.E. 1973. The occurrence of glycolate dehydrogenase and glycolate oxidase in green plants. *Plant Physiol.* 52: 318-323.

Friso, G., Vass, I., Spetea, C., Barber, J. and Barbato, R. 1995. UV-B-induced degradation of the D1 protein in isolated reaction centres of photosystem II. *Biochim. Biophys. Acta* 1231: 41-46.

Frugoli, J.A., Zhong, H., Nuccio, M., McCourt, P., McPeek, M., Thomas, T. and McClung, C.R. 1996. Catalase is encoded by a multigene family in *Arabidopsis thaliana* (L.) Heynh. *Plant Physiol.* 112: 327-336.

Fufezan, C., Gross, C. M., Sjödin, M., Rutherford, A.W., Krieger-Liszkay, A. and Kirilovsky, D. 2007. Influence of the redox potential of the primary quinone electron acceptor on photoinhibition in photosystem II. *J. Biol. Chem.* 282 (17): 12492-12502.

Gerhardt, K.E., Wilson, M.I. and Greenberg, B.M. 1999. Tryptophan photolysis leads to a UVB-induced 66 kDa photoproduct of ribulose-1,5-bisphosphate carboxylase/oxygenase (Rubisco) in vitro and in vivo. *Photochem. Photobiol.* 70(1): 49-56.

Gerstl, S.A., Zardecki, W.A. and Wiser, H.L. 1986. A new UV-B handbook, volume I. In: Worrest, R.C. and Caldwell M.M. (*eds.*) *Stratospheric Ozone Reduction, Solar Ultraviolet Radiation and Plant Life* NATO ASI, Vol. G8, Springer-Verlag, Berlin. pp. 63-74.

Ghetti, F., Fuoco, S. and Checcucci, G. 1998. UVB monochromatic action spectrum for the inhibition of photosynthetic oxygen production in the green alga *Dunaliella salina. Photochem. Photobiol.* 68: 276-280.

Ghetti, F., Herrmann, H., Hader, D.-P. and Seidlitz. 1999. Spectral dependence of the inhibition of photosynthesis under simulated global radiation in the unicellular green alga *Dunaliella salina.* J. *Photochem. Photobiol. B: Biol.* 48: 166-173.

Goyal, A. 2007. Osmoregulation in *Dunaliella*, Part I. Effects of osmotic stress on photosynthesis, dark respiration and glycerol metabolism in *Dunaliella tertiolecta* and its salt-sensitive mutant (HL 25/8). *Plant Physiol. Biochem.* 45: 696-704.

Greenberg, B.M., Wilson, M.I., Gerhardt, K.E. and Wilson, K.E. 1996. Morphological and physiological responses of *Brassica napus* to ultraviolet-B radiation: photomodification of ribulose-1,5-bisphosphate carboxylase/oxygenase and potential acclimation processes. *J. Plant Physiol.* 148: 78-85.

Greenberg, B.M., Wilson, M.I., Huang, X-D. Duxbury, C.L., Gerhardt, K.E. and Gensemer, R.W. 1997. The effects of ultraviolet-B radiation on higher plants. In: *Plants for Environmental Studies.* CRC Press LLC. p. 1-35.

Grotjohann, N., Janning, A. and Eising, R. 1997. In vitro photoinactivation of catalase isoforms from cotyledons of sunflower (*Helianthus annuus* L.). *Arch. Biochem. Biophys.* 346(2): 208-218.

Grzymski, J., Orrico, C. and Schofield, O.M. 2001. Monochromatic ultraviolet light induced damage to photosystem II efficiency and carbon fixation in the marine diatom *Thalassiosira pseudonana* (3H). *Photosynth. Res.* 68: 181-192.

Guindon, S. and Gascuel, O. 2003. A simple, fast, and accurate algorithm to estimate large phylogenies by maximum likelihood. *Syst. Biol.* 52: 696-704.

Häder,D-P, Kumar, H.D., Smith, R.C. and Worrest, R.C. 2003. Aquatic ecosystems: effects of solar ultraviolet radiation and interactions with other climatic change factors. *Photochem. Photobiol. Sci.* 2: 39-50.

Hakala, M., Tuominen,I., Keränen, M., Tyystjärvi, T. and Tyystjärvi, E. 2005. Evidence for the role of the oxygen-evolving manganese complex in photoinhibition of Photosystem. *Biochem. Biophys. Acta (BBA) Bioenergetics* 1706 (1-2): 68-80.

Hall, D.O. and Rao, K.K. 1999. *Photosynthesis* 6th Edition. Cambridge Universtiy Press, Cambridge, UK. p.214.

Halliwell, B. and Gutteridge, J. M. C. 1999. *Free Radicals in Biology and Medicine* 3rd Edition. p.936. Oxford University Press, New York.

Hanlet, D., Huppertz, K. and Nultsch, W. 1992. Photoinhibition of photosynthesis and its recovery in red algae. *Bot. Acta.* 105: 278-284.

Hatchard, C.G. and Parker, C.A. 1956. A new sensitive chemical actinometer II. Potassium ferrioxalate as a standard chemical actinometer. *Proc. Roy. Soc. London* 235A: 518-536.

Hazzard, C., Lesser, M.P. and Kinzie III, R.A. 1997. Effects of ultraviolet radiation on photosynthesis in the subtropical marine diatom *Chaetoceros gracilis* (Bacillariophyceae). *J. Phycol.* 33: 960-968.

He, Y-Y., Klisch, M. and Häder, D-P. 2002. Adaptation of cyanobacteria to UV-B stress correlated with oxidative stress and oxidative damage. *Photochem. Photobiol.* 76(2): 188-196.

Heck, D.E., Vetrano, A.M., Mariano, T.M. and Laskin, J.D. UVB light stimulates production of reactive oxygen species. Unexpected role for catalase. *J. Biol. Chem.* 278 (25): 22432-22436.

Helbling, E., Villafane, V., Ferrario, M. and Holm-Hansen, O. 1992. Impact of natural ultraviolet radiation on rates of photosynthesis and on specific marine phytoplankton species. *Mar. Ecol. Progr. Series* 80: 89-100.

Heraud, P. and Beardall, J. 2000. Changes in chlorophyll fluorescence during exposure of *Dunaliella tertiolecta* to UV radiation indicate a dynamic interaction between damage and repair processes. *Photosynth. Res.* 63:123-134.

Herrmann, H., Ghetti, F., Scheuerlein, R. and Häder, D.-P. 1995. Photosynthetic oxygen and fluorescence measurements in *Ulva laetevirens* affected by solar radiation. *J. Plant Physiol.* 145: 221-227.

Herrmann, H., Häder, D.-P. and Ghetti, F. 1997. Inhibition of photosynthesis by solar radiation in *Dunaliella salina*: relative efficiencies of UV-B, UV-A and PAR. *Plant Cell Environ.* 20: 359-365.

Herrmann, H., Häder, D.-P., Köfferlein, M., Seidlitz, H K. and Ghetti, F. 1996. Effects of UV radiation on photosynthesis of phytoplankton exposed to solar simulator light. *J. Photochem. Photobiol. B: Biol.* 34: 21-28.

Hideg, E. 2006. Detecting stress-induced reative oxygen species in plants under UV stress. In: Ghetti, F (*eds.*) Ghetti, F., Checcucci, G. and Bornman, J.F. (eds.) *Environmental UV Radiation: Impact on Ecosystems and Human Health and Predictive Models.* Springer, The Netherlands. pp.147-157.

Holmes, M. G. 2002. An outdoor multiple wavelength system for the irradiation of biological samples: analysis of the long-term performance of various lamp and filter combinations. *Photochem. Photobiol.* 76, 158-163.

Holm-Hansen, O., Lubin, D. and Helbling, E.W. 1993. Ultraviolet radiation and its effects on organisms in aquatic environments. *In*: Young, A.R., Björn, O., Moan, J. and Nultsch, W. (*eds.*) *Environmental UV Photobiology*. Plenum Press, New York. pp. 379-426.

Hossain, M.A. and Asada, K. 1984. Purification of dehydroascorbate reductase from spinach and its characterization as a thiol enzyme. *Plant Cell Physiol.* 25: 85-92.

Ishikawa, T., Takeda, T., Kohno, H. and Shigeoka, S. 1996. Molecular characterization of *Euglena* ascorbate peroxidase using monoclonal antibody. *Biochem. Biophys. Acta* 1290: 69-75.

Ishikawa, T. and Shigeoka, S. 2008. Recent advances in ascorbate biosynthesis and the physiological significance of ascorbate peroxidase in photosynthesizing organisms. *Biosci. Biotechnol. Biochem.* 72(5): 1143-1154.

Iwanzik,W., Tevini, M., Dohnt, G., Voss, M., Weiss, W., Gräber, P. and Renger, G. 1983. Action of UV-B radiation on photosynthetic primary reactions in spinach chloroplasts. *Physiol. Plant.* 58(3): 401 – 407

Ivanov, A.G., Miskiewicz, E., Clarke, A.K., Greenberg, B.M. and Huner, N.P.A. 2000. Protection of photosystem II against UV-A and UV-B radiation in the cyanobacterium *Plectonema boryanum*: the role of growth temperature and growth irradiance. *Photochem. Photobiol.* 72: 772-779.

Jahnke, L.S. 1995. Acclimation to ultraviolet radiation in *Dunaliella parva*. In: Mathis, P. (*ed*) *Photosynthesis From Light to Bioshpere*. Kluwer Acdemic Publishers, Dordrecht, The Netherlands. pp. 279-282.

Jahnke, L.S. 1999. Massive carotenoid accumulation in *Dunaliella bardawil* induced by ultraviolet-A radiation. *J. Photochem. Photobiol. B: Biol.* 48: 68-74.

Jahnke, L.S. and Sampath-Wiley, P. 2009. Generating a solar UV-B spectrum in the laboratory with fluorescent lamp emissions. Does removing the excessive short-wave radiation transmitted by cellulose acetate make a difference in photosynthesis? *Photochem. Photobiol.* Under review.

Jahnke, L.S., White, A.L. and Sampath-Wiley, P. 2009. The effects of ultraviolet radiation on *Dunaliella*: growth, development and metabolism. Chapter 10 In: A. Ben-Amotz, J.E.W. Polle and D.V. Subba Rao (*eds*) *The alga Dunaliella: Biodiversity, Physiology, Genomics & Biotechnology.* Science Publishers, NH, USA. pp. 231-272.

Jahnke, L. S. and White, A. L. 2003. Long-term hyposaline and hypersaline stresses produce distinct antioxidant responses in the marine alga *Dunaliella tertiolecta. J. Plant Physiol.* 160:1193-1202.

Jeffrey, W.H. and Mitchell, D.L. 1997. Mechanisms of UV-induced DNA damage and response in marine microorganisms. In: Impacts of solar UVR on aquatic microorganisms. *Photochem. Photobiol.* 65(2): 260-263.

Johanson, U. and Zeuthen, J. 1998.The ecological relevance of UV-B enhancement studies is dependent on tube type, tube age, temperature and voltage. *J. Photochem. Photobiol.* 44: 169-174.

Jones, L. W. and Kok, B.1966. Photoinhibition of chloroplast reactions. II. Multiple effects. *Plant Physiol.* 41: 1044-1049.

Jordan, B. R., Chow, W. S., Strid, A. and Anderson, J. M. 1991. Reduction in cab and psb transcripts in response to supplementary ultraviolet-B radiation. *FEBS Lett.* 284:5-8.

Joshi, P.N., Ramaswamy, N.K., Raval, M.K., Desai, T.S., Nair, P.M. and Biswal, U.C. 1997. Response of senescing leaves of wheat seedingls to UVA radiation: inhibition of PSII in light and darkness. *Environ. Exp. Bot.* 38: 237-242.

Joshi, P.N., Ramaswamy, N.K., Iyer, R.K., Nair, P.M., Pradhan, M.K., Gartia, S., Biswal, B. and Biswal, U.C. 2007. Partial protection of photosynthetic apparatus from UV-B-induced damage by UV-A radiation. *Environ. Exp. Bot.* 59: 166-172.

Kato, J., Yamahara, T., Tanaka, K., Takio, S. and Satoh, T. 1997. Characterization of catalase from green algae *Chlamydomonas reinhardtii. J. Plant Physiol.* 151: 262-268.

Kerr, J.B. and McElroy, C.T. 1993. Evidence for large upward trends of ultraviolet-B radiation linked to ozone depletion. *Science* 262: 1032-1034.

Kim, D.-S and Watanabe, Y. 1993. The effect of long wave ultraviolet radiation (UV-A) on the photosynthetic activity of natural populations of freshwater phytoplankton. *Ecol. Res.* 8: 225-234.

Kim, D.-S and Watanabe, Y. 1994. Inhibition of growth and photosynthesis of freshwater phytoplankton by ultraviolet A (UVA) radiation and subsequent recovery from stress. *J. Plankton Res.* 16(12): 1645-1654.

Kimura, S., Tahira, Y., Ishibashi, T., Mori, Y., Mori, T., Hashimoto, J. and Sakaguchi, K. 2004. DNA repair in higher plants; photoreactivation is the major DNA repair pathway in non-proliferating cells while excision repair (nucleotide excision repair and base excision repair) is active in proliferating cells. *Nucleic Acids Res.* 32 (9): 2760-2767.

Krieger-Liszkay, A. 2004. Singlet oxygen production in photosynthesis. *J. Exp. Bot.* 56 (411): 337-346.

Krizek, D.T. 2004. Influence of PAR and UV-A in determining plant sensitivity and photomorphogenic responses to UV-B radiation. *Photochem. Photobiol.* 79(4): 307-315.

Kulandaivelu, G., Maragatham, S. and Nedunchezhian, N. 1989. On the possible control of ultraviolet-B induced response in growth and photosynthetic activities in higher plants. *Physiol. Plant.* 76(3): 398-404.

Laemmli, U.K. 1970. Cleavage of structural proteins during the assembly of the head of bacteriophage T4. *Nature* 227: 680-685.

Langebartels, C., Schraudner, M., Heller, W., Ernst, D. and Sandermann, H. 2002. Oxidative stress and defense reactions in plants exposed to air pollutants and UV-B radiation. In: Inze, D. and van Montagu, M. (*eds.*) *Oxidative Stress in Plants.* Taylor and Francis, NY. pp. 105-135.

Larkum, A.W.D., Karge, M., Reifarth, F., Eckert, H.-J., Post, A. and Renger, G. 2001. Effect of monochromatic UV-B radiation on electron transfer reactions of Photosystem II. *Photosynth. Res.* 68: 49–60.

Leonardis, S. D., Dippierro, N. and Dippierro, S. 2000. Purification and characterization of an ascorbate peroxidase from potato tuber mitochondria. *Plant Physiol. Biochem.* 38:773-779

Lesser, M.P. 1996a. Acclimation of phytoplankton to UV-B radiation: oxidative stress and photoinhibition of photosynthesis are not prevented by UV-absorbing compounds in the dinoflagellate *Prorocentrum micans*. *Mar. Ecol. Prog. Ser.* 132: 287-297.

Lesser, M.P. 1996b. Elevated temperatures and ultraviolet radiation cause oxidative stress and inhibit photosynthesis in symbiotic dinoflagellates. *Limnol. Oceanogr.* 41: 271-283.

Lesser, M.P. 2006. Oxidative stress in marine environments: Biochemistry and physiological ecology. *Annu. Rev. Physiol.* 68: 6.1-6.26.

Lesser, M.P., Barry, T.M. and Banaszak, A.T. 2002. Effects of UV radiation on a Chlorophyte alga (*Scenedesmus* sp.) isolated from the fumarole fields of Mt. Erebus, Antarctica. *J. Phycol.* 38: 473-481.

Lesser, M.P., Neale, P.J. and Cullen, J.J. 1996. Acclimation of Antarctic phytoplankton to ultraviolet radiation: ultraviolet-absorbing compounds and carbon fixation. *Mol. Mar. Biol. Biotechnol.* 5(4): 314-325.

Lesser, M.P. and Shick, J.M. 1989. Effects of irradiance and ultraviolet radiation on photoadaptation in the zooxanthellae of *Aiptasia pallida*: primary production, photoinhibition, and enzymatic defenses against oxygen toxicity. *Mar. Biol.* 102: 243- 255.

Lichtenthaler, H.K. 1987. Chlorophylls and carotenoids: pigments of photosynthetic biomembranes. *Methods Enzymol.* 148: 350-382.

Lichtenthaler, H.K., Buschmann, C., Döll, M., Fietz, H.-J., Bach, T., Kozel, U., Meier, D. and Rahmsdorf, U. 1981. Photosynthetic activity, chloroplast ultrasturcture, and leaf characteristics of high-light and low-light plants and of sun and shade leaves. *Photosynth. Res.* 2: 115-141.

Lichtenthaler, H.K., Ac, A., Marek, M.V., Kalina, J. and Urban, O. 2007. Differences in pigment composition, photosynthetic rates and chlorophyll fluorescence images of sun and shade leaves of four tree species. *Plant Physiol. Biochem.* 45: 577-588.

Lv, X.Y., Qiao, D.R., Xiong, Y., Xu, H., You, F.F., Cao, Y., He, X. and Cao, Y. 2008. Photoreactivation of (6- 4) photolyase in *Dunaliella salina*. *FEMS Microbiol. Lett.* 283: 42-46.

Mackerness, S. A-H., Butt, P.J., Jordan, B. R. and Thomas, B. 1996. Amelioration of ultraviolet-B induced down-regulation of messenger-RNA levels for chloroplast proteins by high irradiance is mediated by photosynthesis. *J. Plant Physiol.* 148: 100-106.

Mackerness, S. A-H., Jordan, B. R. and Thomas, B. 1999. Reactive oxygen species in the regulation of photosynthetic genes by ultraviolet-B radiation (UV-B: 280-320nm) in green and etiolated buds of pea (*Pisum sativum* L.). *J. Photochem. Photobiol. B: Biology* 48: 180-188.

Malanga, G. and Puntarulo, S. 1995. Oxidative stress and antioxidant content *in Chlorella vulgaris* after exposure to ultraviolet B radiation. *Physiol. Plant.* 94: 672-679.

Malanga, G., Calmanovici, G. and Puntarulo, S. 1997. Oxidative damage to chloroplasts from *Chlorella vulgaris* exposed to ultraviolet-B radiation. *Physiol. Plant.* 101: 455-462.

Masi, A. and Melis, A. 1997. Morphological and molecular changes in the unicellular green alga *Dunaliella salina* grown under supplemental UV-B radiation: cell characteristics and photosystem II damage and repair properties. *Biochim. Biophys. Acta.* 1321: 183-193.

McClung, C.R. 1997. Regulation of catalases in Arabidopsis. *Free Rad. Biol. & Med.* 23(3): 489-496.

Melis, A., Nemson, J. A. and Harrison, M. A. 1992. Damage to functional components and partial degradation of photosystem II reaction center proteins upon chloroplast exposure to ultraviolet-B radiation. *Biochim. Biophys. Acta* 1100: 312-320.

Micheletti, M.I, Piacentini, R.D. and Mandronich, S. 2003. Sensitivity of biologically active UV radiation to stratospheric ozone changes: effects of action spectrum shape and wavelength range. *Photochem. Photobiol.* 78, 456-461.

Middleton, E. M. and Teramura, A. H. 1994. Understanding photosynthesis, pigment and growth responses induced by UV-B and UV-A irradiances. *Photochem. Photobiol.* 60: 38-45.

Mirecki, R.M. and Teramura, A.H. 1984. Effects of ultraviolet radiation on soybean. *Plant Physiol.* 74: 475-480.

Mittler, R. and Poulos, T.L. 2005. Ascorbate peroxidase. In: Smirnoff, N. (*ed.*) *Antioxidants and Reactive Oxygen Species in Plants*. Blackwell Publishing Ltd., Oxford UK. pp. 87-100.

Mittler, R., Vanderauwera, S., Gollery, M. and Van Breusegem, F. 2004. Reactive oxygen gene network of plants. *TRENDS Plant Sci.* 9 (10): 490-498.

Mittler, R. and Zilinskas, B.A. 1993. Detection of ascorbate peroxidase activity in native gels by inhibition of the ascorbate-dependent reduction of nitroblue tetrazolium. *Anal. Biochem.* 212: 540-546.

Miyake, C. and Asada, K. 1992. Thylakoid-bound ascorbate peroxidase in spinach chloroplasts and photoreduction of its primary oxidation product monodehydroascorbate radicals in thylakoids. *Plant Cell Physiol.* 33(5): 541-553.

Miyake, C. and Asada, K. 1996. Inactivation mechanism of ascorbate peroxidase at low concentrations of ascorbate; hydrogen peroxidase decomposes Compound I of ascorbate peroxidase. *Plant Cell Physiol.* 37(4): 423-430.

Miyake, C., Wan-Hong, C. and Asada, K. 1993. Purification and molecular properties of the thylakoid-bound ascorbate peroxidase in spinach chloroplasts. *Plant Cell Physiol.* 34(6): 881-889.

Murgia, I., Tarantino, D., Vannini, C., Bracale, M., Carravieri, S. and Soave, C. 2004. *Arabidopsis thaliana* plants overexpressing thylakoidal ascorbate peroxidase show increased resistance to Paraquat-induced photooxidative stress and to nitric oxide-induced cell death. *Plant. J.* 38: 940-953.

Najami, N., Janda,T., Barriah, W., Kayam, G., Tal, M., Guy, M. and Volokita, M. 2008. Ascorbate peroxidase gene family in tomato: its identification and characterization. *Mol. Genet. Genomics* 279(2): 171-182.

Nakano, Y. and Asada, K. 1981. Hydrogen peroxide is scavenged by ascorbate-specific peroxidase in spinach chloroplasts. *Plant Cell Physiol.* 22(5): 867-880.

Nakano, Y. and Asada, K. 1987. Purification of ascorbate peroxidase in spinach chloroplasts; its inactivation in ascorbate-depleted medium and reactivation by monodehydroascorbate radical. *Plant Cell Physiol.* 28:131-140.

Nayak, L., Biswal, B., Ramaswamy, N.K., Iyer, R.K. Nair, J.S. and Biswal, U.C. 2003. Ultraviolet-A induced changes in photosystem II of thylakoids: effects of senescence and high growth temperature. *J. Photochem. Photobiol. B: Biol.* 70: 59-65.

Neale, P. J. 2000. Spectral weighting functions for quantifying effects of UV radiation in marine ecosystems. In: de Mora, S. Demers, S. and Vernet, M. (eds.) *The Effects of UV Radiation in the Marine Environment.* pp. 72-100. Cambridge Univ. Press, New York.

Niyogi, K.K. 1999. Photoprotection revisited: genetic and molecular approaches. *Annu. Rev. Plant Physiol. Plant Mol. Biol.* 50: 333-359.

Nogues, S., Allen, D.J. and Baker, N.R. 2006. Potential effects of UV-B on photosynthesis and photosynthetic productivity of higher plants. In: Ghetti, F., Checcucci, G. and Bornman, J.F. (eds.) *Environmental UV Radiation: Impact on Ecosystems and Human Health and Predictive Models.* Springer, The Netherlands. pp. 137-146.

Osmond, C.B. 1994. What is photoinhibition? Some insights from comparisons of shade and sun plants. In: Baker, N.R. and Boyer, J.R. (*eds.*) *Photoinhibition of Photosynthesis: From Molecular Mechanisms to the Field.* BIOS Scientific Publishers, Oxford, UK. pp. 1-24.

Osmond, C.B., Ramus, J., Levavasseur, G., Franklin, L.A. and Henley, W.J. 1993. Fluorescence quenching during photosynthesis and photoinhibition of *Ulva rotundata* Blid. *Planta.* 190: 97-106.

Peak, M.J., Peak, J.G. and MacCoss, M. 1984.DNA breakage caused by 33nm ultraviolet light is enhanced by naturally occurring nucleic acid components and nucleotide coenzymes. *Photochem. Photobiol.* 39: 713-716.

Peak, M.J. and Peak, J.G. 1986. Molecular photobiology of UVA. In: Urbach, F., Ganga, R.W (*eds.*) *The Biological Effects of UVA Radiation.* Praege Publishing. New York. Pp. 42-52.

Pnueli, L., Liang, H., Rozenberg, M. and Mittler, R. 2003. Growth suppression, altered stomatal responses, and augmented induction of heat shock proteins in cytosolic ascorbate peroxidase (Apx1)-deficient Arabidopsis plants. *Plant J.* 34: 187-203.

Polidoros, A.N. and Scandalios, J.G. 1981. Response of the maize catalases to light. *Free Rad. Biol. Med.* 23 (3): 497-504.

Polle, A. 2001. Dissecting the superoxide dismutase-ascorbate-glutathione-pathway in chloroplasts by metabolic modeling. Computer simulations as a step towards flux analysis. *Plant Physiol.* 126: 445-462.

Quesada, A., Mouget, J.L. and Vincent, W.F. 1995. Growth of Antarctic cyanobacteria under ultraviolet radiaton: UVA counteracts UVB inhibition. *J. Phycol.* 31: 242-248.

Queval, G., Hager, J., Gakiere, B. and Noctor, G. 2008. Why are literature for H_2O_2 contents so variable? A discussion of potential difficulties in the quantative assay of leaf extracts. *J. Exp. Bot.* 59 (2): 135-146.

Raja, R., Hemaiswarya, R. and Rengasamy, R. 2007. Exploitation of *Dunaliella* for b-carotene production. *Appl. Microbiol. Biotechnol.* 74: 517-523.

Redinbaugh, M.G., Sabre, M. and Scandalios, J.G. 1990. The distribution of catalase activity, isozyme protein, and transcript in the tissues of the developing maize seeding. *Plant Physiol.* 92: 375-380.

Rijstenbil, J.W. 2001. Effects of periodic, low UVA radiation on cell characteristics and oxidative stress in the marine planktonic diatom *Ditylum brightwellii. Eur. J. Phycol.* 36:1-8.

Rijstenbil, J.W. 2002. Assessment of oxidative stress in the planktonic diatom *Thalassiosira pseudonana* in response to UVA and UVB radiation. *J. Plankton Res.* 24 (12): 1277-1288.

Rijstenbil, J.W. 2003. Effects of UVB radiation and salt stress on growth, pigments and antioxidative defense of the marine diatom *Cylindrotheca closterium. Mar. Ecol. Prog. Ser.* 254: 37-47.

Roncarati, E., Ristenbil, J.W. and Pistocchi, R. 2008. Photosynthetic performance, oxidative damage and antioxidants in *Cylindrotheca closterium* in response to high irradiance, UVB radiation and salinity. *Mar. Biol.* 153: 965-973.

Salguero, A., Leon, R., Marioti, A., De la Morena, B., Vega, J.M. and Vilchez, C. 2005. UV-A mediated induction of carotenoid accumulation in *Dunaliella bardawil* with retention of cell viability. *Appl. Microbiol. Biotech.* 66: 506-511.

Sano, S., Ueda, M., Kitajima, S., Takeda, T., Shigeoka, S., Kurano, N., Miyachi, S., Miyake, C. and Yokota, A. 2001. Characterization of ascorbate peroxidases from unicellular red alga Galdieria partita. *Plant Cell Physiol.* 42: 433-440.

Savitch, L.V., Pocock, T., Krol, M., Wilson, K.E. Greenberg, B.M. and Huner, N.P.A. 2001. Effects of growth under UVA radiation on CO_2 assimilation, carbon partitioning, PSII photochemistry and resistance to UVB radiation in *Brassica napus* cv. Topas. *Aust. J. Plant Physiol.* 28: 203-212.

Scandalios, J.G. 1994. Regulation and properties of plant catalases. In: Foyer, Christine H.; Mullineaux, Philip M. (*eds.*) *Causes of Photooxidative Stress and Amelioration of Defense Systems in Plants.* CRC Press, Inc. Boca Raton, FL, USA. pp. 275-315.

Scandalios, J.G., Guan, L. and Polidoros, A.N. 1997. Catalases in plants: gene structure, properties, regulation and expression. In: Scandalios, J.G. (*ed.*) *Oxidative Stress and the Molecular Biology of Antioxidant Defenses.* Cold Spring Harbor Laboratory Press. pp. 343-406.

Schaedle, M and Bassham, J. A. 1977. Chloroplast glutathione reductase. *Plant Physiol.* 59:1011-101.

Searles, P.S., Flint, S.D. and Caldwell, M.M. 2001. A meta-analysis of plant field studies simulating stratospheric ozone depletion. *Oecologia* 127: 1-10.

Sedmak, J.J. and Grossberg, S.E. 1977. A rapid, sensitive, and versatile assay for protein using Coomassie brilliant blue G250. *Anal. Biochem.* 79(1-2): 544-552.

Shang, W. and Feierabend, J. 1999. Dependence of catalase photoinactivation in rye leaves on light intensity and quality and characterization of a chloroplast-mediated inactivation in red light. *Photosynth. Res.* 59: 201-213.

Shelly, K, Heraud, P. and Beardall, J. 2002. Nitrogen limitation in *Dunaliella tertiolecta* (Chlorophyceae) leads to increased susceptibility to damage by UV-B radiation but also increased repair capacity. *J. Phycol.* 38: 713-20.

Shelly, K., Heraud, P. and Beardall, J. 2003. Interactive effects of PAR and UV-B radiation on PSII electron transport in the marine alga *Dunaliella tertiolecta* (Chlorophyceae). *J. Phycol.* 39: 509-512.

Shigeoka, S. Ishikawa, T., Tamoi, M., Miyagawa, Y., Takeda, T., Yabuta, Y. and Yoshimura, K. 2002. Regulation and function of ascorbate peroxidase isoenzymes. *J. Exp. Bot.* 53 (372): 1305-1319.

Sicora, C., Mate, Z. and Vass, I. 2003. The interaction of visible and UV-B light during photodamage and repair of photosystem II. *Photosynth. Res.* 75: 127-137.

Siefermann-Harms, D. 1987. The light-harvesting and protective functions of carotenoids in photosynthetic membranes. *Physiol. Plant.* 69:561-568.

Smirnoff, N. 1993. The role of active oxygen in the response of plants to water deficit and desiccation. *New Phytol.* 125(1): 27-58.

Smith, R.C., Prezelin, B. B., Baker, K. S., Bidigare, R. R., Boucher, N. P., Coley, T., Karentz, D., MacIntyre, S., Matlick, H. A., Menzies, D., Ondrusek, M., Wan, Z. and Waters, K. J. 1992. Ozone depletion: ultraviolet radiation and phytoplankton biology in Antarctic waters. *Science* 255: 952-959.

Strid, A. and Porra, R.J. 1992. Alterations in pigment content in leaves of *Pisum sativum* after exposure to supplementary UV-B. *Plant Cell Physiol.* 33(7): 1015-1023.

Taiz, L. and Zeiger, E. 2002. *Plant Physiology* 3rd Edition. Sinauer Associates, Inc. Sunderland, MA, U.S.A. pp.690.

Takeda, T., Ishikawa, T. and Shigeoka, S. 1993. The function of H2O2-scavenging system in *Chlamydomonas reinhardtii*. In: Welinder, K.G., Rasmussen, S.K., Penel, C. and Greppin, H. (*eds.*) *Plant Peroxidases: Biochemistry and Physiology*. University of Geneva. pp. 257-262.

Takeda, T., Ishikawa, T. and Shigeoka, S. 1997. Metabolism of hydrogen peroxidase by the scavenging system in *Chlamydomonas reinhardtii. Physiol. Plant.* 99: 49-55.

Takeda, T., Yoshimura, K., Ishikawa, T. and Shigeoka, S. 1998. Purification and characterization of ascorbate peroxidase in *Chlorella vulgaris. Biochimie* 80: 295-301.

Takeda, T., Yoshimura, K., Yoshii, M. and Kanahoshi, H. 2000. Molecular characterization and physiological role of ascorbate peroxidase from halotolerant *Chlamydomonas* sp. W80 strain. *Arch. Biochem. Biophys.* 376 (1): 82- 90.

Teramura, A.H. 1980a. Effects of ultraviolet-B iradiances on soybean. *Plant Physiol.* 65:483-488.

Teramura, A.H. 1980b. Effects of ultraviolet-B irradiances on soybean. I. Importance of photosynthetically active radiation in evaluating ultraviolet-B irradiances effects on soybean and wheat growth. *Physiol. Plant.* 48: 333-339.

Teixeira, F.K., Menezes-Benavente, L., Galvao, V.C., Marfis, R. and Margis-Pinheiro, M. 2006. Rice ascorbate peroxidase gene family encodes functionally diverse isoforms localized in different subcellular compartments. *Planta* 224: 300-314.

Tommasi, F., Paciolla, C. and Arrigoni, O. 1999. The ascorbate system in recalcitrant and orthodox seeds. *Physiol. Plant.* 105: 193-198.

Turcásanyi, E. and Vass, I. 2000. Inhibition of photosynthetic transport by UV-A radiation targets the photosystem II complex. *Photochem. Photobiol.* 74(2):513-520.

Tyrrell, R.M. 1991. UVA (320-380 nm) radiation as an oxidative stress. In: Sies, H. (*ed*) *Oxidative Stress: Oxidants and Antioxidants*. Academic Press. pp. 57-83.

Tyystjärvi, E. 2008. Photoinhibition of photosystem II and photodamage of the oxygen evolving manganese cluster. *Coordination Chemistry Reviews* 252: 361–376.

van den Hoek, C., Mann, D.G. and Jahns, H.M. 1995. *Algae: An Introduction to Phycology*. Cambridge University Press, Cambridge, UK. pp.627.

Vass, I. 1997. Adverse effects of UV-B light on the structure and function of the photosynthetic apparatus. In: Pessarakli, M. (ed) *Handbook of Photosynthesis*. Marcel Dekker, New York, USA.pp. 931-950.

Vass, I., Cser, K. and Cheregi, O. 2007. Molecular mechanisms of light stress of photosynthesis. *Ann. N.Y. Acad. Sci.* 1113:114-122.

Vass, I., Turcsányi, E. Touloupakis, E., Ghanotakis, D. and Petrouleas, V. 2002. The mechanism of UV- A radiation-induced inhibition of photosystem II electron transport studied by EPR and chlorophyll fluorescence. *Biochemistry* 41: 10200–10208.

Vega, M.P. and Pizarro, R.A. 2000. Oxidative stress and defense mechanisms of the freshwater cladoceran *Daphnia longispina* exposed to UV radiation. *J. Photochem. Photobiol. B: Biol.* 54:121-125.

Walrant, P. and Santus, R. 1974. Ultraviolet and N-formyl-kynurenine-sensitized photoinactivation of bovine carbonic anhydrase: an internal photodynamic effect. *Photochem. Photobiol.* 20(5): 455-460.

Waring, J., Underwood, G.J.C. and Baker, N.R. 2006. Impact of elevated UV-B radiation on photosynthetic electron transport, primary productivity and carbon allocation in estuarine epipelic diatoms. *Plant Cell Environ.* 29: 521-534.

Warner, C.W. and M.M. Caldwell. 1983. Influence of photon flux density in the 400-700 nm wavelengths on inhibition of photosynthesis by UV-B (280-320 nm) irradiation in soybean leaves: Separation of indirect and immediate effects. *Photochem. Photobiol.* 381: 341-346.

West, L.J.A., Greenberg, B.M. and Smith, R.E.H. 1999. Ultraviolet radiation effects on a microscopic green alga and the protective effects of natural dissolved organic matter. *Photochem. Photobiol.* 69: 536-544.

White, A. L. and Jahnke, L. S. 2002. Contrasting effects of UV-A and UV-B on photosynthesis and photoprotection of β-carotene in two *Dunaliella* spp. *Plant Cell Physiol.* 43:877-884.

White, A. L. and Jahnke, L. S. 2004. Removing UV-A and UV-C radiation from UV-B fluorescent lamp emissions. Differences in the inhibition of photosynthesis in the marine alga *Dunaliella tertiolecta* using chromate versus cellulose acetate-polyester filters. *Photochem and Photobiol.* 80:340-345.

Whitehead, R.F., de Mora, S.J. and Demers, S. 2000. Enhanced UV radiation- a new problem for the marine environment. In: de Mora, S.J., Demers, S. and Vernet, M. (eds.) *Effects of UV radiation in the Marine Environment.* Cambridge University Press, New York. pp. 1-34.

Willekens, H., Langebartels, C., Tire, C., Van Montagu, M., Inze, D. and Van Camp, W. 1994. Differential expression of catalase genes in *Nicotiana plubaginifolia* (L.). *Proc. Natl. Acad. Sci.* USA 91: 10450-10454.

Willekens, H., Inze, D., Van Montagu, M. and van Camp, W. 1995. Catalases in plants. *Mol. Breeding* 1: 207-228.

Wolfe-Simon, F., Grzebyk, D., Schofield, O, and Falkowski, P.G. 2005. The role and evolution of superoxide dismutase in algae. *J. Phycol.* 41: 453-465.

Woodbury, W., Spencer, A. K. and Stahmann M. A. 1971. An improved procedure using ferricyanide for detecting catalase isozymes. *Anal. Biochem.* 44(1): 301-305.

Xiong, F., Nedbal, L. and Neori, A. 1999. Assessment of UV-B sensitivity of photosynthetic apparatus among microalgae: short-term laboratory screening versus long-term outdoor exposure. *J. Plant Physiol.* 155: 54-62.

Yoshimura, K., Shikawa, T., Nakamura, Y., Tamoi, M., Takeda, T., Tada, T., Nishimura, K. and Shigeoka, S. 1998. Comparative study on recombinant chloroplastic and cytosolic ascorbate peroxidase isozymes of spinach. *Arch. Biochem. Biophys.* 353:55-63.

Yoshimura, K., Yabuta, Y., Ishikawa, T. and Shigeoka, S. 2000. Expression of spinach ascorbate peroxidase isoenzymes in response to oxidative stresses. *Plant Physiol.* 123: 223-233.

Young, A.J. 1991. The photoprotective role of caroenoids in higher plants. *Physiol. Plant.* 83:702-708.

Zudaire, L. and Roy, S. 2001. Photoprotection and long-term acclimation to UV radiation in the marine diatom *Thalassiosira weissfloggii. J. Photochem. Photobiol. B: Biol.* 62: 26-34.